STRUCTURE OF RUBIDIUM AND STRONTIUM NUCLIDES OF MASS 90 AND 91

STRUCTURE OF RUBIDIUM AND STRONTIUM NUCLIDES OF MASS 90 AND 91

by

JAMES F. A. MASON, B.Sc. (Eng.)

A Thesis

Submitted to the Faculty of Graduate Studies

in Partial Fulfilment of the Requirements

for the Degree

Doctor of Philosophy

McMaster University

September 1969

DOCTOR OF PHILOSOPHY (1969)

McMASTER UNIVERSITY
Hamilton, Ontario

TITLE: Structure of Rubidium and Strontium Nuclides of Mass 90 and 91

AUTHOR: James F. A. Mason, B.Sc. (Eng.)
(Queen's University)

SUPERVISOR: Dr. M. W. Johns

NUMBER OF PAGES: x, 129

SCOPE AND CONTENTS:

The level structures of ^{90,91}Rb and ^{90,91}Sr, as populated in beta decay, have been investigated using Ge(Li) and NaI(Tl) gamma ray and plastic beta ray spectrometers, and standard spectroscopic techniques. Beta-gamma and gamma-gamma coincidence experiments have been used to establish twelve levels in ^{90}Rb, four levels in ^{91}Rb and to determine the ground state Q-values for the decay of both ^{90}Kr and ^{91}Kr. Thirty-one levels have been proposed in ^{90}Sr and eighteen in ^{91}Sr on the basis of gamma-gamma coincidence experiments only. The lifetime of the first excited state in ^{91}Sr has also been measured.

ACKNOWLEDGEMENTS

The author would like to express his appreciation to his research supervisor Dr. M. W. Johns and the other members of his supervisory committee, Dr. W. B. Clarke and Dr. G. L. Keech, for their encouragement and guidance during the course of this investigation. Their comments and suggestions were extremely helpful in solving many of the problems encountered.

The many valuable discussions and generous assistance provided by the members of beta ray spectroscopy group, with whom I have been associated, is gratefully acknowledged. I would also like to thank Drs. T. J. Kennett, J. A. Cameron and W. V. Prestwich and the members of their research groups for making available to me considerable equipment which greatly facilitated the performance of some of the experiments.

It is a pleasure to thank the staff of the McMaster reactor and Computation Centre for the assistance in the innumerable sample irradiations and the running of the computer programs used in this study.

I would like to express my thanks to Dr. W. L. Talbert, Jr. of Iowa State University, for his generosity in making available some preliminary results of experiments on the same nuclides as have been investigated here.

The ability of Miss Susan Wignall in transforming the hieroglyphics of the original manuscript into the present document has been remarkable. The efforts of Mr. Tom Dececchi in plotting graphs for data analysis and the preparation of drawings is gratefully acknowledged.

The financial assistance of the National Research Council of Canada and the Government of Ontario was essential to the continuation of these studies.

Also essential was the support, both financial and moral, provided by my parents, Professor and Mrs. F. E. Mason. I am greatly indebted for their continued encouragement.

The exclusive final position in this list of acknowledgements has been reserved for my wife, Rosemary. I am sure that many times during the course of our stay in this city, she has felt that she was managing a boarding house rather than a household; for her understanding, a great big thank you.

TABLE OF CONTENTS

LIST OF TABLES

LIST OF FIGURES

CHAPTER I

DESCRIPTION OF NUCLEAR STATES

INTRODUCTION

The understanding and interpretation of nuclear properties within a theoretical framework is a fundamental problem of nuclear physics. The most direct approach to this problem would be to determine all the components of the total nucleon-nucleon interaction and using these, to derive the total nuclear wave function. This wave function would then contain or could be used to calculate all the properties which characterize a nuclear state e.g. spin, parity, energy, magnetic moment, quadrupole moment.

Such an approach is, however, unrealistic both because of uncertainties in the form of the nucleon-nucleon interaction and the enormity of the calculations required to account for all the degrees of freedom of all the particles involved. Even if such a calculation could be performed the results would probably vastly exceed one's ability to comprehend them. Hence it has become standard procedure to describe nuclear properties with the help of models; each of which may be more or less limited in scope. The usefulness of any model is, of course, determined by its ability to reproduce easily and understandably, observed experimental facts.

1.1 The Shell Model

The shell model, or individual particle model, is a relatively

simple but rather successful model. It is based on the assumption that the nucleons within the nucleus move as independent particles describing orbits determined by some average potential due to the presence of all the other nucleons. The particular form of the potential which is used in any calculation depends upon the degree of sophistication of the calculation and is usually chosen in a phenomenological or semi-phenomenological fashion for ease of calculation.

The potential employed when the model was introduced originally by Mayer (1949, 1950) and independently by Haxel, Jensen and Suess (1949, 1950) was of the form $Vc - V_{\ell s}\vec{\ell}\cdot\vec{s}$. The central term (Vc), produces nuclear states which can be characterized by three quantum number - (n, ℓ, j). This indicates that, as a result of the spherical symmetry of the potential, both the orbital angular momentum designated by ℓ and the total angular momentum, designated by j, are constants of the particle motion. There may, however, be a degeneracy in energy of several of these states. The addition of the $\vec{\ell}\cdot\vec{s}$ term partially removes this degeneracy without destroying the angular momentum properties so that the quantum numbers (n, ℓ, j) continue to characterize the states.

A further degeneracy with respect to the orientation of the total angular momentum still exists. This means that each (n, ℓ, j) state is actually as superposition of $(2j + 1)$ states each with a different value for m_j, the quantum number representing the orientation of j. For $V_{\ell\cdot s}$ a positive number the states with $j = \ell + 1/2$ are depressed from the original position while the states with

$j = \ell - 1/2$ are raised.

Because nucleons are fermions and therefore obey the Pauli Exclusion principle each (n, ℓ, j) level can contain at most (2j + 1) nucleons of a specific type. The structure of any nucleus is thus determined by filling the lowest possible energy levels with neutrons and protons until all the particles have been placed. By properly selecting the value of $V_{\ell \cdot s}$, relatively large gaps can be made to occur in the energy required to add another nucleon, at occupation numbers corresponding to the observed "magic numbers" of inherently extra stable nuclei. The levels which are isolated between any two of these gaps taken together are referred to as a major shell while each level separately may be referred to as a minor shell.

Figure 1.1.1 shows the generally accepted ordering of levels for neutrons in the simple shell model, labelled by $n\ell_j$. For protons the ordering is similar although minor variations do occur because of the additional energy of Coulomb repulsion. Such corrections depend on the spatial distribution of the nuclear change and hence quantitatively upon the exact wave functions of the particles. Qualitatively, however, it is found that in the fifth shell (Z > 50) the $2d_{5/2}$ or $1g_{7/2}$ are inverted as are the $3s_{1/2}$ and $2d_{3/2}$.

Another phenomenon which must be considered in determining the filling of levels is the pairing energy. Whenever two nucleons with the same (n, ℓ, j) quantum number occur with opposite m_j i.e. with their spins alligned in opposite directions, they tend to interact strongly together to form a "zero coupled pair". Such a pair, which has zero resultant angular momentum, is considerably more stable

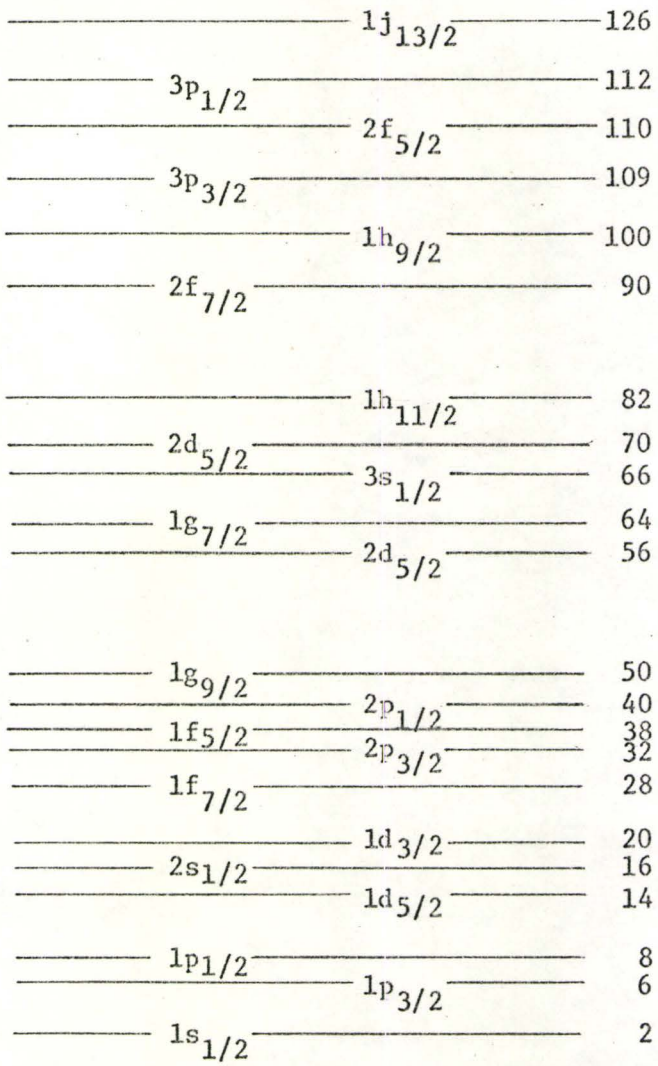

Figure 1.1.1 Simple Shell Model Energy Levels for the First 126 Neutrons

and hence energetically more favourable than a pair formed by the interaction between two nucleons with the same (n, ℓ, j) but m_j which are not exactly opposite. The magnitude of the gain in energy depends on the value of the orbital angular momentum, being larger for higher values of momentum. Because of this pairing energy it is sometimes energetically more favourable for a nucleon to be in a level of higher intrinsic energy if there is another particle already there available to form a pair.

1.2 Spins and Parities of Ground States

With these considerations it is possible using the simple shell model to determine the spins and parities of many multi-nucleon configurations. In particular, configurations which contain an even number of nucleons of the same (n, ℓ, j) type will have a resultant angular momentum of zero since the nucleons will couple pair-wise to zero thus gaining the pairing energy. Also since such a configuration is symmetric with respect to the pair-wise exchange of all the space co-ordinates of all the particles the system will have a positive parity. Since each individual level can contain an even number of particles, all filled levels will have 0 spin and positive parity (0+ configurations). Thus the shell model predicts the experimentally observed fact that all nuclei with even numbers of protons and neutrons (even-even nuclei) will have 0+ ground states.

In nuclei which have an even number of protons and an odd number of neutrons, the protons will form a 0+ configuration, as will all the filled levels of the neutron configuration. The neutrons remaining in the unfilled shell will couple pair-wise, as much as

possible, to 0+ configurations so that the spin and parity characteristics of the ground state of the total nucleus will be given by that of the final unpaired neutron. The situation for odd Z even N nuclei is the same but with the roles of neutrons and protons interchanged.

If the simple shell model is expanded to include residual interactions between all the nucleons in an unfilled shell the results obtained above are not altered. Generally the states produced by different combinations of identical particles are energy degenerate but the inclusion of the residual interaction removes this degeneracy. Provided the interaction between levels of different ℓ and j is smaller than the interactions within the unfilled level the pairing force will still dominate and even numbers of particles will couple to resultant spin 0 and odd numbers of particles will couple pair-wise to zero with the resultant spin being that of the final remaining nucleon.

In the case of nuclei which have an odd number of both neutrons and protons the predictions are not so unique. The residual interaction between the final neutron and final proton contains a part which depends on the relative orientation of the respective intrinsic spins of the particles. Brennan and Bernstein (1960), from an analysis of a number of unambiguous ground state assignments, proposed the following rules to aid with configuration determinations. For ($j_p - \ell_p$) (p designates proton) and ($j_n - \ell_n$) (n designates neutron) of opposite sign, the strength of the spin dependent part of the residual interaction is such that the state with resultant angular momentum $J = |j_n - j_p|$ is energetically well below the other possible states, and hence becomes the ground state of the configuration. For ($j_p - \ell_p$) and

$(j_n - \ell_n)$ of the same sign the interaction is such that either the state with $J = j_n + j_p$ or the state with $J = |j_n - j_p|$ will be favoured over the intermediate spin values. Thus, for these cases, the ground state spin of the configuration may be either $|j_n - j_p|$ or $(j_n + j_p)$.

Using these principles it is possible, in a reasonable manner, to account for a good many observed ground state spins and parities and hence determine the nucleonic structure of the ground state configuration. With a straightforward extension it is also possible in some cases to account for the properties of low lying excited states.

1.3 Excited State Spins and Parities

In this interpretation, low lying excited states are formed by exciting one or more of the nucleons into levels which are unoccupied. The properties of the state are then determined as before. It must be remembered, however in interpreting excited states, that levels may arise solely from rearranging the ground state configuration, as mentioned above. These levels may, therefore, not have a true single particle nature because the residual interaction has the effect of admixing certain amounts of other states into the wave function of the original state. This configuration mixing may make interpretation of the low lying excited states difficult.

1.4 Justification of the Shell Model and Limitations

The remarkable success of this model considering the incongruity between its basic assumption and the established facts about the strength and nature of the nucleon-nucleon interaction is of con-

siderable interest. In fact, the assumption of independent motion has been borne out in nuclear matter calculations where it is found that unless the nucleons are quite close togehter ($\lesssim$ 1.0 fm; i.e. $\lesssim 1.0 \times 10^{-13}$ cm) their wave function are essentially those of free particles. Since the average separation of nucleons in nuclear matter is about 1.66 fm the particles act by and large as free particles.

The reason for this behaviour is that in order for two nucleons to interact in an observable fashion they must be in different states after the interaction than before. However, all the available momentum states are occupied up to the Fermi momentum, determined by the density of the particles, and since nucleons obey Fermi-Dirac statistics only those states above the Fermi momentum are available as final states. Since large momentum transfer collision are improbable only those nucleons near this momentum will undergo noticeable interaction while the remaining deep lying nucleons will act as essentially free. Since the interior of larger A nuclei resembles nuclear matter this same condition will exist with only some slight modification for the density variation at the nuclear surface.

The success of the Shell model is, of course, limited to quantities such as spin and parity which do not depend in detailed fashion on the wave function. Such quantities as magnetic moments, quadrupole moments, transition probabilities and spins and parities of many excited states are difficult to explain with the shell model and indeed suggest the existence of strong collective behaviour.

1.5 Collective Motion

One type of collective behaviour, already introduced, is the

preferred interaction of two nucleons in similar (n, ℓ, j) states but with oppositely aligned spin vectors. If this is extended to include interaction between such zero-coupled pairs in both the same and different orbitals a description of the nucleus is obtained in which the motion of these pairs is also correlated. This is the so-called BCS description (Bardeen, Cooper and Schreiffer (1957)) originally applied to the problem of superconductivity. The application to nuclear physics was made by Bohr, Mottelson and Pines (1958).

The correlation produced by the interaction between pairs of particles is such that the single (n, ℓ, j) levels of the simple shell model are no longer filled or empty in the usual sense. Instead the pairs of particles are distributed amongst these levels in a correlated fashion. Thus in a given state of the nucleus a particular (n, ℓ, j) shell model level has a probability $V^2_{n\ell j}$ of being occupied by a pair and $U^2_{n\ell j}$ of being empty. In the same state, a different (n, ℓ, j) level will be characterized by a different set at U^2 and V^2. Each state thus consists of a particular arrangement of pairs amongst the shell model levels and its wave function may be written as

$$\Psi^{BCS} = \pi(U_{n\ell j} + V_{n\ell j}\ a^{+}_{n\ell j}\ a^{+}_{\overline{n\ell j}})\ |\ 0\rangle$$

where $a^{+}_{n\ell j}\ a^{+}_{\overline{n\ell j}}$ represents the creation of a pair in the nℓj shell model level and $|0\rangle$ represents the state with no particles present. A different arrangement of pairs i.e. a different set of $U_{n\ell j}$'s and $V_{n\ell j}$'s will have a different wave function and therefore constitute a different nucleon state. These different configurations plus the

states formed by breaking a pair and exciting a single particle with the required re-arrangement of the other pairs form the excited states of even-even nuclei.

The description of these excited states is generally done in terms of quasi-particles. These arise from the formalism in which a simple transformation changes the problem from one of interacting pairs of particles to independent entities which have properties of both particles and holes; hence the term quasi-particle. Under this transformation the single particle energies associated with (n, ℓ, j) shell model orbits ($\varepsilon_{n\ell j}$) are replaced by single quasi-particle energies

$$E_{n\ell j} = \left[(\varepsilon_{n\ell j} - \lambda)^2 + \Delta^2 \right]^{1/2}$$

where λ and Δ are parameters of the problem. Also the ground state of an even-even nucleus becomes the quasi-particle vacuum.

From the equation it can be seen that the minimum energy a quasi-particle can have is Δ. Thus, rearrangement of the pairs in even-even nuclei, which correspond to the excitation of two quasi-particles, must differ by at least 2Δ. The occurence of intrinsic excited states i.e. states involving the excitation of individual particles as opposed to collective states involving excitation of all the particles, is then limited to the region above 2Δ above the ground state. The existence of this energy gap has been experimentally verified.

The excitation of a single quasi-particle amounts to the creation of an extra particle and thus constitutes the ground state

and low lying excited states of the neighbouring odd mass nuclei.

Other types of collective motion may exist, particularly types which involve all the nucleons as a whole. If for example one of the quasi-particles was to undergo a slight perturbation from its orbit it could interact with other quasi-particles to produce a coherent oscillation. Depending on the frequency of this oscillation these states may occur below the 2Δ gap imposed on intrinsic excitations.

A phenomonological description of such vibrations has been established in an harmonic approximation which predicts excited states containing "phonons" of vibration of frequencies ω_λ and hence at energies $E_{n\lambda} = n_\lambda \omega_\lambda$ $n = 1, 2, 3.....$ These phonons carry an associated angular momentum λ and parity $(-1)^\lambda$. Thus coupling these phonons with the ground state of even-even nucleus will produce the low lying excited states listed in Table 1.5.1

λ	n_λ	$J\pi$ excited states	Energy of excited state
2	1	0+	$\hbar\omega_2$
	2	0+, 2+, 4+	$2\hbar\omega_2$, $2\hbar\omega_2$, $2\hbar\omega_2$
3	1	3-	$\hbar\omega_3 \simeq 2\hbar\omega_2$

TABLE 1.5.1

Characteristics of Some Low Lying Vibrational States

The degeneracy of the 2 phonon state is generally lifted to create an

expected triplet. However, only a few of these triplets have so far been observed experimentally.

In odd A nuclei, as previously mentioned, it is frequently assumed that the (A-1) particles couple to form an inert core equivalent to the neighbouring even-even nucleus. Thus, in odd A nuclei, if the single particle excitation energies of the odd particle are fairly large so that the excited levels are well spaced, states may exist which consist of vibrational excitations of the even-even core coupled to the single particle level. The number of these states depends on the vector coupling of the odd particle angular momentum and that of the phonon. If the constraint on the single particle excitation energy is not met, then different single particle states and their vibrational relations may all be considerably admixed by residual interactions to produce states of no definite character.

1.6 Rotational Description

Another type of collective motion has been extensively considered in the literature but will be only briefly mentioned here as it is currently felt that it is not particularly applicable in the mass region of interest in this thesis. In this description the nucleus is assumed to have a large stable deformation. This accounts for the large ground state quadrupole moments observed in many heavier nuclei. The lowest lying excitations of these nuclei, turn out to be quantised rotations of the deformed equilibrium shape giving rise to excited states with spins and parities 2+, 4+, 6+ etc. for the even-even case. At higher excitations the vibrations described above

become energetically possible and can be divided into types which retain any axial symmetry of the original shape and those which destroy it.

In the odd A nuclei, the situation is as above with a coupling of rotations and vibrations to the various single particle excitations. Here however, the single particle state is generally taken to be that of a particle in a non-spherical deformed potential. The energies of these deformed states differs considerably from the spherical case, the deviation depending on m_j and the amount of deformation, and many level crossings occur. Thus the order of level filling depends on the equilibrium deformation and has in many cases been used to determine the ground state deformation.

These considerations have formed the basis for much of the interpretation of experimental observations of nuclear structure. Although many other calculations, models, and approximations exist, the most widely used seem to be the shell model, the vibrational model and the rotational (Nilsson) model.

CHAPTER 2

RADIOACTIVE DECAY

INTRODUCTION

Any unstable configuration of nuclear states will attempt to become more stable by the process of radioactive decay. Several processes exist for this transformation and all compete in each decay to a greater or lesser degree. However, in most cases the probability of one particular mode is so great as to essentially eliminate all other possibilities. Of these various types of decay only those which relate to the problem under investigation in this thesis will be described.

2.1 Fission

Fission is the process by which an unstable configuration achieves greater stability by separating into two sections. The gain in stability is indicated in Figure 2.1.1 which shows the potential energy of the two fragments as a function of their separation. The probability of fission depends on the position of the level I, which represents the initial state, relative to the peak in the potential function. For levels well below this peak the quantum mechanical tunneling effect will produce fission but with a very low probability. As the level approaches the peak however, the probability increases rapidly exhibiting a threshold behaviour. This is indicated by Figure 2.1.2 where the initial state is an excited state formed by the cap-

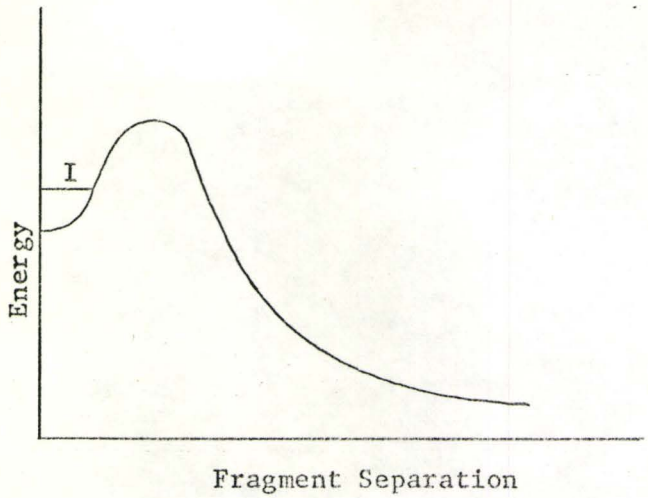

Figure 2.1.1 Potential Energy of Fission Nucleus as a Function of the Fragment Separation (Segrè (1965)).

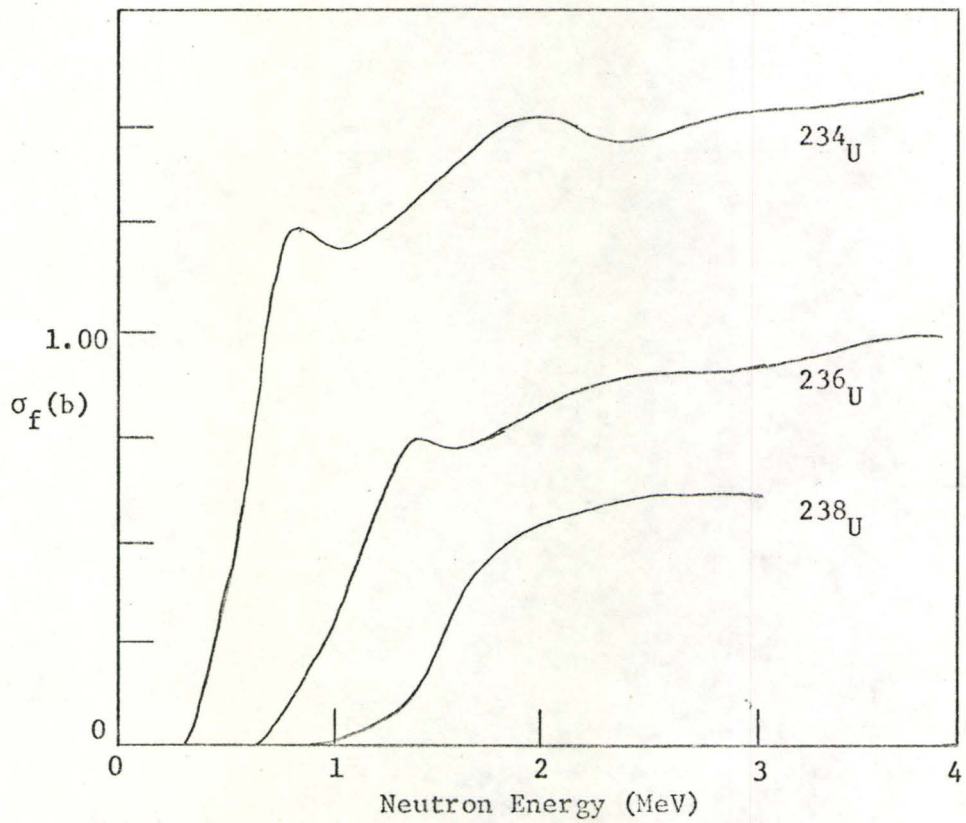

Figure 2.1.2 Neutron Fission Cross Sections (Segrè (1965)).

ture of a neutron by the indicated even A nucleus. The position of this state thus can be increased from its initial position at the binding energy of the neutron by increasing the incident neutron energy. For the neighbouring odd A nuclei, an extra amount of excitation energy is acquired from the pairing of the captured neutron with the one already present. This lowers the threshold energy by a similar amount so that while neutrons of 0.4 MeV are required to cause fission in ^{234}U, the threshold in ^{233}U and ^{235}U is <0, and even thermal neutrons (energy ~0.025 ev) will induce fission.

The masses of the fragments produced in fission are neither equal nor constant. The distribution as a function of mass is shown in Figure 2.1.3 for thermal neutron fission of ^{233}U, the isotope used in this investigation. The use of the lighter uranium isotope tends to shift the centroid of the lighter mass hump to a lower value. Beside being distributed in mass, the fission fragments are also distributed in charge for any given mass. Here the distribution is well described by a gaussian function whose width seems to be constant for all masses (Wolfsburg (1965));(Norris and Wahl (1966)). Figure 2.1.4 shows a composite curve for both the mass 90 and 91 chains centred about the most probable nuclear charge Z_p. This charge is, generally, two or three units away from the beta stability line and consequently most fission fragments themselves are unstable against beta-decay.

2.2 Beta Decay

Beta decay in the form involved in the investigation discussed in this thesis consists of a transformation of one nucleus to another

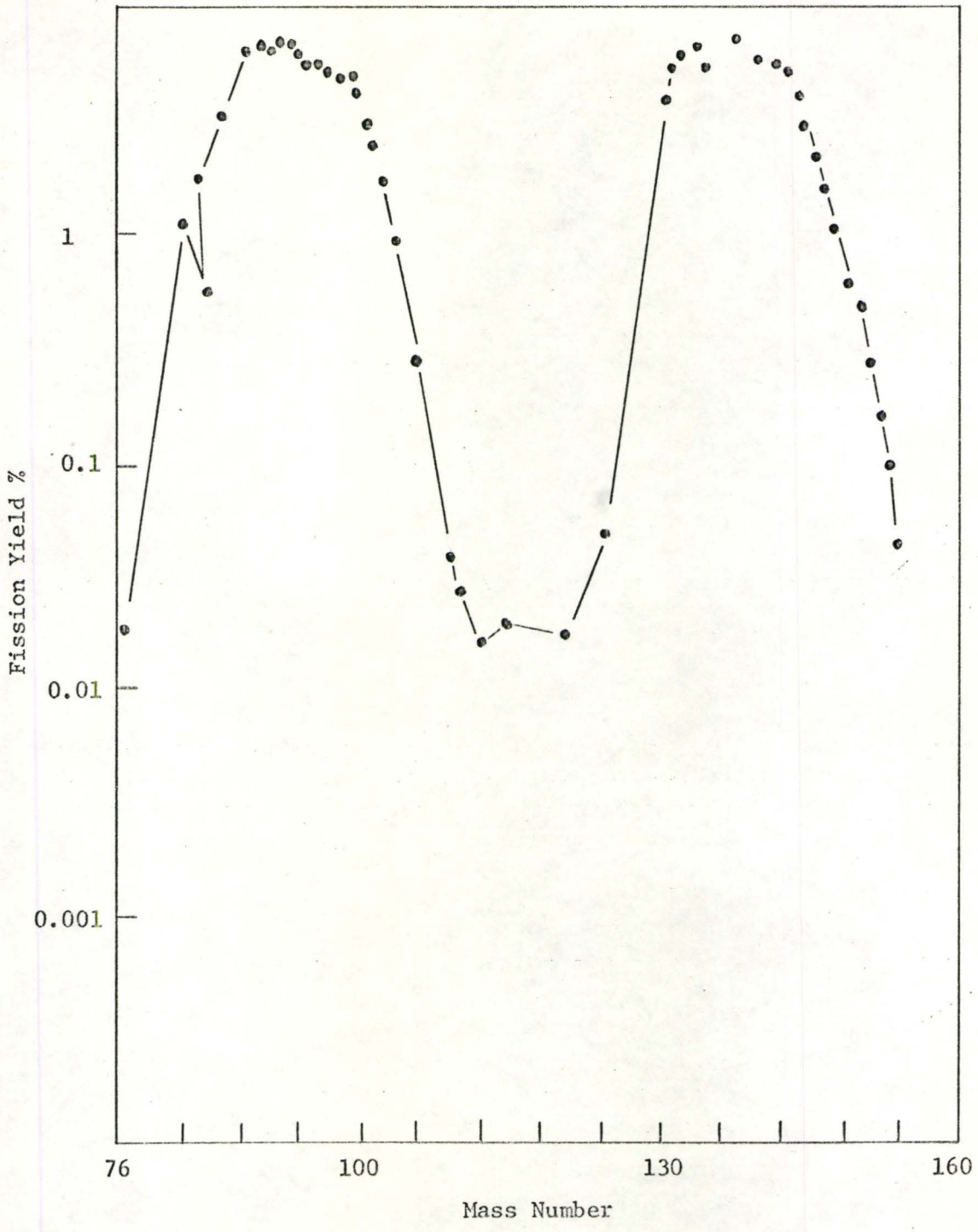

Figure 2.1.3 Frequency Distribution of Mass Number of Fission Fragment from Thermal Neutron Fission of ^{233}U (Segrè (1965)).

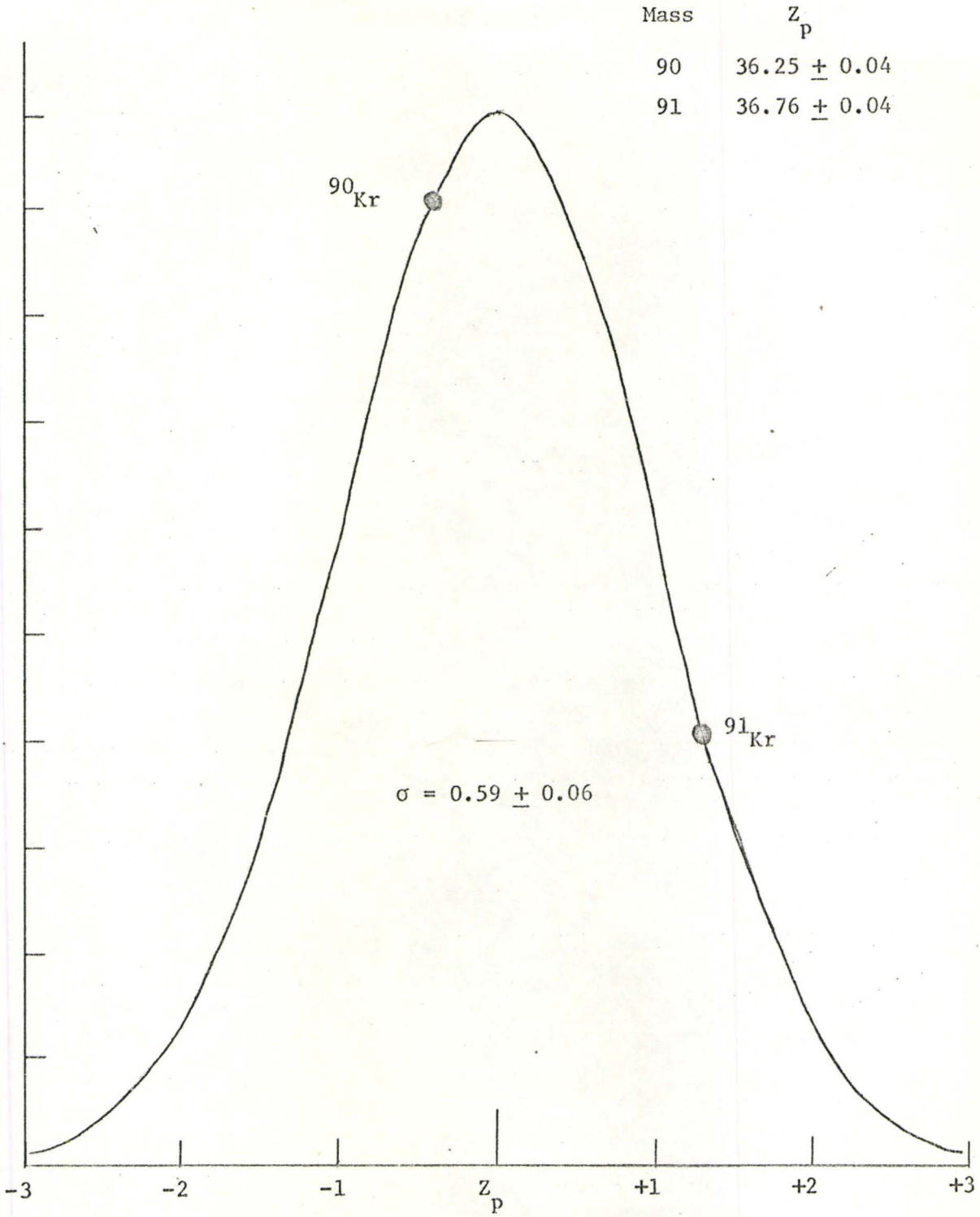

Figure 2.1.4 Charge Distribution of Constant Mass Fission Fragments in Units of σ.

through the changing of a neutron to a proton accompanied by the emission of an electron and an anti-neutrino. Although other modes of beta decay exist, including positron emission, orbital electron capture and muon decays, the references in the following discussion are mainly to the mode of negatron or electron emission.

All types of β-decay are thought to proceed due to a universal weak interaction. The classification of this interaction as weak stems from its strength relative to the other currently known types of interaction. These are the strong interaction, responsible for specifically nuclear forces, the electromagnetic interaction between electric charges, the weak interaction, and the gravitational interaction. The relative strengths of these are respectively 10: $1/137 : 10^{-23} : 10^{-45}$ (Preston (1962)).

The three body character of beta decay was originally hypothesized (Pauli (1931)) to account for the continuous distribution of the emitted electron's energy, and to satisfy spin and statistics requirements. The third particle, called the neutrino, was thus assumed to have zero charge, intrinsic spin 1/2 and probably zero mass. Its existence was indirectly verified through the inverse neutrino-induced reaction by Reines and Cowan (1959).

The transition probability for beta decay from an initial state $|\psi_{in}>$ to a final state $|\psi_{fin}>$ can be written as

$$T = \frac{2\pi}{h} \left| <\psi^*_{fin} \left| H_\beta \right| \psi_{in} > \right|^2 \rho \qquad 2.2.1$$

where ρ is the density of final states and H_β is the weak interaction Hamiltonian. If the emission, or creation, of the anti-neutrino

involved in electron emission is considered, instead, as the absorption or destruction of a neutrino, both the initial and final states can be written as products of a nucleonic part, $|\Psi>$, and a leptonic part, $|\phi>$. Thus $|\psi_{in}> = |\Psi_{in}\phi_{in}>$, and the transition probability is symmetric.

The weak interaction, H_β, has been found to violate the principle of conservation of parity (Wu et al (1957)) by the observation of the angular distribution of electrons emitted from aligned ^{60}Co nuclei. This possibility was suggested by Lee and Yang (1956) and admits the possibility of experimentally observing both scaler and pseudoscaler quantities. Of the five possible interactions of these types i.e. scaler (S), pseudoscaler (P), vector (V), axial-vector (A) and tensor (T), experiment has shown only the V and A terms to be non-zero. Each of these terms contain two parts, the second of which is of the order of v_n/c of the first, where v_n is the velocity of the transforming nucleon. The V interactions contain a term proportional to the isotopic spin ladder operation which changes the neutron to a proton and a second smaller term involving both the isotopic spin operator and the velocity operator for the nucleon. The larger portion of the A interaction arises from a term involving the same iso-spin operator and the regular spin operator while the smaller contributions are generated by an iso-spin, helicity combination. (Helicity is defined as $\frac{\vec{p}\cdot\vec{\sigma}}{|\vec{P}||\vec{\sigma}|}$)

The evaluation of 2.2.1 with these operators is done by approximation methods, each successive approximation being required when selection rules cause all preceeding terms to be zero. Thus the

approximation leading to allowed transitions involves retaining only the larger terms of the V and A interaction. The form of these operators imposes certain constraints on the spin and parity of the nuclear states involved as is indicated in Table 2.2.1.

Another approximation involved in the allowed transitions involves the leptonic wave functions. If these are taken as the wave functions of free particles (plane waves) the evaluation of 2.2.1 yields a term like $e^{-i(p+q)\cdot r}$ where p and q are the momenta of respectively the electron or neutrino and r is the nuclear co-ordinate at which the transition occurs. In evaluating allowed transition probabilities this exponential is replaced by the leading term in its series expansion. The resulting electron energy distribution for allowed decay is then given by (Segrè (1965))

$$\omega(\varepsilon)d\varepsilon = \frac{g^2 m^5 c^4}{2\pi^3 \hbar^7} |M_{if}|^2 F(Z,\varepsilon) (\varepsilon_o - \varepsilon)^2 \varepsilon\eta \, d\varepsilon \qquad 2.2.2$$

The nuclear transition matrix elements are lumped in M_{if} and $F(Z,\varepsilon)$ has been introduced to account for the distortion of the electronic wave function by the interaction between the electron and the nucleus. The electron energy (ε) is measured in units of $m_e c^2$ and the electron momentum (η) in units of $m_e c$. Both are arranged to include the effect of the rest mass of the particle.

If the initial and final nuclear states do not satisfy the spin and parity requirements of the allowed approximation, the transition cannot occur by these interactions. It is then necessary to include the remaining two terms of the V and A interactions and successively higher terms in the exponential series expansion until spin

and parity requirements are obtained which can be satisfied and hence yield a non-zero transition probability. For each term of the series after the leading term which must be included an additional degree of forbiddenness is encountered. The spin and parity changes imposed by several forbidden transitions are also indicated in Table 2.2.1.

The total probability for beta decay may be obtained by integrating 2.2.2 from 0 to the maximum beta energy assuming $|M_{if}|^2$ is constant.

$$\lambda = \frac{g^2|M_{if}|^2}{2\pi^3\hbar^7} \int_1^{\varepsilon_o} F(Z,\varepsilon_o)\,(\varepsilon_o - \varepsilon)^2\,\varepsilon\,\eta\,d\,\varepsilon \qquad 2.2.3$$

$$= \frac{g^2\,|M_{if}|^2}{2\pi^3\hbar^7}\; f\,(Z,\varepsilon_o) \qquad 2.2.4$$

The integral involved is a calculable quantity depending only on the end point of the beta transition and the charge of the nucleus. Since λ is inversely proportional to the half life 2.2.4 can be re-written as

$$f(Z,\varepsilon_o)\; T_{1/2} = \frac{A}{|M_{if}|^2} \qquad A \text{ constant} \qquad 2.2.5$$

Thus the "ft" of a beta transition is inversely proportional to the square of the nuclear matrix element and should be an indicator of the type of transition. Since each degree of forbiddenness introduces a factor of about 100 in $|M_{if}|^2$ it is more usual to compare log(ft) values. Log (ft) values for various transition are also listed in Table 2.2.1.

TABLE 2.2.1

COMPARISON OF SOME PROPERTIES OF SOME BETA TRANSITIONS

Transition	ΔJ	$\pi_i \pi_f$	Log(ft)	Interaction and Restriction
allowed	0	+	4-6	V
	$\pm 1,0$	+	4-6	A no $0 \to 0$
first forbidden	$\pm 1,0$	-	~ 7	V no $0 \to 0$
	$\pm 1,0$	-	~ 7	A no $0 \to 0$
				no $1/2 \to 1/2$
				no $0 \to 1$
first forbidden unique	± 2	-	7.4-9.0	A
second forbidden	$\pm 3,\pm 2$	+	12-14	V + A
third forbidden	$\pm 4,\pm 3$	-	~ 18	V + A
fourth forbidden	$\pm 5,\pm 4$	+	$23(^{115}I_n)$	V + A

2.3 Gamma Emission

Following the process of beta decay, the final nucleus may be left in an unstable configuration from which the largest probability of decay is emission of a gamma ray. This occurs by rearrangement of one or more nucleons and, because of the charges and magnetic moments of these nucleons, this rearrangement is manifest by a perturbation in the electromagnetic field surrounding the nucleus. The energy associated with this perturbation is just the difference in energy of the two nuclear configurations.

As with beta decay, the probability of gamma emission can be calculated from the formula

$$T = \frac{2\pi}{h} \left| < \psi^*_{fin} \left| H_\gamma \right| \psi_{in} > \right|^2 \rho \qquad 2.3.1$$

In this case, the interaction H_γ is that of the configuration of A particles with the electromagnetic field surrounding it, properly quantized to account for the emission or absorption of energy in units or photons. It is also usual to expand H_γ in terms of quantized angular momentum since the interaction, in general, causes a change in total angular momentum of the system in going from $|\psi_{in}>$ to $|\psi_{fin}>$ and this angular momentum is carried off by the photon. The creation of this photon can then be attributed to one particular term of the expansion. The transition probability can then be written

$$T(\sigma\lambda\mu) = \frac{2\pi}{h} |< \psi_{fin} \mid O^\sigma_{\lambda\mu} \mid \psi_{in}>|^2 \qquad 2.3.2$$

where $T(\sigma\lambda\mu)$ represents the transition associated with the emission of a photon carrying angular momentum λ with projection μ due to the

operator $O^{\sigma}_{\lambda\mu}$. $O^{\sigma}_{\lambda\mu}$ represents the quantized operator for either an oscillating electric (σ=E) or magnetic (σ=M) field of (2λ) multipole order. The form of these operators imposes the following restrictions on the spins and parities of the initial and final states:

$$J_i + J_f \geq \lambda \geq |J_i - J_f|$$

$$\pi_i\pi_f = (-1)^{\lambda} \quad \text{for electric multipole transitions}$$

$$= (-1)^{\lambda+1} \quad \text{for magnetic multipole transitions}$$

(π_i represents the parity, + or -, of the initial state, π_f the parity of the final state.)

Evaluation of transition probabilities depends explicitly on the form of the wave functions used for the initial and final configurations. Order of magnitude estimates, however, independent of the form of these wave functions indicates that the probability decreases rapidly with increasing multipole order, and for the same order that electric transitions are considerably more probable than magnetic ones when both are allowed by the selection rules. A notable exception to this arrangement frequently occurs for M1 and E2 transition. The collective nature of many states may enhance the E2 transition probability between them while on the other hand the M1 transition, allowed by the general selection rules between the same states, may be hindered by some other selection rule. In this instance, the M1 and E2 strengths may compete favourably and the radiation has a mixed multipole character. A particular set of single particle transition rates frequently used as reference values is listed in Table 2.3.1.

TABLE 2.3.1

GAMMA RAY TRANSITION PROBABILITIES

(Weisskopf Estimates; E_γ in MeV)

Transition Character	Transition Probability (sec^{-1})
E1	$1.03 \times 10^{14} \; A^{2/3} \; E^3$
M1	$3.09 \times 10^{13} \; E^3$
E2	$7.39 \times 10^{7} \; A^{4/3} \; E^5$
M2	$2.22 \times 10^{7} \; A^{2/3} \; E^5$
E3	$3.50 \times 10 \; A^{2} \; E^7$
M3	$1.05 \times 10 \; A^{4/3} \; E^7$

2.4 Internal Conversion

Besides emitting a gamma ray, an excited state may de-excite by the process of internal conversion. In this decay mode, the energy of the transition is transferred directly to an atomic electron, which is then ejected from the atom with an energy equal to that of the transition less the binding energy of the electron shell from which the electron originated. The competition between internal conversion and gamma ray emission is measured by the conversion coefficient

$$\alpha = \frac{N_e}{N_\gamma} \qquad 2.4.1$$

where N_e is the number of electrons and N_γ is the number of photons emitted in the transformation per unit time. This coefficient is further subdivided depending on the atomic shell from which the electrons originated. (α_k, α_{LI}, α_{LII}, α_{LIII} etc.)

These coefficients are strongly increasing functions of multipole order and atomic number and strongly decreasing functions of transition energy. In addition, if the associated gamma ray has mixed multipole character, the conversion coefficient will exhibit the same amount of mixing. Since these coefficients depend only on the atomic electron wave functions and the electromagnetic multipole interaction their values may be theoretically predicted (e.g. Hager and Seltzer (1968)) and a comparison of these predictions with experimental observations can be used to determine the multipolarity of the transition.

CHAPTER 3

SOURCE PREPARATION, DATA COLLECTION, AND DATA REDUCTION

3.1 Source Preparation

Sources were prepared using an irradiation facility developed by Okendon and Tomlinson (1962). This is shown in figure 3.1.1. A quantity of ^{233}U was deposited as a thin layer on hydrous zirconium oxide plates, thus producing a large surface area with good emanating power for the gaseous fission products and long lifetime under constant irradiation by thermal neutrons (Archer (1965)). The irradiation chamber was surrounded by a cadmium sheath with a hinged, gravity-operated shutter on the front end. Normally closed, this shutter could be opened by remotely retracting the sheath thus lifting the shutter over the front end of the chamber. Moving the sheath forward again allowed the shutter to fall back to its normally closed position. This arrangement permitted irradiation of the Uranium for variable lengths of time.

Following irradiation, the inert noble gas fission products Krypton and Xenon were rapidly emanated from the source material while the highly reactive halogen products, Bromine and Iodine, remained attached to surrounding material. The Krypton and Xenon fractions could then be preferentially removed from the chamber by flushing it with Helium gas. The Xenon fraction was removed by passing the Helium carrier plus Xenon and Krypton traces through a

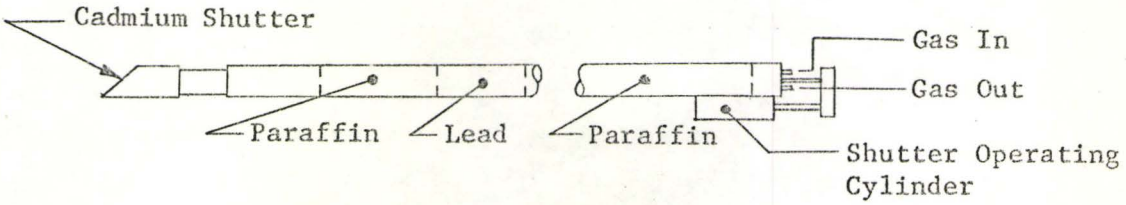

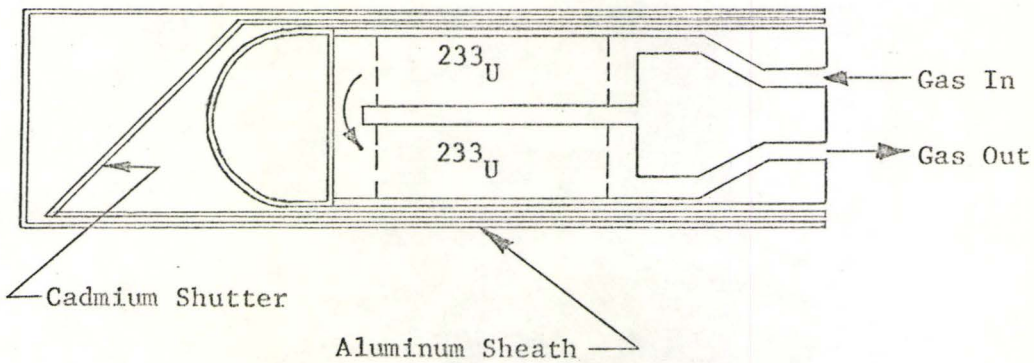

Figure 3.1.1 Irradiation Facility

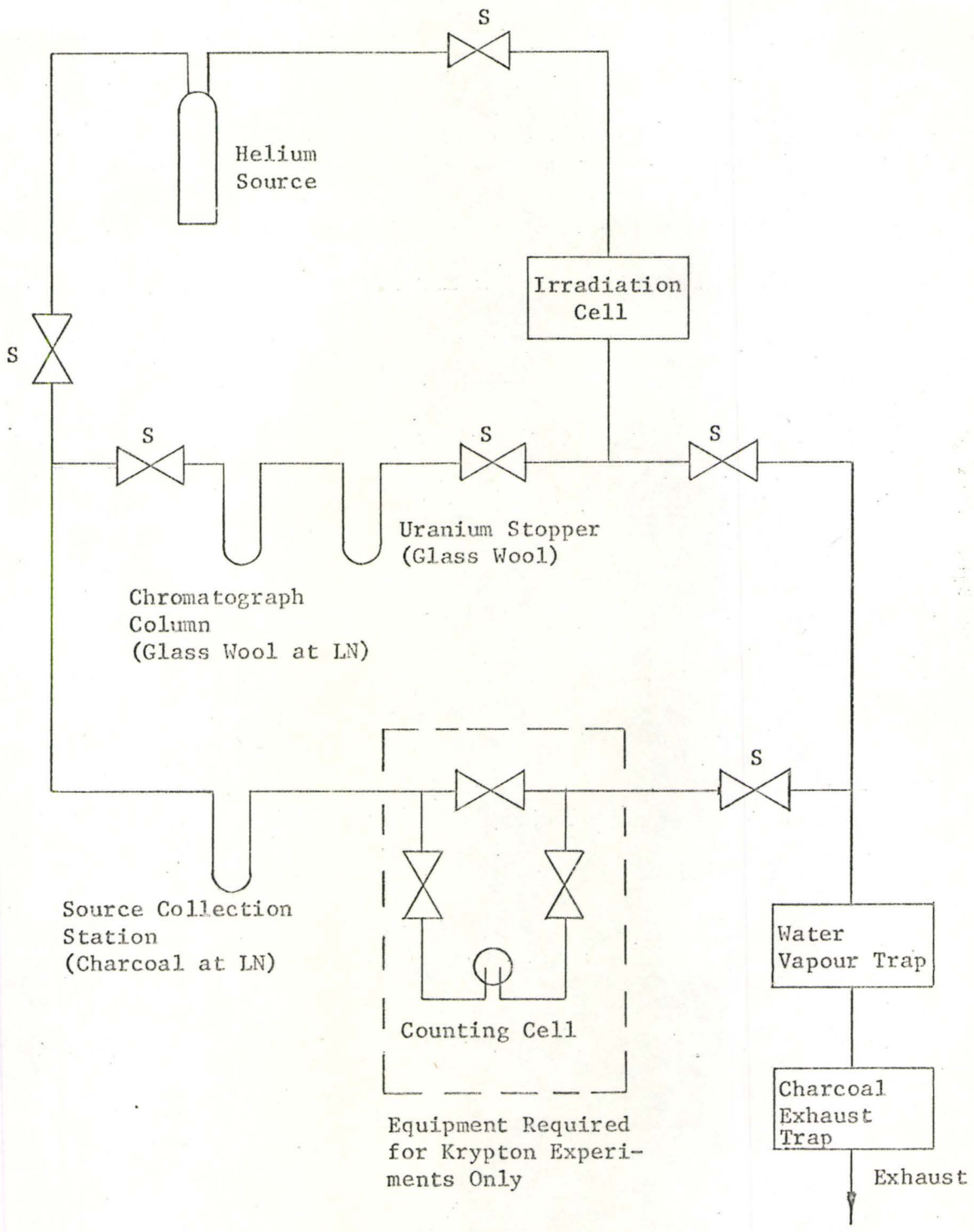

Figure 3.1.2 Gas Transport System

chromatograph column of glass wool at liquid nitrogen temperatures (Archer (1965)). Here the gases were absorbed and then re-emitted at a rate depending exponentially on their molecular weight. Thus the Helium and Krypton were re-emitted essentially instantaneously while the Xenon was effectively permanently trapped. The Krypton which passed the chromatograph column was subsequently collected on a small amount of activated charcoal also at liquid nitrogen temperatures. This accumulated the Krypton activity, produced in the relatively capacious fission chamber, into a small volume more amenable to experimental purposes.

The gas system used to transport the radioactive samples is shown schematically in Figure 3.1.2. The valves marked by S were solenoid operated and were controlled by relays remotely activated by hand operated switches. The unmarked valves were smaller hand operated types.

3.1.1 Krypton Sources

In order to investigate the radiations resulting from the decay of the Krypton isotopes, the Krypton collected on the charcoal was immediately released by heating the charcoal, contained in a glass U-tube, in boiling water. The radioactive gas was then transported to a counting cell, again using Helium carrier gas. The level of activity in the counting cell was monitored on a scaler, and as the counting rate reached a maximum the valves were closed to trap the sample in place.

The Krypton gamma counting cell shown in Figure 3.1.3 was developed in an attempt to remove contamination due to the daughter

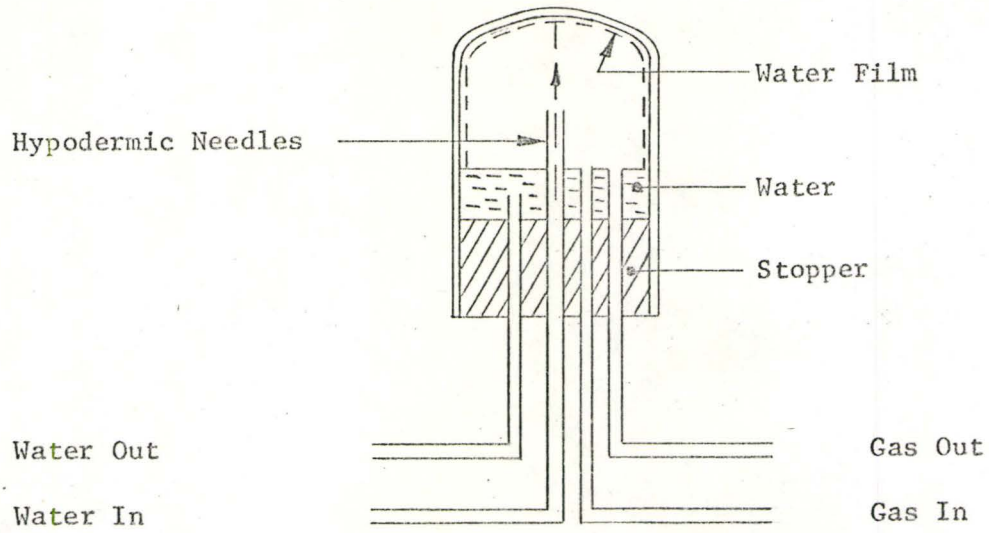

Figure 3.1.3 Krypton Gamma Counting Cell

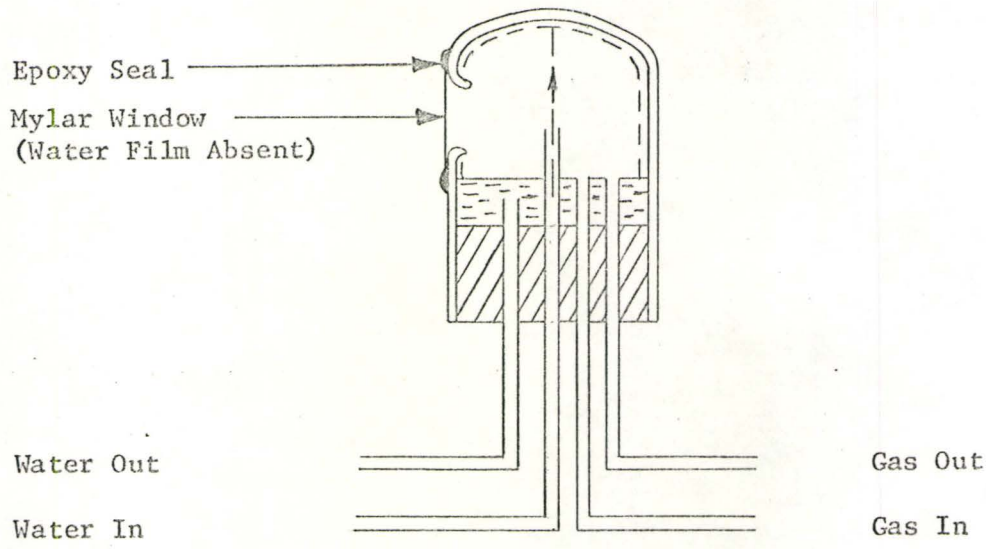

Figure 3.1.4 Krypton Beta Counting Cell

Rubidium activities and proved to be about 95% effective. It consisted of a small section of a glass test tube approximately 1 cm dia. x 2.5 cm long with 1 mm thick walls, inverted and stoppered at the open end. Two 18 gauge x 3" long stainless steel hypodermic needles inserted through the stopper provided an inlet and outlet for the gas system. Two other hypodermic needles similarly inserted were inlet and outlet respectively for a pressurized water system. The water, entering through the central needle under sufficient pressure, shot up to the glass top and then washed all the interior of the cell. Thus, much of the Rubidium produced, which would otherwise adhere to the walls, was removed in solution. The flow rate of the water was $\sim$ 1800 cc/hr so that the small volume ($\sim$ 1 cc) of water which collected on the bottom of the cell was removed in a few seconds thus contributing little background contamination.

The counting cell used in experiments involving Krypton beta particles is shown in Figure 3.1.4. Similar in design and operation to the gamma cell, it had a hole of approximately 7 mm dia. covered with a layer of 2.7 mgm/cm^2 mylar through which the betas were detected. Since the beta feeds all had end point energies greater than 2.5 MeV this window caused negligible degradation of the energies. The window was held in place by epoxy resin and was both gas and water tight. The mylar, however, was not washed by the water and consequently Rubidium activity tended to collect upon it. As a result frequent waiting periods were required in these experiments to allow the Rubidium activity to decay.

In the production of a source there were five time intervals

which could be varied independently to maximize the desired activity with respect to that of the other isotopes which were always present. These times were:

i) irradiation time: the time which the cadmium shutter was kept open. This had a practical minimum of about 5 sec.

ii) hold-up time: the time after irradiation during which the sample remained in the irradiation cell before being flushed to the collection station.

iii) transfer time: the time required to deliver the source from the irradiation cell to the collection station. This had a practical minimum of about 10 sec.

iv) delay time: the time after complete collection until the source was positioned near the detector ready for counting. This includes the time required to transfer the collecting charcoal to boiling water, heat it and transfer the gas to the counting cell.

v) counting time: the length of time for which events were recorded.

Thus the number of events from the decay of the i^{th} isotope recorded for a single source would be proportional to

$$N_i^{Kr} \sim [1-\exp(-\lambda_i t_{irr})]\cdot[\exp(-\lambda_i t_{hold\text{-}up})]\cdot[\exp(-\lambda_i t_{trans})]$$
$$\cdot[\exp(-\lambda_i t_{delay})]\cdot[1-\exp(-\lambda_i t_{count})]$$

Solution of this equation for i=89, 90, 91 to obtain the proper times for the best 91: 90: 89 ratios was done experimentally and yielded the

Table 3.1.1 Source Prescriptions (All Times in Secs)

Source	Irradiation Time	Hold up Time	Transfer Time	Decay Time	Delay Time	Counting Time
Kr Standard	10	0	10	0	10	30
Kr Delayed	10	0	10	0	40	30
$^{90}_{Rb}$	30	20	10	30	15	180
$^{91}_{Rb}$	10	10	10	10	15	70

times shown in Table 3.1.1. When possible, minimum times were used to reduce the amount of ^{89}Kr present, since this possesses a complex, high energy gamma spectrum.

3.1.2 Rubidium Sources

In order to investigate the radiations from the Rubidium isotopes, the Krypton, which was collected in the charcoal, was allowed to remain there and decay to the Rubidium isotopes which then became strongly adsorbed. This introduces another time interval, t_{decay}, into the source preparation. After this interval the remaining excess Krypton was removed by heating the charcoal and cleansing it with Helium. In this case the counting cell was the U-tube containing the charcoal.

The number of events due to the i^{th} Rubidium isotope from a single source is then proportional to

$$N_i^{Rb} \sim [1-\exp(-\lambda_i^{Kr} t_{irr})]\cdot[\exp(-\lambda_i^{Kr} t_{hold\text{-}up})]\cdot[\exp(-\lambda_i^{Kr} t_{trans})]$$

$$\cdot\frac{\lambda_i^{Kr}}{\lambda_i^{Rb}-\lambda_i^{Kr}}\cdot[\exp(-\lambda_i^{Kr} t_{decay})-\exp(-\lambda_i^{Rb} t_{decay})]$$

$$\cdot[\exp(-\lambda_i^{Rb} t_{delay})]\cdot[1-\exp(-\lambda_i^{Rb} t_{count})]$$

Again experimentation was adopted to determine the most appropriate times for each isotope as listed in Table 3.1.1.

3.2 Single Parameter Experiments

Single parameter experiments were performed to determine the energy, intensity and nuclide of origin of each of the gamma rays observed. A Ge(Li) detector of approximately 12 cc active volume was

used with the associated electronics shown schematically in Figure 3.2.1. This system had an optimum resolution of 3.2 keV on the 1.333 MeV gamma ray of ^{60}Co with a peak/compton ratio of about 16:1. In practice, this performance was not quite realized because of gain shifts associated with the rapidly decaying activity.

The analysis of the spectra obtained in these experiments was performed using a computer program ("Jagspot") developed at Chalk River (AECL) and modified by the Beta Ray Spectroscopy group at McMaster. This program performed a non-linear, least-squares fit of the data in the region of a peak, or group of peaks (≤ 6), to an analytical function of the form

$$I(x) = \alpha + \beta x + \sum_{i=1}^{\leq 6} I_i \int_{-\infty}^{z_i} e^{\varepsilon(y-z_i)}\, e^{-\delta(x-y)^2}\, dy \qquad 3.2.4$$

where α, β, δ, ε, I_i, z_i were the parameters for which the calculations were performed. The function is essentially a linear background ($\alpha+\beta x$) plus an intensity weighted sum of gaussians ($(\text{variance})^2 = 1/2\delta$) convoluted from $-\infty$ to an upper limit z_i with an exponential decaying from z_i towards $-\infty$ at a rate depending on ε. This form was chosen to account for the assymetric low energy tail sometimes observed on full energy peaks from large volume Ge(Li) detectors.

This highly non-linear problem was linearized by starting with a first order approximation to each of the various parameters and then doing a least squares calculation to obtain the best corrections to add to these to obtain second order approximations. This process was repeated until the correction obtained for each parameter was less than the error associated with the same parameter. Provision was also

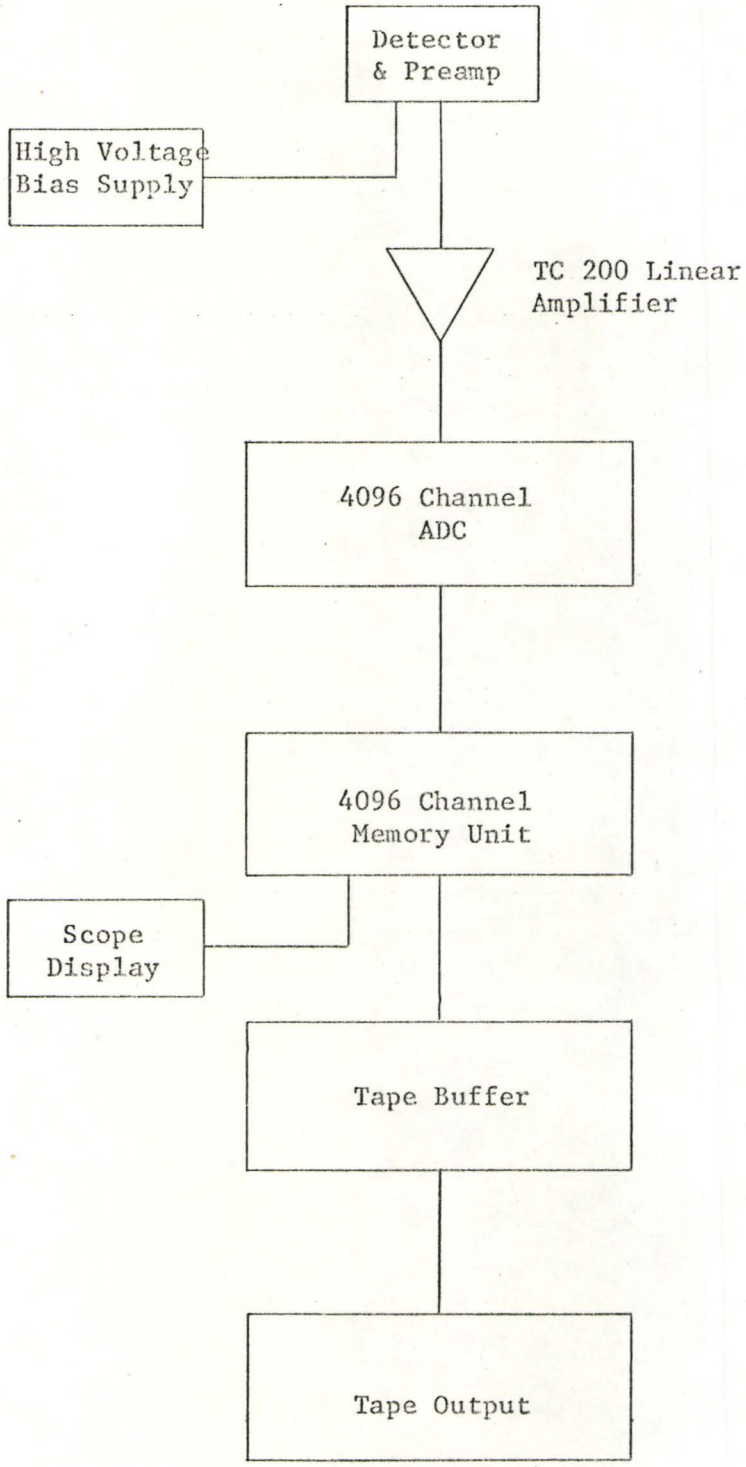

Figure 3.2.1 Schematic Diagram of Electronic Configuration Associated with Single Parameter Experiments.

included to allow the values of δ and/or ε to be fixed during the calculations, at a value predetermined from either a curve calculated using prominent peaks in the spectrum or from input data. This procedure proved particularly useful in fitting weak peaks.

The energies of the unknown gamma rays from the nuclides under investigation were determined by collecting spectra including gamma rays whose energies are well known, along with the unknowns. The positions of all the prominent peaks were then determined using the computer program and a calibration curve of energy versus peak position calculated using the standard gamma rays in the spectrum. This curve could be up to fourth order in peak position although a cubic was generally found to be sufficient to reproduce the non-linearity of the analogue-to-digital converter (ADC). The energies of the prominent unknown peaks were then calculated using the curve, and these values used as standard energies for the analysis of spectra obtained without standard sources.

Above 2.754 MeV, where standard gamma ray energies with half lives in a range to make them useful for this purpose are rare, energy calibration was done by using the accurate 0.511 MeV and 1.022 MeV differences between escape peaks and full energy peaks. In order to identify the escape peaks associated with various full energy peaks, curves giving the ratio of single and double escape peak areas, respectively, to that of the full energy peak were obtained from the relatively simple, high energy spectra obtained from (n,γ) reactions of S (Kennett et al (1967)) and Si (Lycklama et al (1967)). These curves are shown in Figure 3.2.2.

The relative intensities of the various gamma rays were de-

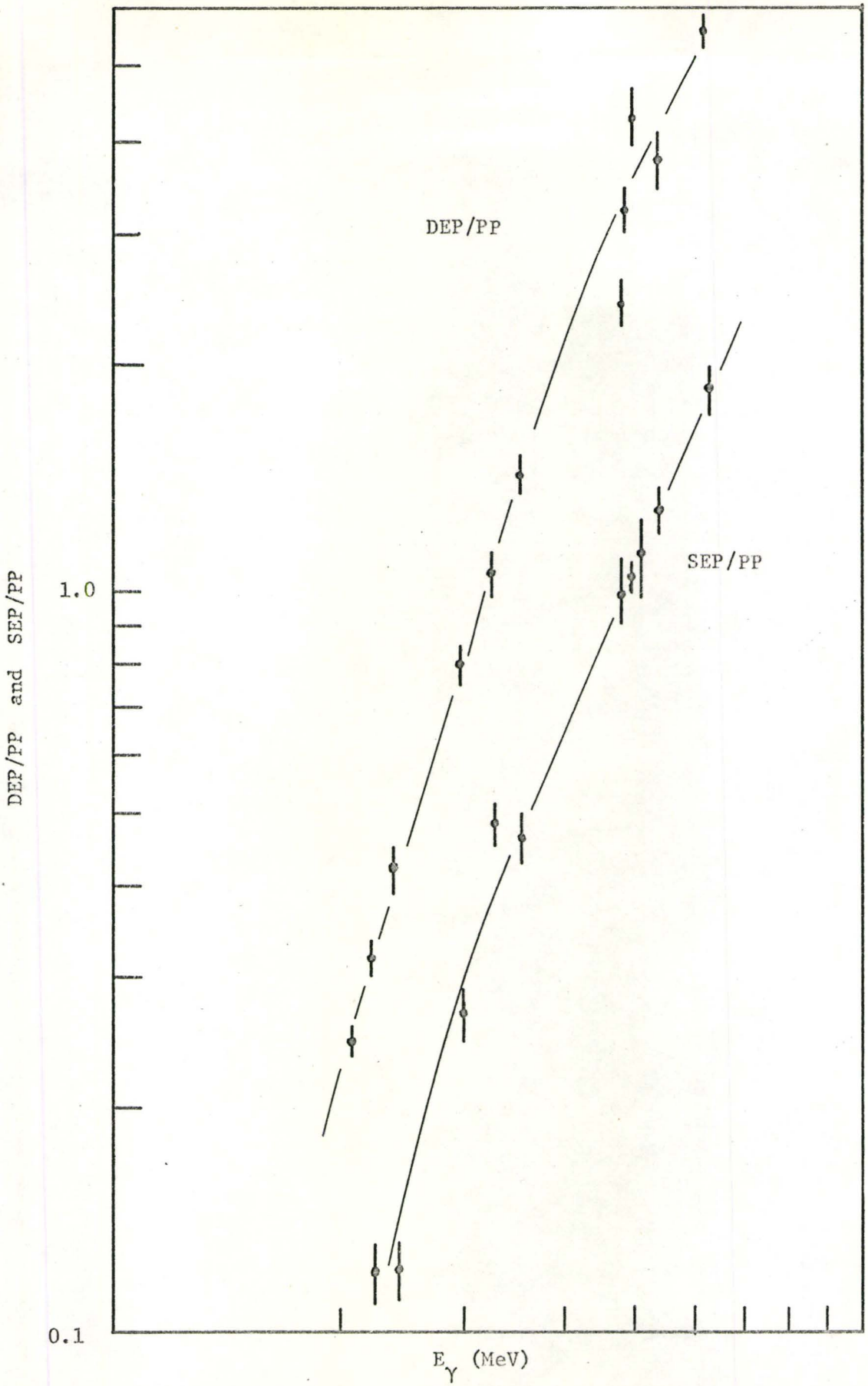

Figure 3.2.2 Ratio of Double Escape Peak (DEP) and Single Escape Peak (SEP) to Full Energy Peak (PP) as a Function of Energy

termined using the relationship between the relative intensity and the area of the full energy peak

$$N_i = (\varepsilon\omega)_i \, I_i \qquad 3.2.5$$

where N_i is the area of the full energy of the peak associated with the i^{th} gamma ray,

I_i is the relative intensity for the i^{th} gamma ray and $(\varepsilon\omega)_i$ is the relative efficiency of the detector at the energy of the i^{th} gamma ray.

The variation of $(\varepsilon\omega)$ with energy was determined by analyzing spectra from sources in which the intensities (I_i) were well known. The separate curves obtained from these sources (^{180m}Hf, ^{152}Eu, S(n,γ) and Si(n,γ)) were then overlapped to obtain the composite curve shown in Figure 3.2.3. This curve is characteristic of the 12 cc Ge(Li) detector with an absorber composed of 7.5 mm lead, 3 mm Cadmium and 0.5 mm Copper placed between the detector and the source. The purpose of this absorber was to attenuate strong, low energy transitions which might otherwise consume most of the data acquisition time at the expense of higher energy events. The relative efficiency for this detector without an absorber, as obtained using ^{152}Eu and ^{180m}Hf is shown in Figure 3.2.4.

The decay chain with which each gamma ray are associated was determined by comparing the areas of the corresponding full energy peaks in two different spectra, acquired in experiments designed to alter the composition of the sources. For the Krypton isotopes, this variation in composition was accomplished by making t_{delay} = 40 sec, as indicated in Table 3.1.1. This caused the relative activity of

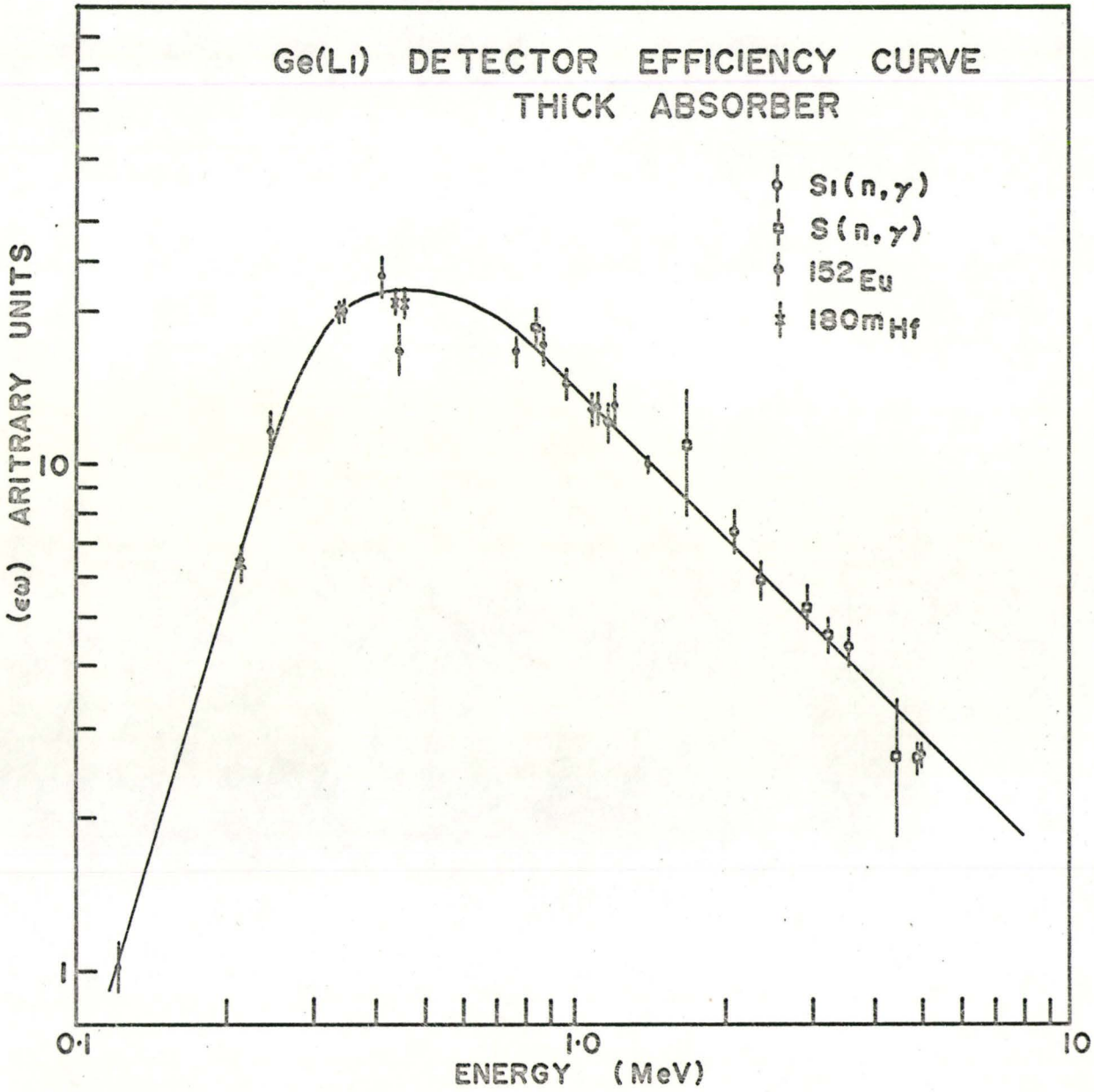

Figure 3.2.3 Ge(Li) Detector Efficiency Curve - Thick Absorber

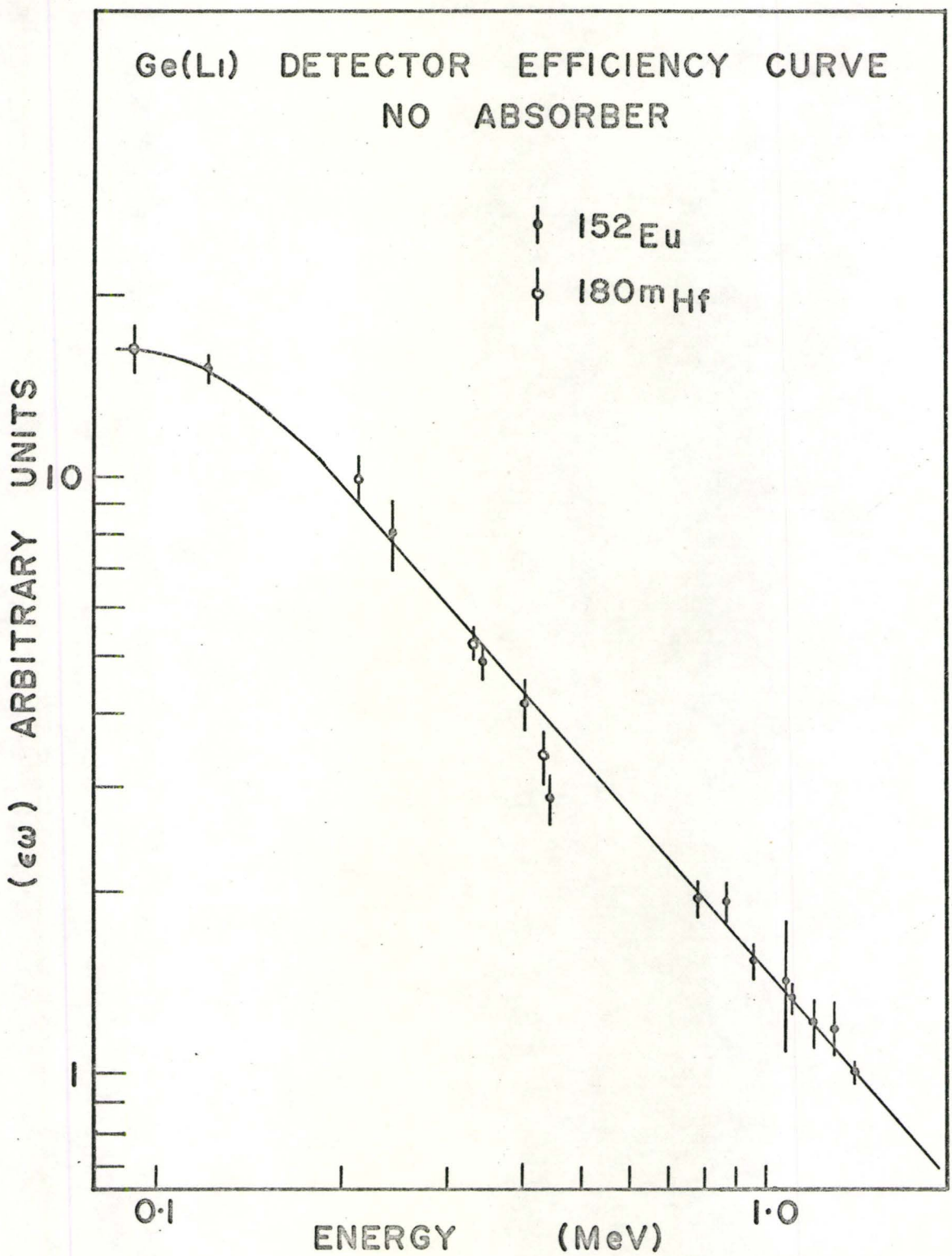

Figure 3.2.4 Ge(Li) Detector Efficiency Curve - No Absorber

the mass 91 isotope to be reduced considerably, while that of the mass 90 isotope was reduced only slightly and the mass 89 isotope was increased. For the Rubidium isotopes, the variation was accomplished by using the different source prescriptions indicated in Table 3.1.1.

3.3 Two Parameter Gamma-Gamma Experiments

In order to establish gamma cascade relationships to aid in determining the level structure of the nuclei, gamma-gamma coincidence experiments were performed using a 12 cc Ge(Li) detector and a 3" x 3" NaI(Tl) detector in the experimental arrangement shown in Figure 3.3.1. The bi-polar output pulses from the main amplifiers were fed to timing, single channel analyzers (TSCA)(Canberra 1436) which generated timing markers at the zero-crossing point of each pulse respectively. One of these timing markers was used to start a time-to-amplitude converter (TAC) while the other was used to stop it. The output of the TAC was then a pulse with an amplitude proportional to the time difference between start and stop pulses. For events which are associated with gamma cascades though non-isomeric levels this time difference will just be that due to the different time delays of the circuitry associated with each detector, and all TAC output pulse from these events will have the same height. In addition to these events, TAC output will also be generated by unrelated events which occur randomly in each detector but which generate consecutive start and stop signals during the operating period of the converter. These chance coincidences will be uniformly distributed in time and should therefore produce a uniform distribution of output pulse heights. The output pulse height spectrum from the TAC as collected in the 512 channel multichannel analyzer is shown in Figure 3.3.2. The large width of the

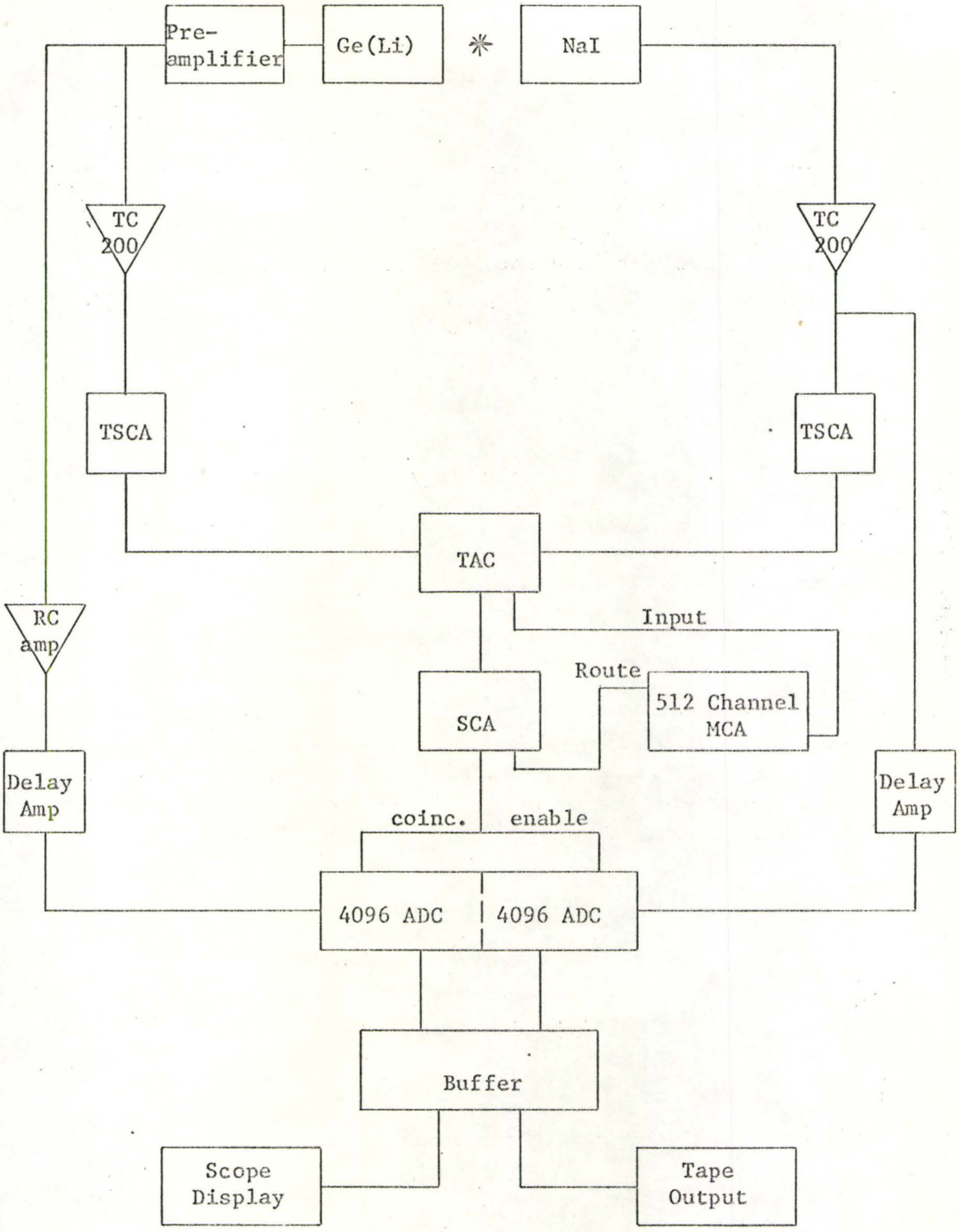

Figure 3.3.1 Electronic Configuration Associated With Two-Parameter Coincidence Experiment

"prompt" coincidence fraction, relative to that expected, can be traced to the poor timing characteristics of large volume Ge(Li) detectors.

The output pulses from the TAC were processed by a third TSCA (Canberra 1435) which generated an output pulse only if the height of the input pulse was within the region indicated in Figure 3.3.2. This "window" thus included most of the true coincidences plus a small chance contribution. The output from this TSCA was used to open a linear gate at the input to two ADC's, one for the linear output from each detection system. Thus the ADC's, only digitized information from the detectors which had occured in coincidence. For the NaI spectrometer, the bi-polar pulse used for timing was also used as the linear signal. However, for the Ge(Li) spectrometer, in order to obtain better resolution, a uni-polar linear signal was generated with a second, low noise amplifier. In each case, a delay amplifier with unity gain and switchable delay times was used to properly align, in time, the arrival of the two linear pulses and the coincidence enable pulse.

The address output from the two ADC's, when taken as a pair, form the co-ordinates of a coincidence in a two dimensional matrix, whose axes represent the energy detected by each detector. These address pairs were collected in blocks of 2048 and written on magnetic tape. An IBM 7040 computer later processed this address recorded data to accumulate the total number of events that occured at each co-ordinate of the matrix. The data were collected in a grid of 1024 channels along the Ge(Li) direction and 128 channels along the

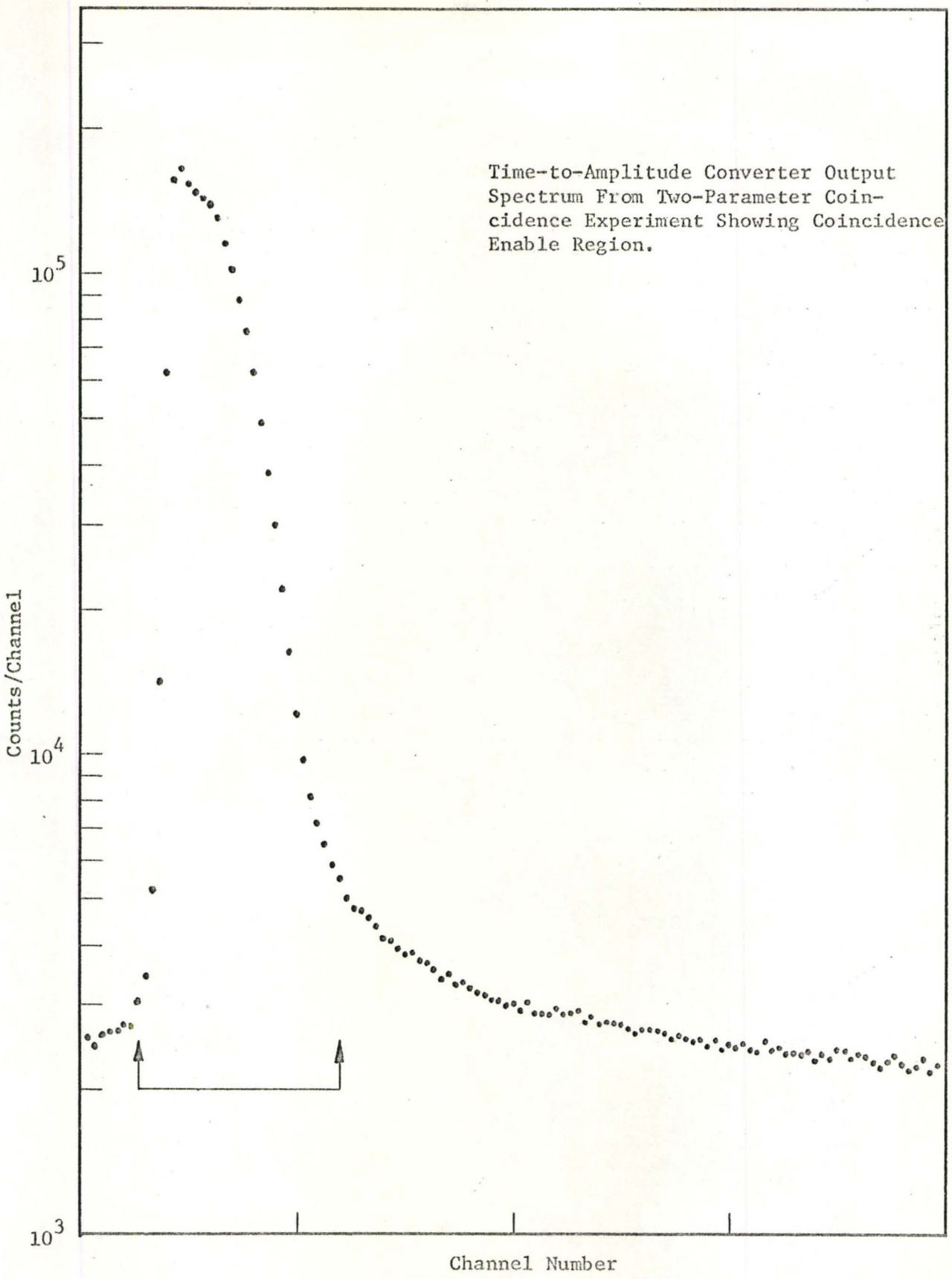
Time-to-Amplitude Converter Output Spectrum From Two-Parameter Coincidence Experiment Showing Coincidence Enable Region.
10^5
10^4
10^3
Counts/Channel
Channel Number

Figure 3.3.2

NaI(Tl) direction.

In order to extract the coincidence information from this matrix this procedure was followed: The total summed projections of all coincidence events unto the Ge(Li) and NaI axes were obtained. "Gates" were then set along either dimension by instructing the computer to select certain channels along that dimension and sum the spectra in coincidence with these channels along the other dimension. For well defined peaks, the events due to underlying Compton distributions of higher energy gamma rays could be removed by subtracting an amount equivalent to this underlying portion using channels immediately above or below the region of interest. In general, this subtraction process was applicable to only the peaks occuring in the Ge(Li) projection although it also worked with some prominent peaks in the NaI projection. However, the NaI gates usually consisted of the sum of ten channels with no background contribution subtracted.

The spectra generated by these gates were then analyzed to obtain the coincidence probabilities between the gamma rays observed in the gated spectrum and the gating transition. Experimentally, this is given by

$$N_{ij} = N_0(\varepsilon\omega)_i \ (\varepsilon\omega)_j \ C_{ij} \qquad 3.3.1$$

where N_{ij} is the number of coincidence events occuring between the full energy peaks of the i^{th} and j^{th} gamma rays, $(\varepsilon\omega)_i$ and $(\varepsilon\omega)_j$ are the corresponding efficiencies (one NaI, one Ge(Li)) and C_{ij} is the coincidence probability. Since N_0 was not known, the coincidence probabilities were determined by normalizing the calculations to a

strong transition occuring in the gate, for which it was felt that the true coincidence probability was well known. A comparison of these probabilities with those predicted from the assignment made in the decay scheme provided a quantitative test of the assignment.

Because of the large range of gamma ray energies, these coincidence experiments were performed in two sections for each element. The first section constituted a "Lo-Lo" experiment in which the electronics associated with both detection systems were adjusted to cover approximately the same energy region. For the Krypton isotopes this upper limit was approximately 1.9 MeV while for the Rubidium isotopes the Ge(Li) dimension spanned 0 - 2.77 MeV and the NaI dimension spanned 0 -3.1 MeV. In the other section, the "Hi-Lo" experiment, the energy region accepted by the NaI detection system was left unchanged from that in the corresponding "Lo-Lo" experiment, while that accepted by the Ge(Li) system was arranged to cover the upper portion of the gamma ray spectrum with some overlap with the "Lo-Lo" experiment. Thus for the Krypton isotopes the Ge(Li) system covered the region 1.6 to 4.49 MeV while for the Rubidium isotopes the range was 2.7 to 5.9 MeV.

3.4 Two Parameter Beta-Gamma Experiments

As an aid to establishing level ordering, a two-parameter beta-gamma experiment was performed on the Krypton isotopes only. The experimental configuration was the same as that shown in Figure 3.3.1 except the NaI(Tl) detector was replaced by a 1.75 in diameter x 2.0 in Nel02 plastic beta detector, and the gamma counting cell of Figure 3.1.3 was replaced with the beta counting cell. The beta

detector was mounted on a Dumont 6292 photo tube with optical coupling provided by silicone fluid (Dow Corning #200). The plastic was held firmly in place by a cardboard tube with a small lip projecting over the detector to provide mechanical strength. The tube in turn was firmly fastened to the lower portion of the photo tube with light-tight black plastic tape. The exposed end of the plastic was covered with three layers of Aluminum foil, each 0.228 mgm/cm^2 thick, to exclude light without affecting the beta spectra except at the very low energy end.

A collimator consisting of 0.3 mm copper and 0.6 mm lead was placed between the source and the beta detector. This had a conical hole (30° half angle) with a 0.5 mm dia. intersection with the front surface of the copper portion. This collimator served three functions:

i) to ensure that the detector could only "see" a portion of the source holder covered by the thin mylar window;

ii) to make the efficiency essentially independent of energy by making the shortest straight line path through the detector longer than the range of the expected electrons;

iii) to absorb the strong 0.1086 MeV and 0.1215 MeV transitions in the ^{91}Kr and ^{90}Kr decays respectively, which originated in the portion of the source not "seen" through the hole in the collimator. These gamma rays would otherwise contribute a large gamma-gamma component to the observed coincidences.

Although this gamma contribution to the coincident beta spectra would only become appreciable at $\sim$ 1.0 MeV (1.118 MeV Compton edge)

for the ^{90}Kr decay and at ∿ 0.34 MeV (0.506 MeV Compton edge) for the ^{91}Kr decay, i.e. approximately 1.6 MeV below the end point of the lowest energy beta group expected in ^{90}Kr, an attempt was made to correct for it. This was done by performing a separate gamma-gamma coincidence experiment in the same geometry, but with the Copper portion of the collimator replaced by a similar piece without the conical hole. The two experiments were normalized by comparing the areas of the full energy peaks in singles spectra from the Ge(Li) spectrometer recorded during the collection of the coincidence data in each case. The corrections ranged from ∿ 20% to ∿ 50% depending on the relative size of the beta-gamma and gamma-gamma coincidence probabilities of the gating transition and its coincidence radiations.

The data were accumulated and gates were generated as described for the gamma-gamma case (Section 3.3) with the exception that no beta gates were used and the beta dimension grid was reduced to 51 from 256 to increase the number of events in each channel. The coincident beta spectra were corrected for the expected coincident gamma contribution, and for the response of the plastic detector (Slavinskas et al (1965)). Energy calibration was obtained using the beta spectra of ^{198}Au, ^{28}Al and ^{38}Cl by the following iterative procedure. A first approximation to the calibration was used to generate Fermi plots of the three standards. Weighted, least-squares, straight-line fits to these Fermi plots yielded channel number intercepts which were used to obtain a second approximation to the energy calibration. This procedure was repeated until the standard end points were recalculated within the generated error. This final energy calibration

was then used to generate the Fermi plots of the coincidence spectra and consisted of a gain of approximately 0.114 MeV/channel. The above mentioned least-squares fit to the coincidence Fermi plots then yielded the end-points of the various beta groups.

The beta-gamma coincidence probabilities were determined from the Fermi plots using the relationship

$$N_{ij}(W) = N_0 \, (\varepsilon\omega)_i \, (\varepsilon\omega)_j \, \phi_j(W) \, C_{ij} \qquad 3.4.1$$

where $N_{ij}(W)$ is the number of coincidences between the i^{th} gamma ray and the electrons in the j^{th} beta group that occur at an energy W, $\phi_j(W)$ is the probability of an electron in the j^{th} group occuring with energy W and the other symbols are as previously described. $\phi_j(W)$ is just the beta spectrum shape of equation 2.2.2 (with ε replaced by W) normalized to unit area and may therefore be calculated for the various beta groups involved. As with the gamma-gamma calculations, N_0 was unknown and it was necessary to normalize the calculations to a coincidence where it was felt that the probability was well known.

3.5 Delayed Coincidences and Lifetime Measurement

During the course of this investigation it became evident that the first excited state in ^{91}Sr at 0.0931 MeV possessed a measurable lifetime. This lifetime was subsequently measured using the standard fast-slow coincidence technique, and the experimental arrangement shown in Figure 3.5.1 (Prestwich et al (1968)). TAC start pulses were generated from both beta and gamma events above about 0.150 MeV in energy as detected in a 1.5 in thick by 1.8 in dia. NATON 136 plastic detector while stop pulses were generated from events in the region of the 0.093 keV full energy peak detected in the 1 in x 1 in NaI(Tl)

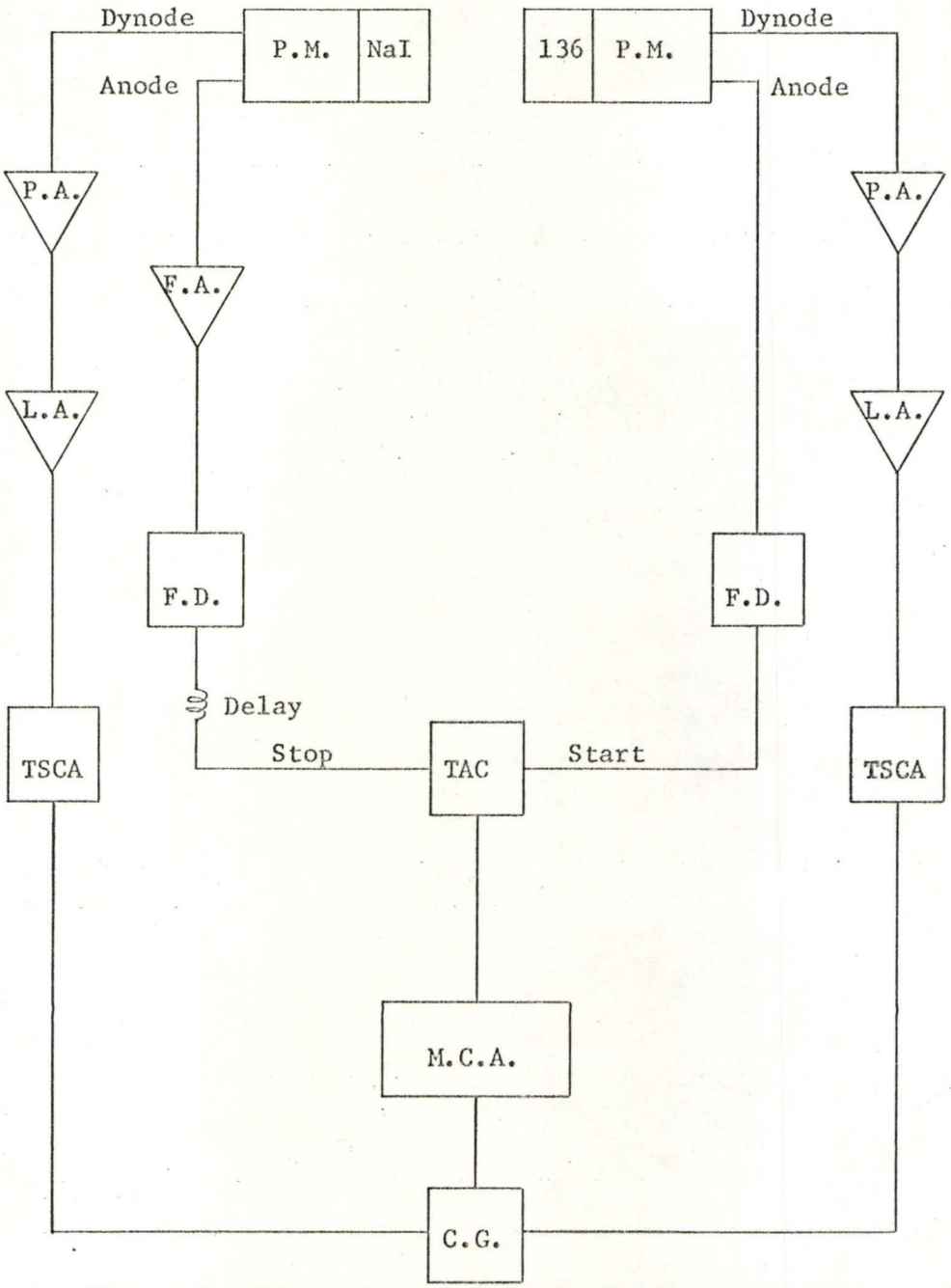

P.M. - Photomultiplier Tube
P.A. - Preamplifier
L.A. - Linear Amplifier
TSCA - Timing Single Channel Analyzer
C.G. - 100 ns Coincidence Gate
F.A. - Wide Band Amplifier
F.D. - Fast Discriminator
TAC - Time-to-Amplitude Converter
MCA - Multi-Channel Analyzer

Figure 3.5.1 Schematic Diagram of Electronic Configuration Associated with Lifetime Measurement.

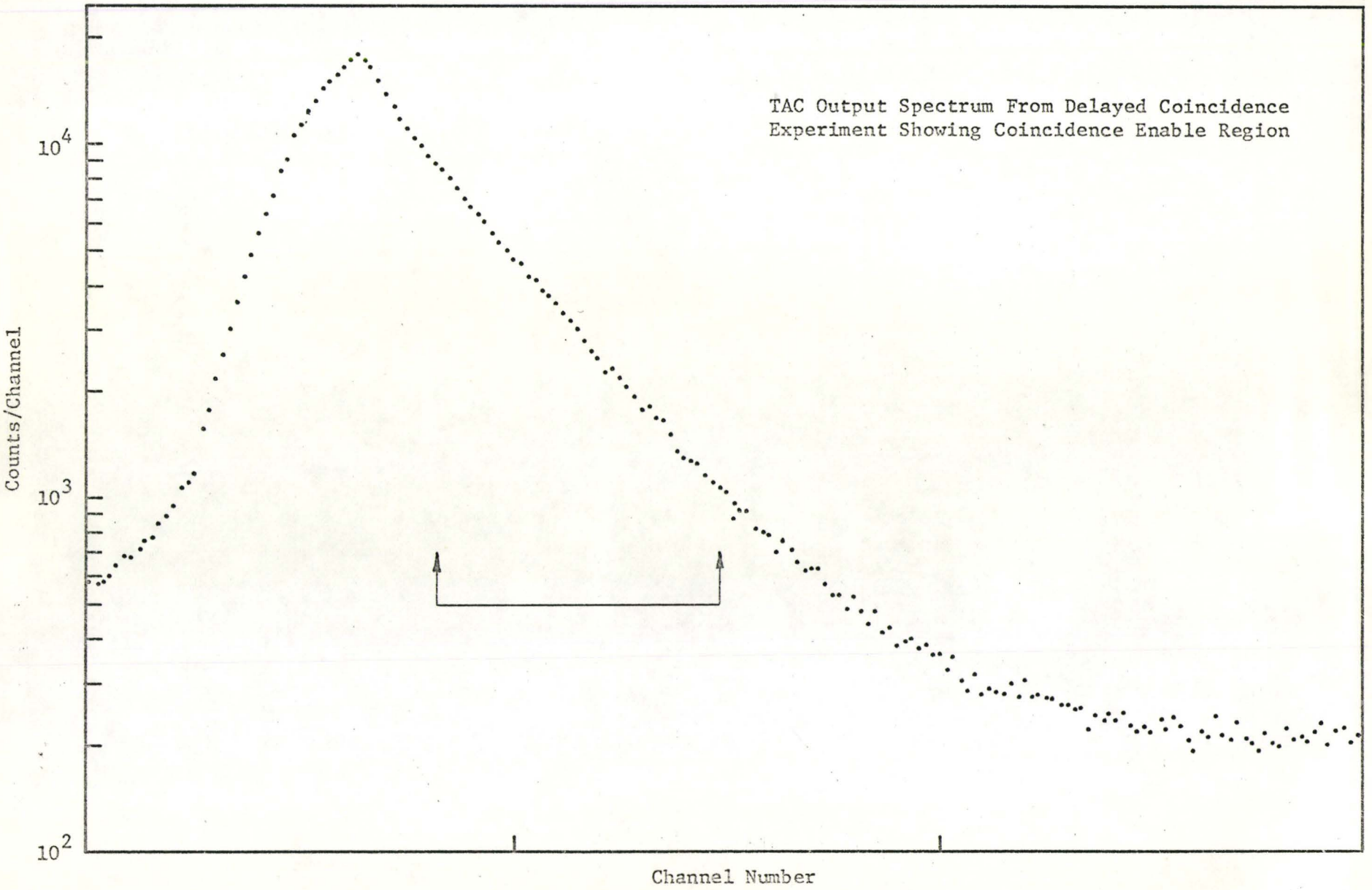
TAC Output Spectrum From Delayed Coincidence
Experiment Showing Coincidence Enable Region
10^4
10^3
10^2
Counts/Channel
Channel Number

Figure 3.5.2

scintillator. The TAC output spectrum was collected in a multi channel analyzer. The shape of the "prompt" curve, due to undelayed coincidences for this equipment was obtained using the annihilation radiation from ^{22}Na. Time calibration was also performed using this source by introducing successive additional delays of 100 ns into the circuits generating the stop pulses. Another measure of the lifetime was provided by the TAC output collected during the course of the delayed coincidence experiment described below. "Prompt" response and time calibration were determined in the same fashion as above.

The existence of this lifetime provided an effective means for determining which transitions were connected to the first excited state, either directly or in cascade. By using the configuration shown in Figure 3.3.1 with a 0.125 in thick x 1 in dia. NaI(Tl) detector gated on the region of the 0.093 MeV full energy peak (instead of the ungated 3" x 3" NaI(Tl) detector) to generate the stop pulses, a TAC output spectrum as shown in Figure 3.5.2 was obtained. Setting the window of the SCA which generated the analyzer enabled pulse on the indicated region of this spectrum, effectively rejected all un-delayed events. Thus only those events associated with the population of the 0.0931 MeV level were analyzed. The events had to be delayed a longer time than usual in order that they arrive at the analyzer at the instant coinciding with the opening of the linear gate. The chance contribution to the collected spectrum, which was larger than that for an ordinary coincidence experiment due to the increased size of the window on the TAC spectrum, was readily corrected for using the strong transitions in the ^{90}Rb decay.

CHAPTER 4

RESULTS AND DISCUSSION - ^{90}Kr AND ^{91}Kr

4.1 Previous and Concurrent Work

The decay scheme of ^{90}Kr has been previously investigated by Goodman et al (1964) and the results of this investigation are presented in Figure 4.1.1. Gamma-gamma and beta-gamma measurements were performed using 2" x 2" NaI detectors and an NE102 plastic beta detector. The gamma spectra obtained were analyzed by hand stripping procedures while the analysis of the beta spectrum required the use of a correction factor for the plastic detector efficiency, which was a function of energy because of the method of operation. As a result, the decay scheme of Figure 4.1.1 might be expected to be in error in many of the weaker transitions.

More recently Carlson et al (1969) have investigated the radiations associated with the decay of ^{90}Kr using a mass separator to produce isotopically pure samples, and have determined the half-life to be 32.32 $\pm$ 0.09 sec. In addition, from measurements of the decay of the ^{90}Rb daughter, they have discovered an isomer with a beta half life of approximately 255 sec. Talbert (1969) using the same equipment, has also measured the gamma ray spectrum associated with the decay of ^{90}Kr with high resolution Ge(Li) detectors and has identified this isomer as a level at 0.1069 MeV in ^{90}Rb. Talbert's investigation, as well as the present one indicates the existence

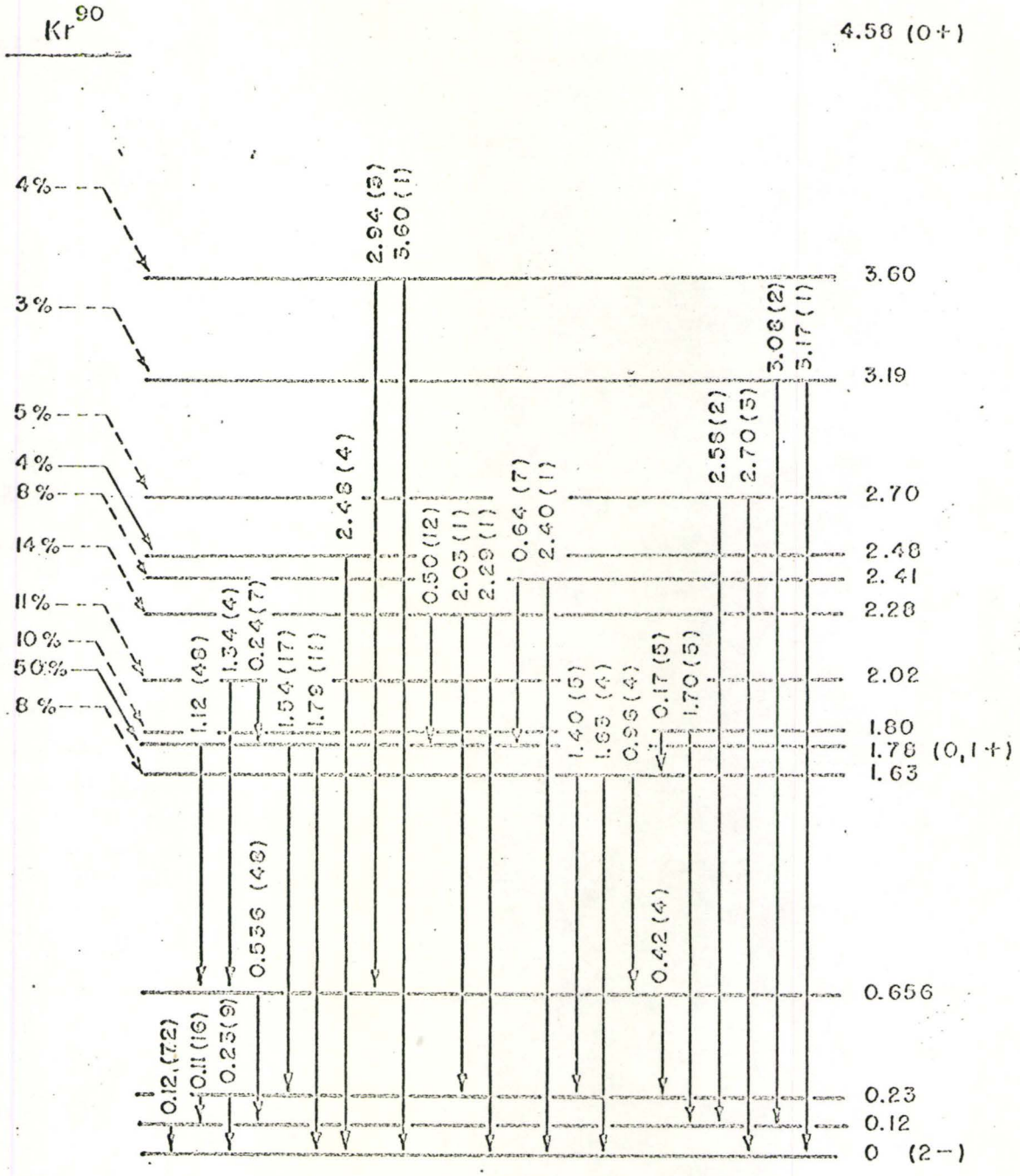

Figure 4 .1.1 Decay Scheme of ^{90}Kr Proposed by Goodman et al (1964).

of many more transitions than the previous measurements of Goodman.

4.2 Identification of the Origin of Gamma Rays

Figure 4.2.1 presents the spectrum obtained from sources prepared using the standard ^{90}Kr prescription of Table 3.1.1. All of the ^{90}Kr full energy peaks have been labelled as have most of the prominent peaks due to contaminant activity. A few of the weaker contaminant peaks have not been labelled for the sake of clarity. A portion of this spectrum is shown expanded in Figure 4.2.2 along with the corresponding section from the spectrum obtained from the "delayed" sources. This section contains gamma rays from all three nuclides present in the samples and indicates the type of behaviour observed for peaks associated with each of these. A representative sample of the numerical values generated by the procedure outlined in Section 5.3.2 is shown in Table 4.2.1 to illustrate the quality of the distinction that can be made between the nuclides. Although this classification procedure was generally quite successful, some of the weaker gamma rays were assigned to particular decay chains on the basis of comparison with the results of Talbert (1969). In addition, many weak high energy transitions were observed in this latter investigation which were not seen in the present one due to the large contamination from high energy ^{89}Kr events.

4.3 ^{90}Kr Decay

4.3.1 ^{90}Kr Energy and Intensity Measurements

The energy and intensity of the gamma rays assigned to the decay of ^{90}Kr are summarized in Table 4.3.1. The errors in the energy

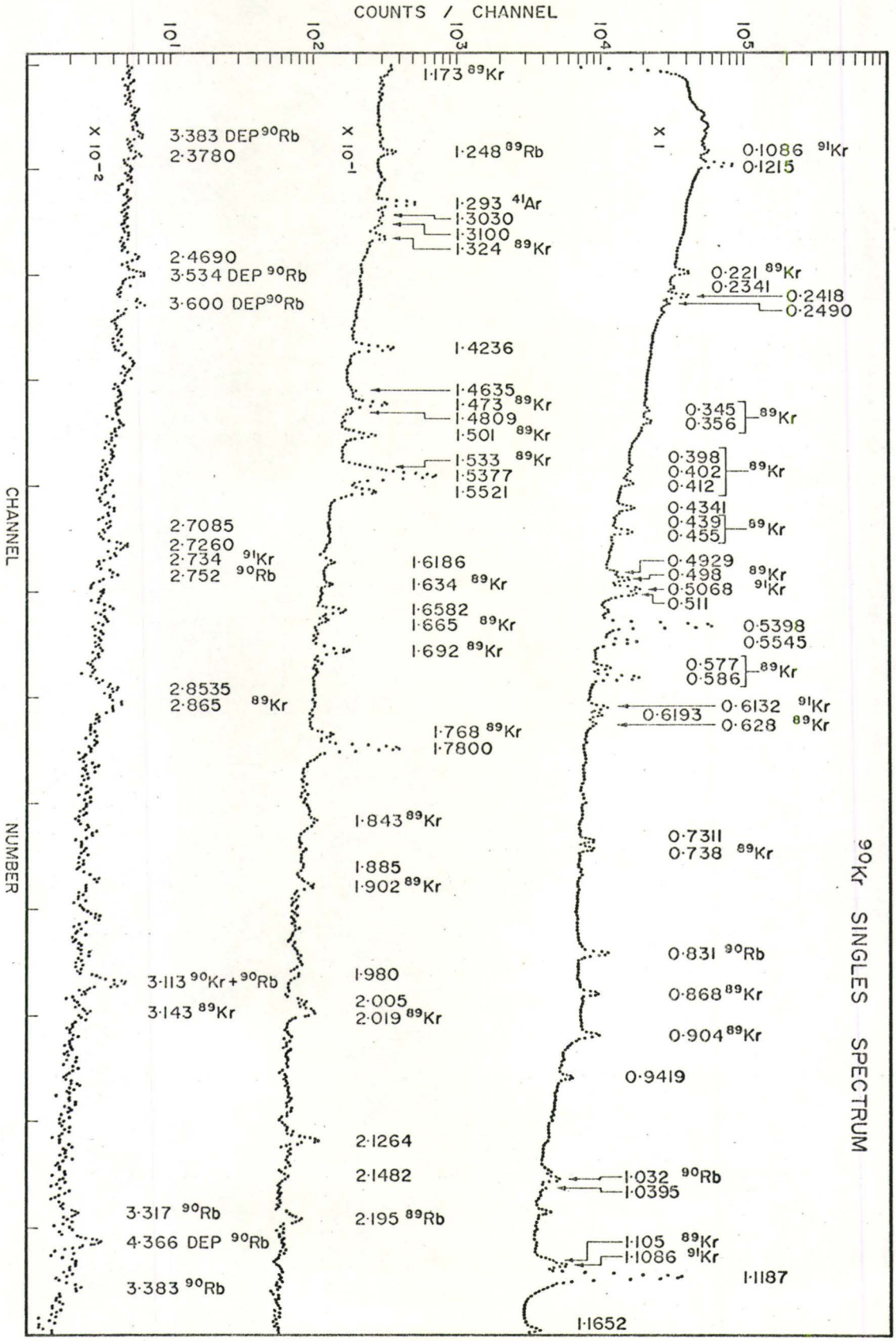

Figure 4.2.1 ^{90}Kr Singles Gamma Spectrum

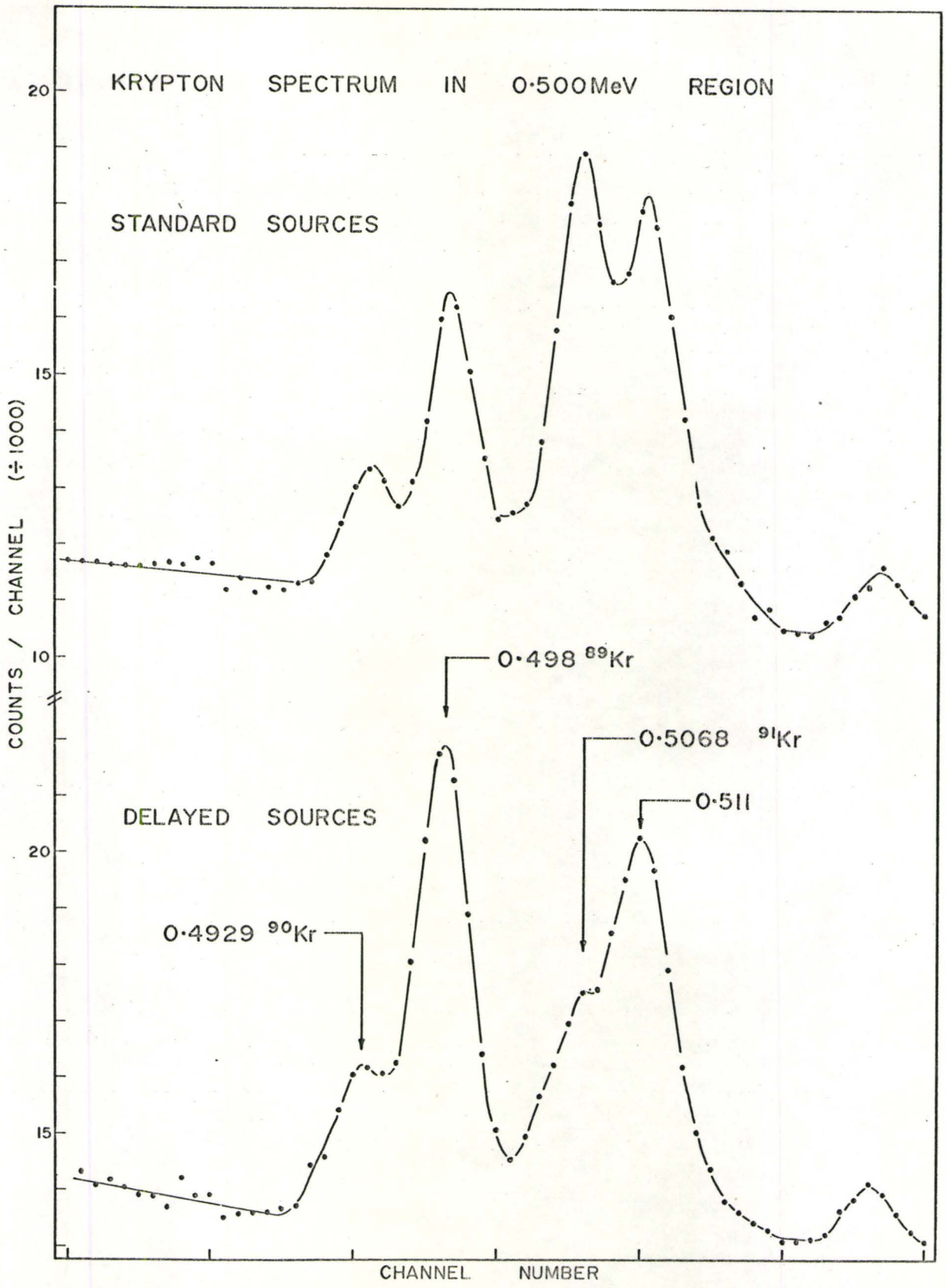

Figure 4.2.2 Krypton Spectrum in 0.500 MeV Region

TABLE 4.2.1

Ratio of Some Peaks Observed in Krypton Singles Experiment

(Ratio is Peak Area Delayed Source/Peak Area Standard Source)

E_γ(MeV)	Ratio	Isotope Classification
0.1086	0.47	91
0.1215	1.10	90
0.2206	1.35	89
0.2341	0.92	90
0.2419	1.01	90
0.3564	1.56	89
0.4120	1.48	89
0.4341	1.22	90
0.5068	0.50	91
0.5398	1.15	90
0.6132	0.53	91
0.7311	1.30	90
0.8675	1.96	89
1.1187	1.20	90

TABLE 4.3.1

Gamma Rays Observed in the Decay of ^{90}Kr

Energy (MeV)				Intensity		Classification	Basis for Classification	
Present Work		Talbert (1969)		Present Work	Talbert (1969)		E**	
		0.1059	2		0.64	1.7998→1.6735	E	
0.1064	5	0.1069	3		251 sec Isomer	0.1069→0.0	E	
0.1215	2	0.1216	1	58	58	0.1215→0.0	E many γ-γ (2.59β)	
0.2341	2	0.2344	1	4.6	3.1	0.3557→0.1215	E 4.2(0.121)	3.1(1.423) 1.3(2.69β)
0.2419	2	0.2422	1	17	11.5	0.2419→0.0	E 0.7(0.419)	15(1.537) 10(2.64β)
0.2490	2	0.2493	1	3.0	1.6	0.3557→0.1069	E 1.9(1.423)	
0.4193	2	0.4193	2	0.3*	0.35	0.6612→0.2419	E 0.7(0.242)	
0.4341	2	0.4335	1	3.2	1.6	1.6735→1.2402	E 2.7(0.121)	2.2(1.187) 3.5(2.80β)
		0.4702	3		0.35			
0.4929	2	0.4926	2	1.5*	1.6	0.6144→0.1215	1.6(0.121)	
0.5398	2	0.5395	1	38	39.5	1.7798→1.2402	E 38(0.121)(n)	38(1.118)(n) 38(2.63β)(n)
0.5545	2	0.5544	2	6.5	6.7	0.5545→0.0	E 7.5(1.118)	5(2.73β) 0.7(3.86β)
0.6193	2	0.6190	2	1.4	1.4	0.7408→0.1215	E 1.7(0.121)	
0.6772	2	0.6777	3	0.5	0.5			

Energy (MeV)				Intensity		Classification	Basis for Classification	
Present Work		Talbert (1969)		Present Work	Talbert (1969)		E	
0.6906	2	0.6904	3	0.5	0.5			
0.7311	2	0.7313	4	1.9	2.1	0.7311→0.0	E 1.7(0.942)(n)	(2.75β)
0.9419	2	0.9417	2	1.6	1.8	1.6735→0.7311	E 1.7(0.731)(n)	
1.0395	4	1.0391	5	0.5	0.64	1.7798→0.7408	E 0.5(0.121)	∿0.6(0.619)
1.1187	2	1.1185	2	45	60.4	1.2402→0.1215	E 43(0.121)	38(0.540)(n) 49(2.55β)
				7		1.6735→0.5545	E 8.2(0.555)	5(3.11β)
1.1652	3	1.1653	3	1.1	1.3	1.7798→0.6144	E 1.2(0.492)	
		1.2405			0.29	1.2402→0.0	E	
1.3030	5	1.3045	6	0.7	0.2			
1.3100	5	1.3098	4	0.6	0.5			
		1.3414	4		0.3			
1.3862	3	1.3862	4	0.3	0.35	2.1261→0.7408	E	
1.4237	3	1.4230	4	3.7	5.2	1.7798→0.3557	E 2.0(0.121)	3.1(0.234) 1.9(0.249)
1.4635	2	1.4656	4	0.4	0.45	2.1261→0.6612	E	
1.4809	5			0.2				
1.5377	2	1.5372	4	13.2	17.5	1.7798→0.2419	E 15(0.242)	
1.5521	2	1.5516	4	3.1	4.0	1.6735→0.1215	E 2.8(0.121)	
1.6186	4	1.6195	7	0.15*	0.29			

Energy (MeV)				Intensity		Classification	Basis for Classification
Present Work		Talbert (1969)		Present Work	Talbert (1969)		E**
1.6582	2	1.6577	4	1.6	2.3	1.7798→0.1215	E 1.3(0.121)
		1.6921	5		0.1		
1.7800	2	1.7797	2	9.6	12.5	1.7798→0.0	E no γ-γ
1.885	4	1.8849	4	0.2*	0.46	2.1261→0.2419	E
1.980	5	1.9805	4	0.3*	0.29		
2.005	5	2.0059	4	0.5*	0.3	2.1261→0.1215	E
2.1264	4	2.1271	3	1.5	2.7	2.1261→0	E
2.1482	4	2.1494	4	0.3*	0.52		
		2.1911	5		0.23		
		2.205	1		0.2		
		2.353	1		0.2	3.0937→0.7408	E
2.3780	9			0.5			
		2.4171	5		0.35		
		2.4323	5		0.3	3.0937→0.6612	E
2.469	5	2.4680	4	0.6	1.0		
2.7085	13						
2.7260	8	2.7265	4	1.0	1.7		

Energy (MeV)				Intensity		Classification	Basis for Classification
Present Work		Talbert (1969)		Present Work	Talbert (1969)		E**
2.8535	9	2.8543	4	1.0	0.81	3.0937→0.2419	E
2.865	6	2.865	6	0.3	0.38		
		2.9481	8		0.11		
		2.971			~0.2	3.0937→0.1215	
3.1130	6			0.3			
		3.2689	10		0.15		
		3.308					
		4.354					

Note

* Indicates transition identified as belonging to ^{90}Kr decay by comparison with Talbert's results.

** E indicates energy fit.

(n) Indicates this cascade used for normalization in calculation of coincidence probabilities.

are presented as that in the last significant figure of the energy while errors in intensity are not quoted. These are believed to be about 10% for strong transitions where the error is generated largely from uncertainties in the detector efficiency curve and to rise to about 20% for the weak transitions where there is an additional error associated with determining the area of the full energy peak. The results of Talbert are listed for comparison.

Table 4.3.1 also indicates the classification within the decay scheme for those gamma rays which have been placed, as well as the basis for this classification. The latter is given in terms of observed coincidence probabilities from both gamma-gamma and beta-gamma experiments. These probabilities were determined from an analysis of the coincidence data as outlined below.

4.3.2 ^{90}Kr Coincidence Measurements and Decay Scheme Construction

Figure 4.3.1 shows the Fermi plots of the partial beta spectra in coincidence with the 0.1215, 0.2341, 0.2419, 0.4341, 0.5398, 0.5545, 0.7311 and 1.1187 MeV full energy peaks. Each of these has had coincidences due to underlying Compton events removed and all but the 0.1215 MeV gate have been corrected for gamma-gamma contributions. The 0.1215 MeV gate is presented in an uncorrected form to indicate the magnitude of this contribution to the low energy portion of the spectrum. From these it is immediately evident that the 0.1215, 0.2341, 0.2419, 0.5398 and 1.1187 MeV transitions are in coincidence with the same beta group with an energy of 2.60 $\pm$ 0.05 MeV. The 1.1187 MeV gamma ray also shows indications of being in

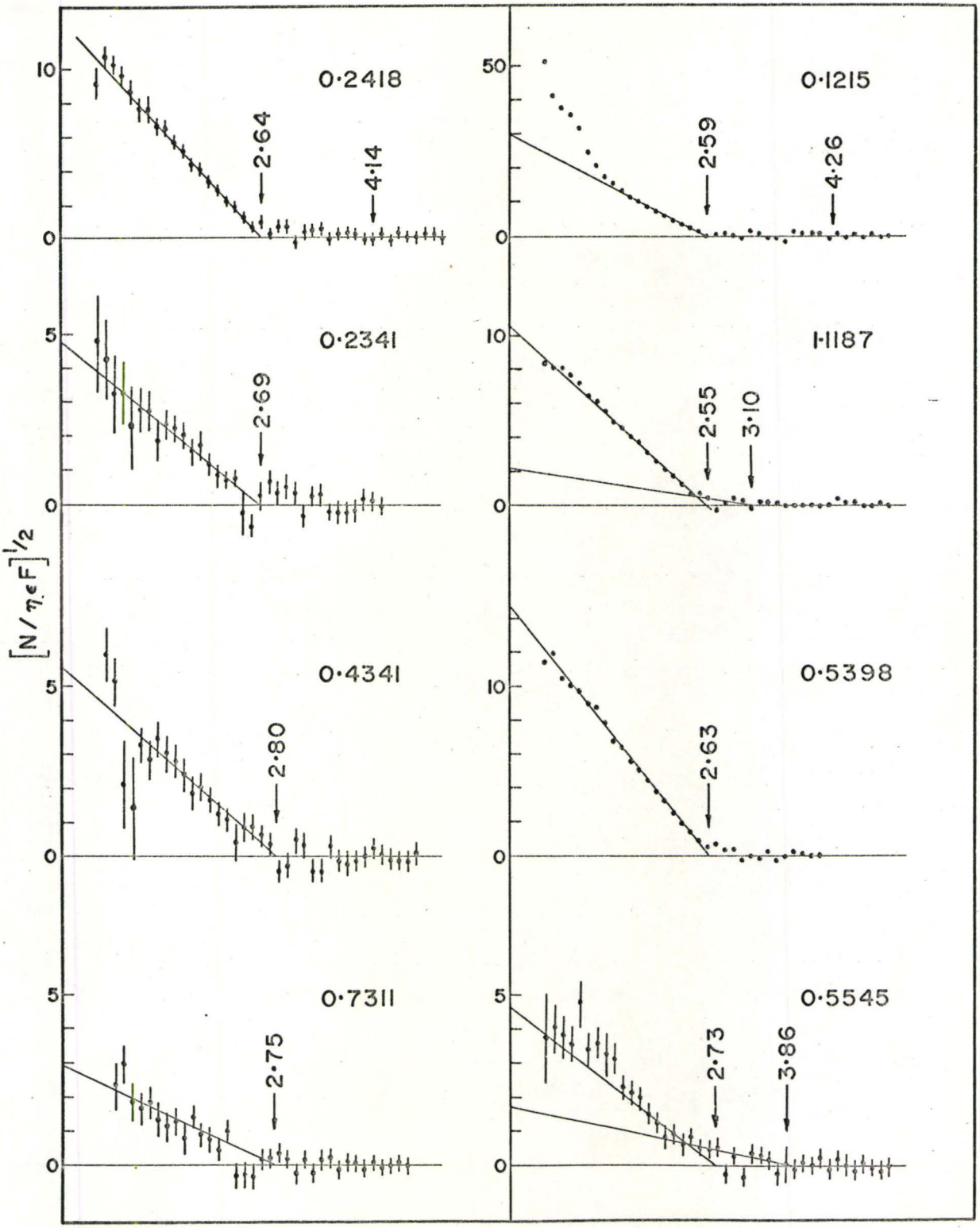

Figure 4.3.1

Fermi Plots of Beta Spectra in Coincidence with ^{90}Kr Gating Transitions

coincidence with a beta group of a slightly higher endpoint of 3.11 ± 0.1 MeV.

In particular, the beta group in coincidence with the 0.4341 MeV radiation is observed to have an endpoint of 2.8 ± 0.1 MeV, somewhat higher than the strong group making the multiple coincidences. The endpoint of the beta group exciting the 0.7311 MeV transition, which appears to be approximately that of the group exciting the 0.4341 MeV gamma ray, is difficult to determine. It is calculated to be 2.6 ± 0.2 MeV or 2.9 ± 0.2 MeV depending on whether the three consecutive negative points generated by the Compton subtraction process are included. Thus a value of 2.75 ± 0.2 MeV was adopted.

Finally the 0.5545 MeV gate indicates that this transition is in coincidence with two beta groups of energy 3.86 ± 0.2 MeV and 2.73 ± 0.2 MeV.

The three coincidence spectra associated with NaI photopeaks of the 0.1215, 0.5398 and 1.1187 MeV transitions, as generated from the "Lo-Lo" gamma-gamma experiment, are shown in Figures 4.3.2, 4.3.3 and 4.3.4 respectively. These demonstrate the existence of a strong triple cascade of the three gating transitions themselves and establishes a level at 1.7800 MeV, de-excited also by a ground state transition, regardless of how this cascade is ordered. From the intensity of the 0.1215 MeV transition it can be assumed to be the ground state transition thus establishing a level at this excitation. The appearance of strong 0.4341 - 1.1187 MeV and equally strong 0.4341 - 0.1215 MeV coincidences suggests that of the remaining pair the 1.1187 MeV gamma ray is the lower. This would establish levels

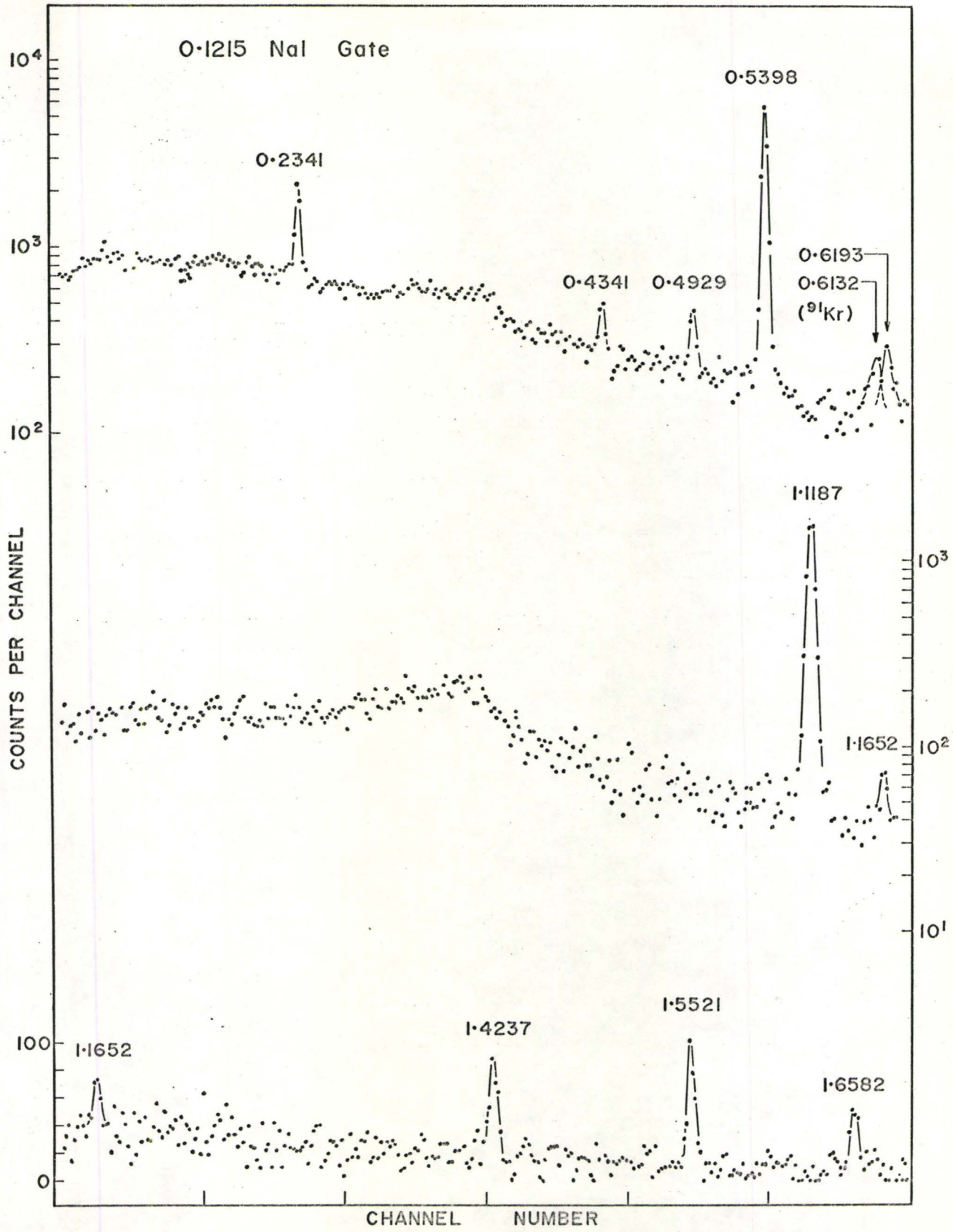

Figure 4.3.2 ^{90}Kr Gamma Coincidence Spectrum - 0.1215 MeV NaI Gate

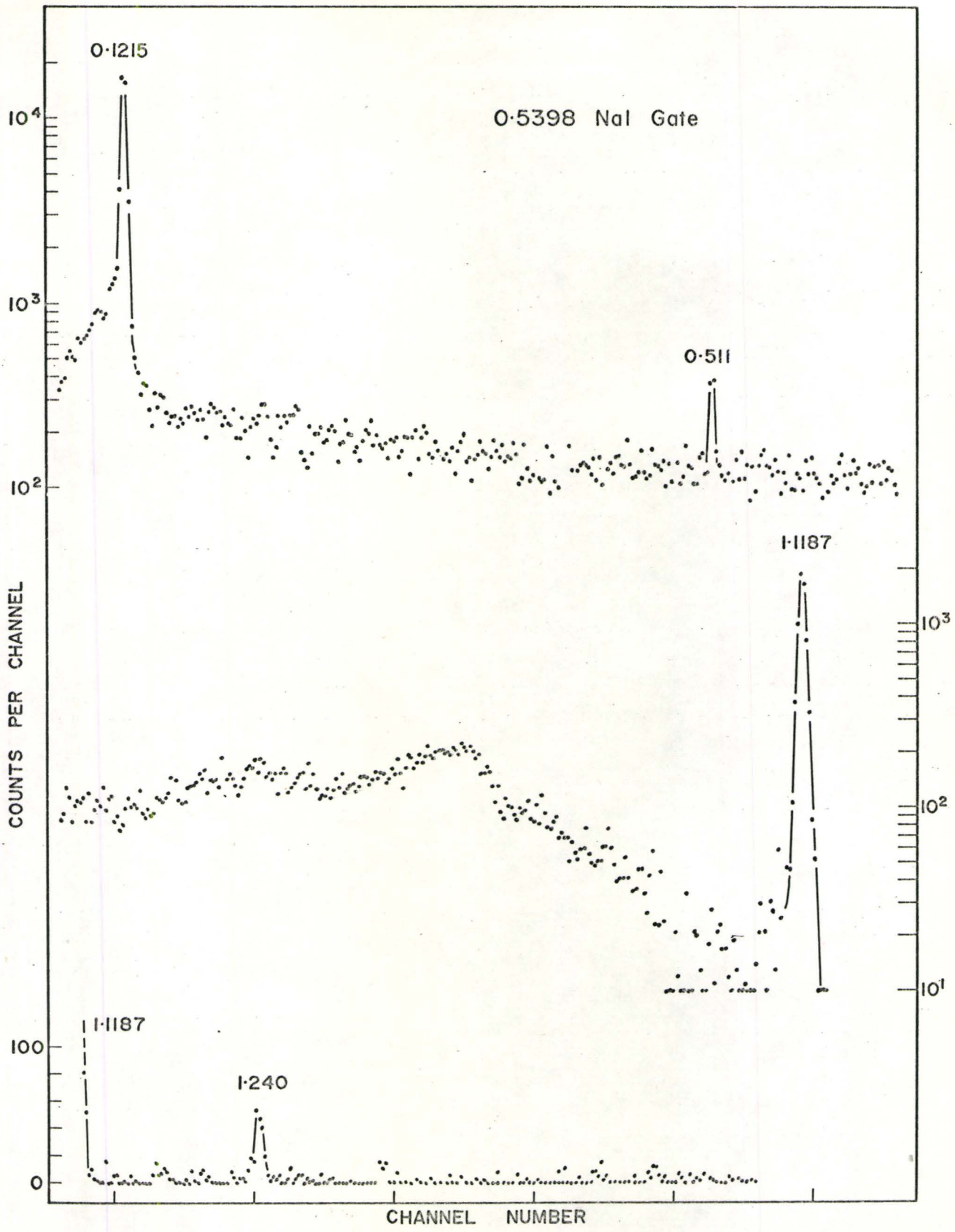

Figure 4.3.3 ^{90}Kr Gamma Coincidence Spectrum - 0.5398 MeV NaI Gate

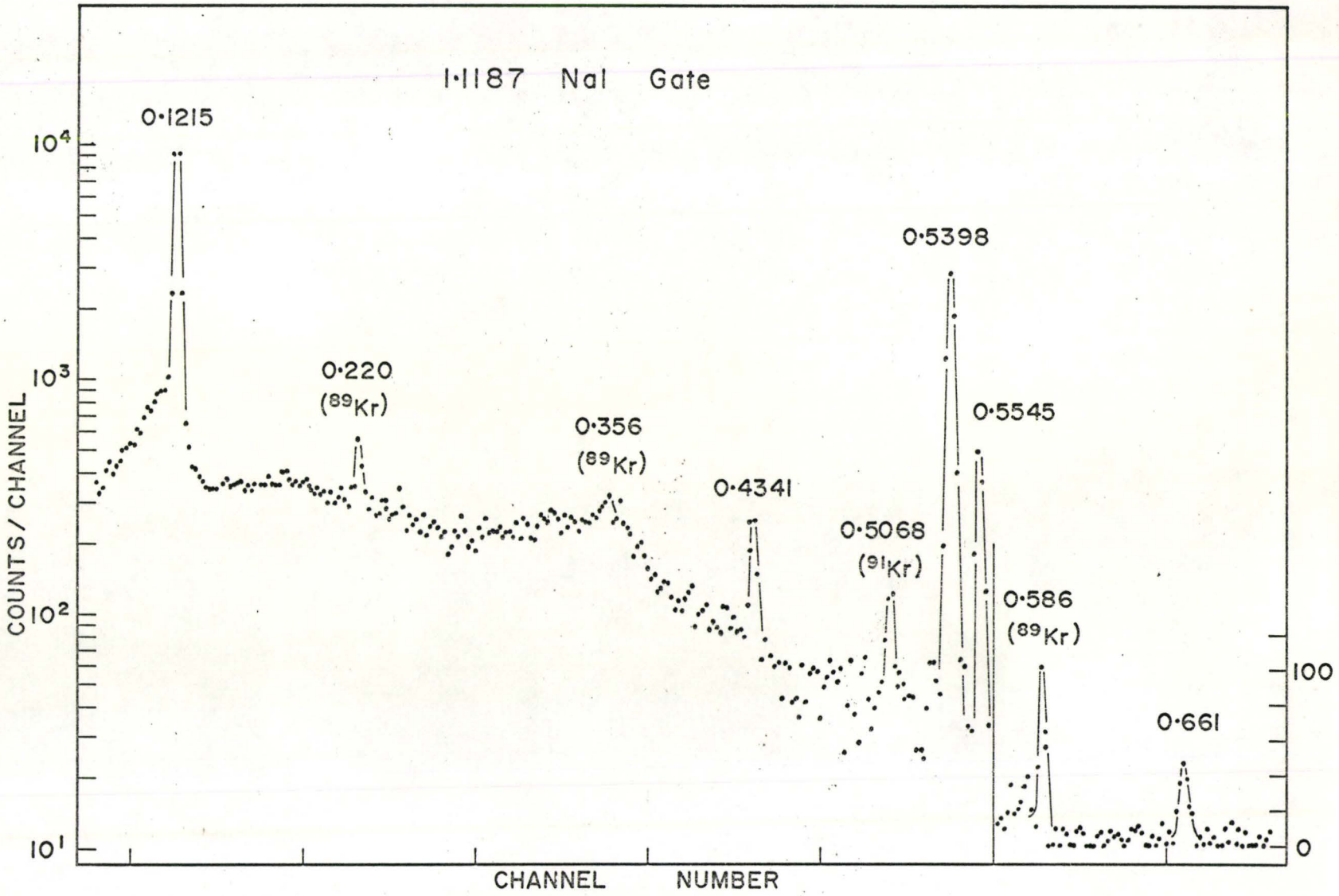

Figure 4.3.4 ^{90}Kr Gamma Coincidence Spectrum - 1.1187 MeV NaI Gate

at 1.6736 and 1.2402 MeV, the latter of which would accommodate the transition of approximately this energy observed by Talbert. The 1.2402 MeV peak appearing in the 0.5398 MeV gate cannot be used as evidence directly since a 0.6616 MeV peak also occurs in the 1.1187 MeV gate. These are both believed to be largely due to coincidence summing in the Ge(Li) detector. However, under the assumption that the latter peak is entirely due to summing the relationship

$$\frac{N^{540}_{cs\ 121-1118}}{N^{1118}_{cs\ 121-540}} = \frac{(\varepsilon\omega)^{NaI}_{540}}{(\varepsilon\omega)^{NaI}_{1.118}} \times \frac{(\varepsilon\omega)^{Ge}_{1118}}{(\varepsilon\omega)^{Ge}_{540}} \times \frac{c_{121-1118}}{c_{121-540}}$$

may be used to estimate that approximately 1/7 of the 1.2402 MeV peak is not due to summing effects. This would correspond to a gamma ray of intensity $\sim$ 0.25 as compared to the 0.29 observed by Talbert. Because of the errors involved in the peak areas and the efficiencies, this result cannot be regarded as proof for the transition ordering. The strongest evidence for this ordering is provided by the observed 0.4341 gamma coincidences. The ordering proposed by Goodman would require a 0.227 MeV transition of intensity equal to that of the 0.4341 MeV transition and such a gamma ray has not been observed in either singles or coincidence experiments. The currently proposed ordering is supported by the endpoint of the partial beta spectrum exciting the 0.4341 MeV gamma ray and the existence of the upper group in the partial beta feed to the 1.1187 MeV transition.

The 1.1187 MeV NaI gated spectrum clearly shows 1.1187-0.5545 MeV coincidence events. The lack of corresponding 0.1215-0.5545 MeV events in the 0.1215 MeV NaI and 0.5545 MeV gated spectra (Figures

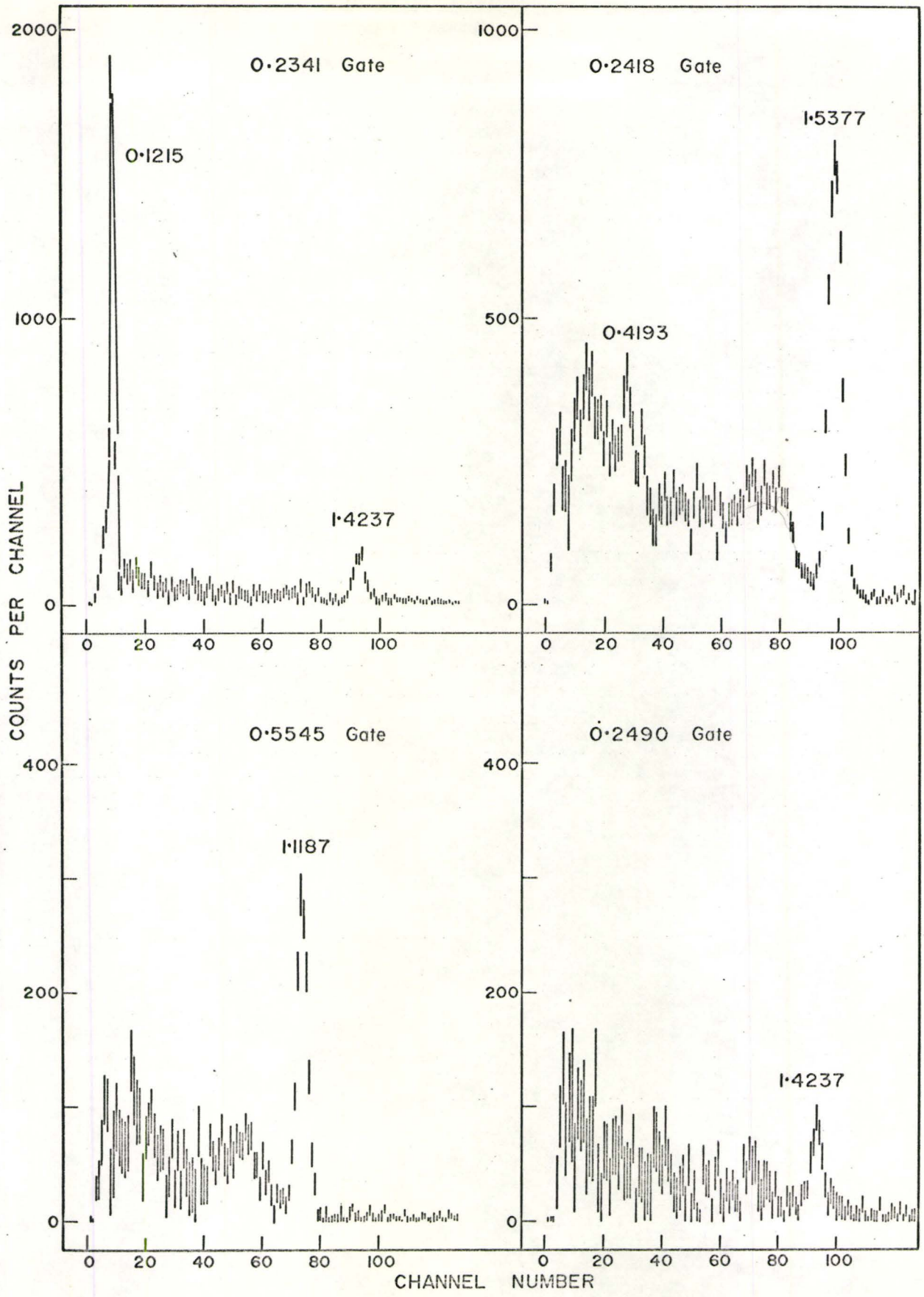

Figure 4.3.5 ^{90}Kr Gamma Coincidence Spectra - Ge(Li) Gates

4.3.2 and 4.3.5 respectively) just as clearly indicates that the 0.5545 MeV gamma ray cannot feed the 1.2402 MeV level. This and the coincidence probabilities suggests that the 1.1187 MeV radiation is a complex of two gamma rays one of intensity approximately 7% which feeds the 0.5545 MeV transition and the other of approximately 45% intensity which feeds the second excited state at 0.1215 MeV. The end point of the higher energy group in the beta spectrum in coincidence with the 0.5545 MeV gamma ray suggests that the 0.5545 MeV transition is the lower member of the 1.1787-0.5545 MeV cascade. This cascade has been placed between the 1.7798 and 0.1064 MeV levels as a mechanism for populating the latter state. On an energy fit, it could equally well be located between the 1.6735 and ground states. The end points of the beta groups feeding the 0.5545 MeV transition are compatible with either interpretation.

The 0.2341 and 1.4237 MeV coincidences observed in the 0.1215 MeV NaI gated spectra, in con junction with the 1.4237 MeV peak in the 0.2341 MeV Ge(Li) gated spectrum, in Figure 4.3.5, establishes another cascade from the 1.7800 MeV level. Events at 1.4237 MeV in the 0.2490 MeV Ge(Li) gated spectrum (Figure 4.3.5) and energy fit suggest orderings of 1.4237-0.2341-0.1215 and 1.4237-0.2490-0.1064 MeV respectively thus establishing a level at 0.3557 MeV.

Two further cascades from the 1.7800 MeV level to the 0.1215 MeV excited state are established from the 0.4929, 0.6193 and 1.1652 MeV coincidences in the 0.1215 MeV gated spectrum and the 1.1652 and 1.0395 MeV events in the Ge(Li) gated spectra associated with the 0.4929 and 0.6193 MeV radiations (Figure 4.3.6). Using intensities to order the transitions establishes levels at 0.6144 and 0.7408 MeV

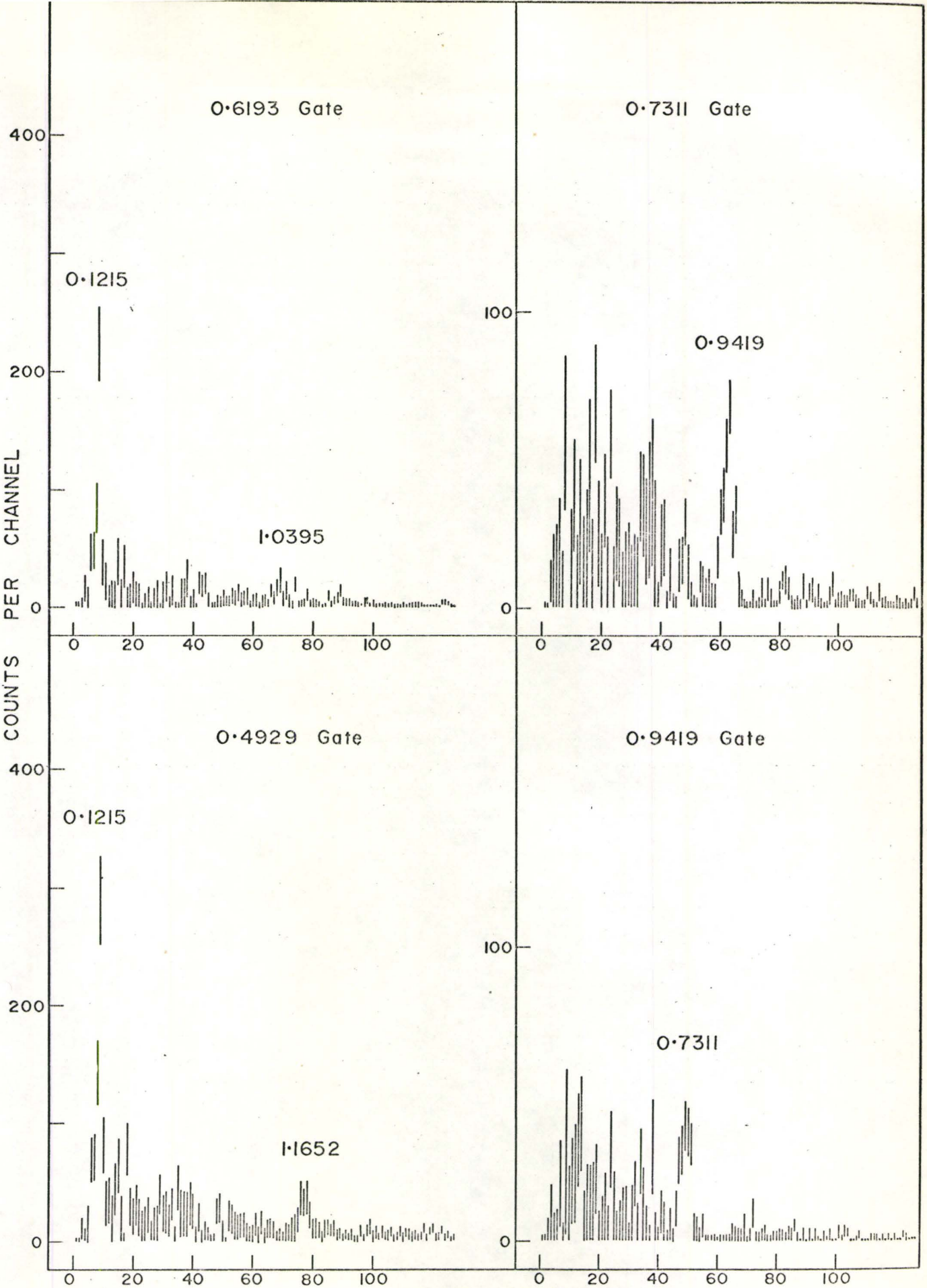

Figure 4.3.6 ^{90}Kr Gamma Coincidence Spectra - Ge(Li) Gates

respectively.

Of the remaining gamma rays in the 0.1215 MeV NaI gated spectrum the one at 1.6582 MeV cascades directly from the 1.7800 MeV level to the second excited state while the one at 1.5521 MeV provides further evidence for the 1.6736 MeV level. The 0.9429-0.7311 MeV cascade whose existence is determined from the corresponding Ge(Li) gated spectra shown in Figure 4.3.6 can be fitted either between the 1.7798 and 0.1064 MeV levels or between the 1.6735 MeV and ground states. The former choice has been made to provide a larger feed to the isomer. The beta spectra in coincidence with the 0.7311 MeV level is consistent with either interpretation.

The beta group with end point at 2.6 MeV which appears in coincidence with the 0.2419 MeV radiation is explained by the Ge(Li) gated spectrum associated with this same radiation as shown in Figure 4.3.5. This figure establishes yet another cascade from the 1.7800 level involving the 1.5377 and 0.2419 MeV gamma rays. The pressence in this spectrum of the 0.4193 MeV peak which defines the 0.4193-0.2419 MeV cascade, offers further support for the levels at 0.2419 and 0.6612 MeV.

The Krypton "Hi-Lo" experiment which was performed yielded no information and consequently is not discussed. This negative result is due to the weak intensity of the gamma rays above 1.780 MeV and the small number of events recorded during the experiment.

4.3.3 ^{90}Kr Decay Scheme and Discussion

The results of the foregoing analysis are presented graphically

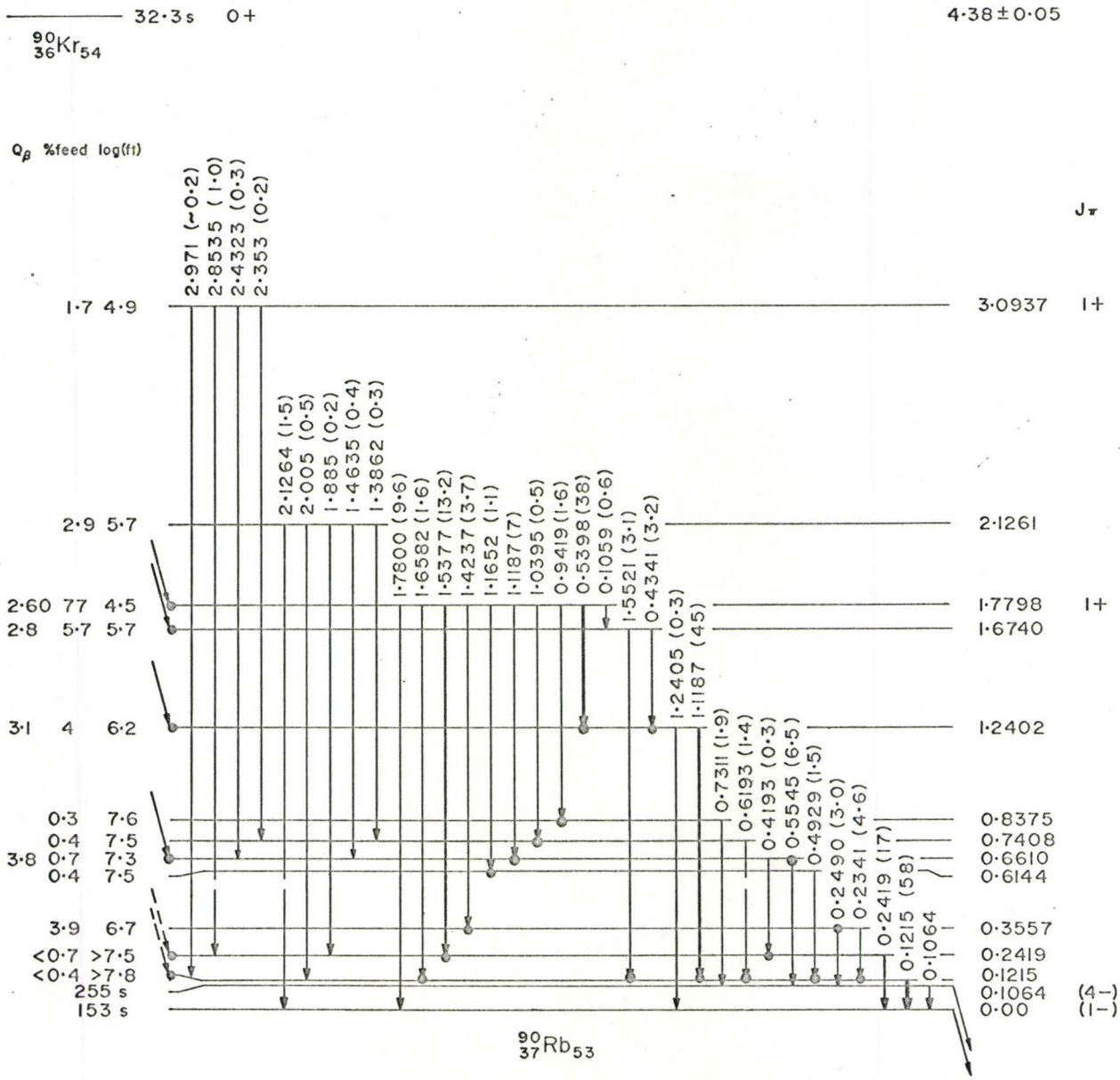

Figure 4.3.7 ^{90}Kr Decay Scheme

in the decay scheme of Figure 4.3.7. Solid dots at the terminus of transitions indicate that this radiation has been observed in coincidence. Included on this scheme are two levels at 3.0937 and 2.1261 MeV respectively which have been established tentatively on the basis of multiple energy fit only, making use of several gamma rays observed by Talbert. Also included on the basis of energy fit is the 0.1059 MeV transition placed between the 1.7798 and 1.6735 MeV levels. The level energies have been recalculated taking into account all well established modes of decay and as a result the values shown, in some cases, differ from the corresponding values mentioned in the text.

The beta groups indicated by solid arrows are those whose end points were determined, as shown, from beta-gamma measurements. These end points along with the energy of the associated levels give a weighted average value of 4.38 ± 0.05 MeV for the ground state Q-value. The intensities of the beta feeds with the exception of those indicated by dashed arrows were established by intensity balance at each level and normalized to total 100. For this purpose the ground state feed was assumed to be 0. This normalization was then used to calculate the gamma ray intensities in photons/100 decays.

The upper limits to the intensities of the beta feeds to the 0.1215 and 0.2418 MeV levels which are shown, were determined from the beta spectra observed in coincidence with these radiations. This was done by determining the intensity of the directly feeding transitions relative to that of the 2.6 MeV group using the net number of observed events between the end points of these two groups.

An analysis of the various configurations available for the low lying levels in ^{90}Rb in an effort to postulate tentative spin assignments yields very ambiguous results. The ground state of ^{87}Rb in which the neutrons form a complete major shell, indicates that the proton configuration consists of a $(p_{3/2})^{-1}$ arrangement in which the 37^{th} proton has been promoted to fill the $f_{5/2}$ level. Similarly the ground states of ^{89}Sr and ^{91}Zr indicate that the 51^{st} neutron, and therefore presumably also the 53^{rd} neutron, is in the $d_{5/2}$ level. The latter assumption is also supported by the $5/2^+$ assignment to the ^{93}Zr ground state.

The ground state and low lying states of ^{90}Rb would then be expected to be formed as a coupling of the $d_{5/2}$ neutron particle state and $(p_{3/2})$ proton hole state to produce states of negative parity and spins 1, 2, 3 and/or 4. Using Brennan and Bernstein's rules, since l and s are parallel for both neutron and proton, the lowest state in this multiplet should be either 1^- or 4^-. However, the even Rubidium isotopes systematically have a 2^- ground state, including ^{88}Rb.

The log (ft) of 4.5 for the beta decay to the 1.7798 MeV level indicates an allowed transition and hence a spin of 0 or 1 and positive parity for this level. A spin of 0 would imply a pure Fermi transition from the 0^+ parent which occurs only between isobaric analogue states. Since the neutrons are in the next major shell above the protons, the excitation of approximately 2 MeV is unlikely sufficient to justify classification of this level as the analogue of the ground state of ^{90}Kr. Consequently an assignment of 1^+ for this state can be made with confidence. For the same reason, the levels at 2.1261 and 3.0937 also have spin 1 and positive parity.

The 1.7798 MeV level subsequently decays directly to all the lower lying states except the 0.1069 MeV isomer. This decay pattern indicates that such a transition involves a large spin charge and suggests a possible assignment of 4^- for the isomer. This arrangement would account for the beta decay of this state to a level in ^{90}Sr tentatively established as 4^+, (see following chapter), and a 1^- ground state configuration would satisfy both Brennan and Bernstein's Rules and the observed weak gamma branching from the isomer. The intensity of the beta feed from the ^{90}Rb ground state as deduced from the gamma intensity balance in the ^{90}Sr level structure is consistent with the 1^- assignment.

From Figure 4.3.7, it is apparent that at least 11.4% of the transition intensity feeds the isomeric state. From the ^{90}Rb decay, it will be shown that the isomeric transition, including internal conversion, has an intensity of $\sim$1.3% leaving >10% to be de-excited by beta decay. This estimate is in fair agreement with the 18% figure deduced from the ^{90}Sr level structure.

It is quite possible, of course, that the simple shell model levels and the simple coupling schemes discussed are completely inadequate for even a simple minded description of these states. More likely, considerable configuration mixing included recoupling of the three neutrons, as well as such proton configurations as $|(p_{3/2})^4\ (f_{5/2})^5>$ or $|(p_{3/2})^3\ (f_{5/2})^6>$ with the $(p_{3/2})^3$ configuration recoupled or even $|(p_{3/2})^2\ (f_{5/2})^6\ (p_{1/2})^1>$ may be involved. Further insight into the actual nature of these states will need to await both theoretical calculations and further experimental investigations, if possible, into the multipolarities of the transi-

tions connecting these low lying levels.

4.4 ^{91}Kr Decay

4.4.1 ^{91}Kr Energy and Intensity Measurements

The information obtained concerning the decay of ^{91}Kr is very meagre as it was really only gleaned from the experiments on ^{90}Kr. Since the irradiation facility was operated at essentially its maximum rates in order to produce the ^{90}Kr sources it was not possible to make sources maximizing the ^{91}Kr activity. In fact, the ^{91}Kr was a contaminant in the ^{90}Kr experiments and something was learned of its decay because the effects which were observed had to be accounted for.

The energies and intensities of the gamma rays observed to belong to the decay of ^{91}Kr are listed in Table 4.4.1. Some of these were assigned by comparison with the work of Talbert, whose results are also listed. Some 97 transitions have been omitted from the latter list since they were not observed, even faintly, in the present investigation.

4.4.2 ^{91}Kr Coincidence Measurement and Decay Scheme Construction

The only gamma-gamma coincidence information that was obtained came from the 0.1215 MeV and 1.1187 MeV NaI gates of Figures 4.3.2 and 4.3.3 respectively. As well as the strong ^{90}Kr gating transitions these also contained lesser amounts of ^{91}Kr radiations of 0.1086 and 1.1086 MeV respectively. The 0.1086-0.6132 MeV coincidences establish a level at 0.7218 MeV for which the 0.7215 MeV radiation observed by Talbert is probably the ground state transition. The 1.1086-0.5068

TABLE 4.4.1

Gamma Rays Observed in the Decay of ^{91}Kr

Energy (MeV)				Intensity		Comments
Present Work		Talbert (1969)		Present Work	Talbert (1969)	
0.1086	2	0.1088	1	197	206	
		14 γ's				
0.5068	2	0.5066	1	100	100	
		4 γ's				
0.6132	2	0.6128	1	42	41	
		4 γ's				
		0.7215	2	3		
		18 γ's				
1.1086	5	1.1086	1	35*	43	strongly contaminated by ^{89}Kr
		22 γ's				
1.5012	3	1.5014	3	36*	37	strongly contaminated by ^{89}Kr
		35 γ's				
2.488	2	2.4844	3	17	23	
		7 γ's				
2.734	2	2.7356	4	11	10	
		28 γ's				

* Indicates assigned to ^{91}Kr decay by comparison with results of Talbert (1969).

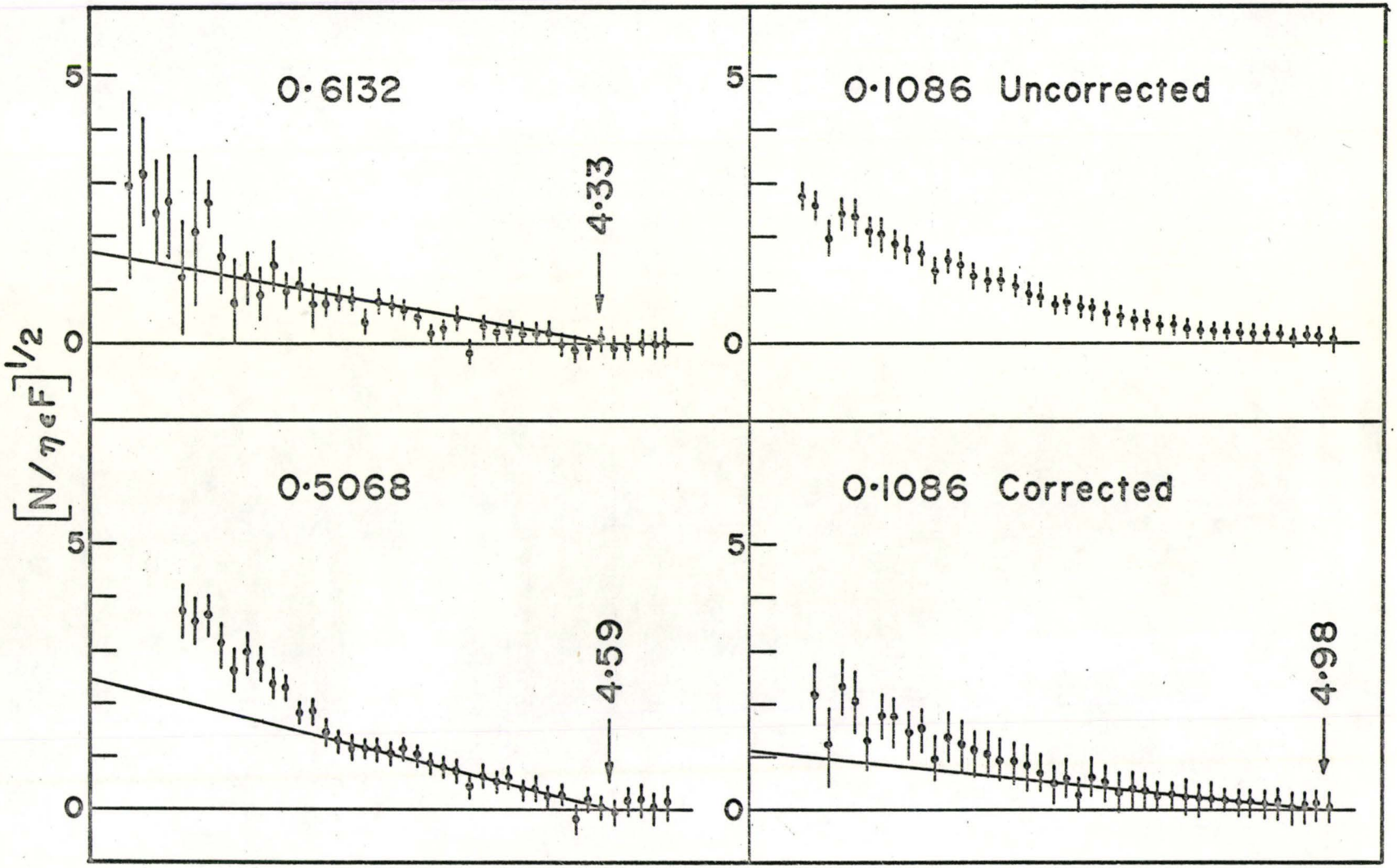

Figure 4.4.1 Fermi Plots of Beta Spectra in Coincidence with ^{91}Kr Gating Transitions

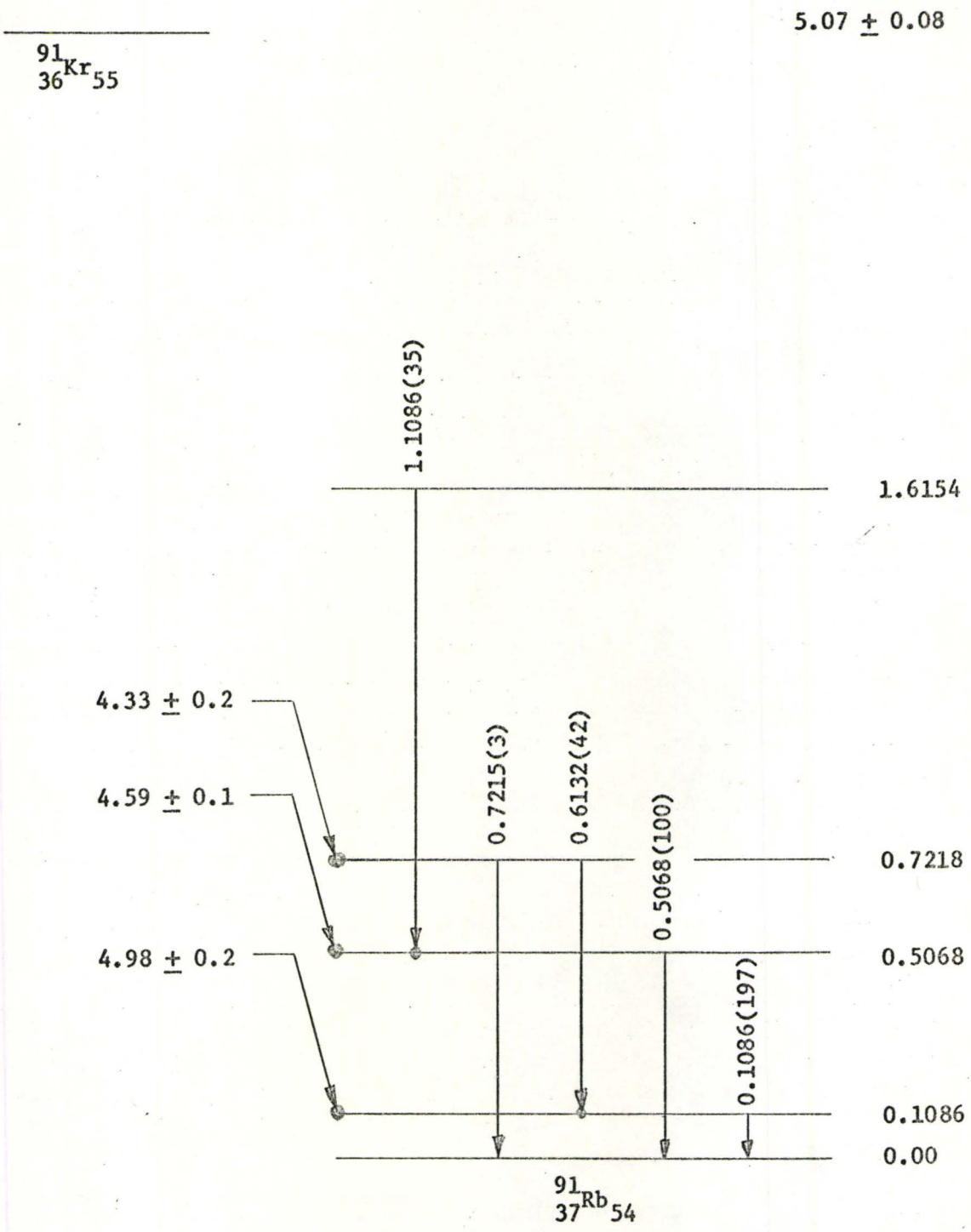

Figure 4.4.2 Partial Decay Scheme of ^{91}Kr as Delineated by This Investigation.

MeV coincidences observed in the other gate place a level at 1.6154 MeV from which there does not appear to be any ground state decay.

The results of the beta-gamma coincidence experiment for ^{91}Kr are shown in Figure 4.4.1 which presents the Fermi plots of the partial beta spectra in coincidence with the 0.1086, 0.5068 and 0.6132 MeV full energy peaks. Since the 0.6132 and 0.1086 MeV radiations are in coincidence, the latter gate contains both a directly feeding component and a cascade through the 0.7218 MeV level. Using the spectrum observed in coincidence with the 0.6132 MeV gamma ray, to correct the 0.1086 MeV gate for this contribution yields the results which are also shown in Figure 4.4.1. Analysis of these Fermi plots gives end points of 4.33 $\pm$ 0.2, 4.59 $\pm$ 0.1 and 4.98 $\pm$ 0.7 MeV for the beta groups feeding the 0.7218, 0.5068 and 0.1086 MeV levels respectively.

4.4.3 ^{91}Kr Decay Scheme and Discussion

The results of the above discussion are presented in Figure 4.4.2 as a decay scheme in miniature. From the observed beta decays the ground state separation of ^{91}Kr and ^{91}Rb is calculated to be 5.07 $\pm$ 0.08 MeV. In view of the extremely limited information embodied in this decay scheme any discussion seems to be even more unreasonable than that for the decay of ^{90}Kr.

CHAPTER 5

RESULTS AND DISCUSSION - ^{90}Rb AND ^{91}Rb

5.1 Previous and Concurrent Work

The radiations associated with the decay of ^{90}Rb have been investigated by several workers. The halflife has been measured by Kofoed-Hansen and Nielsen (1951), Johnson et al (1964), Amarel et al (1967) and Carlson et al (1969). The first of these two obtained single values of 2.74 and 2.91 min respectively, while the latter two showed that there were actually two components present with half-lives of approximately 255 sec and 153 sec,with the longer lived component being rather weak. In addition, Talbert (1969) has determined that the 255 sec activity is associated with an isomeric state at 0.1069 MeV in ^{90}Rb, as described in Chapter 4.

The beta and gamma decay scheme has also been investigated by Johnson et al (1964), by Zherebin et al (1967), and by Talbert (1969). The first two groups obtained very similar results, measuring the ground state Q-value to be 6.60 $\pm$ 0.10 MeV and 6.64 $\pm$ 0.12 MeV respectively. However, both groups were limited in their gamma ray investigations by the resolution of the NaI scintillation spectrometers used. The more recent work of Talbert employing an isotope separator arranged on line with an irradiation facility at a research reactor as well as better resolution Ge(Li) spectrometers, indicates, as does the present investigation, that the decay scheme is much more

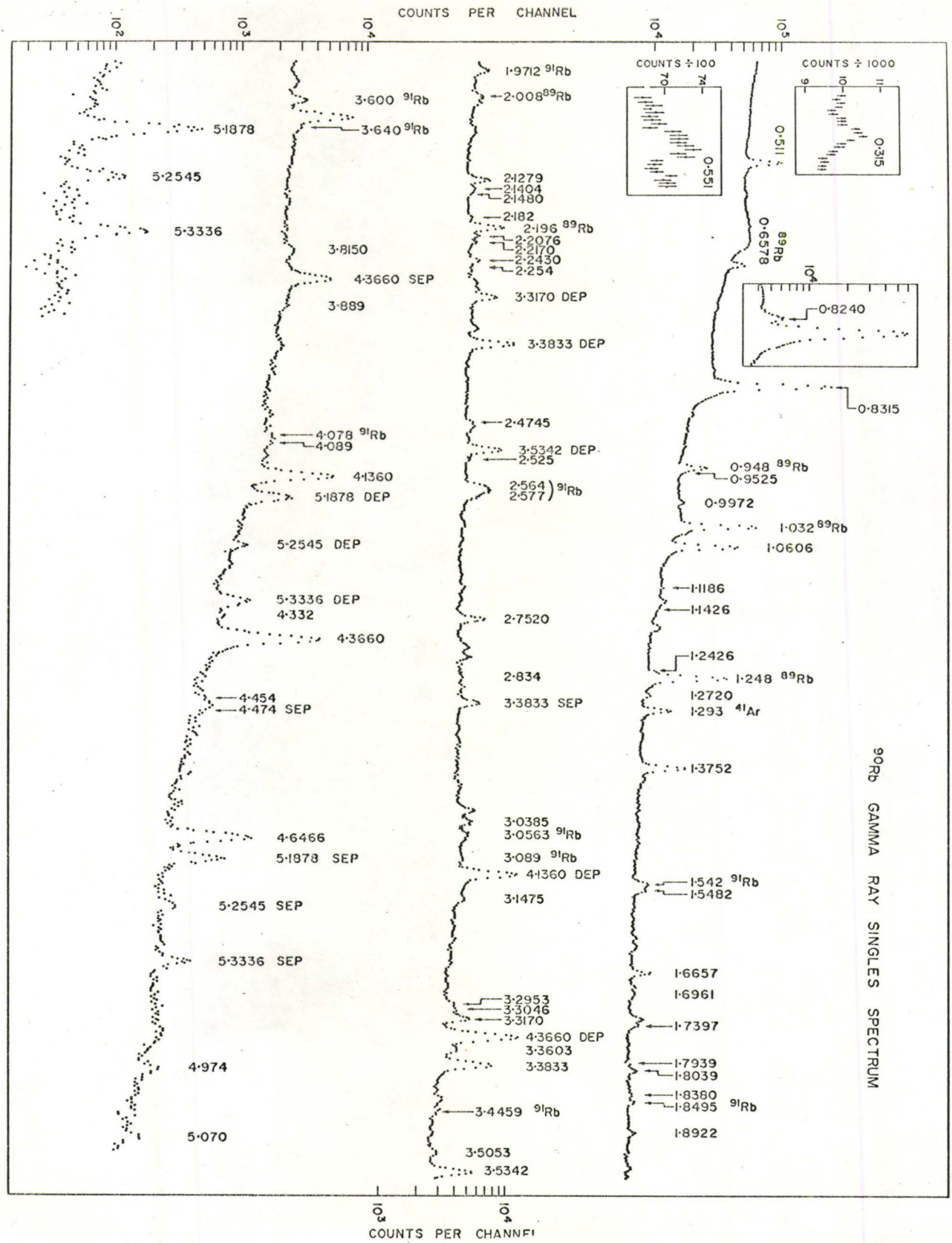

Figure 5.2.1 ^{90}Rb Singles Gamma Spectrum

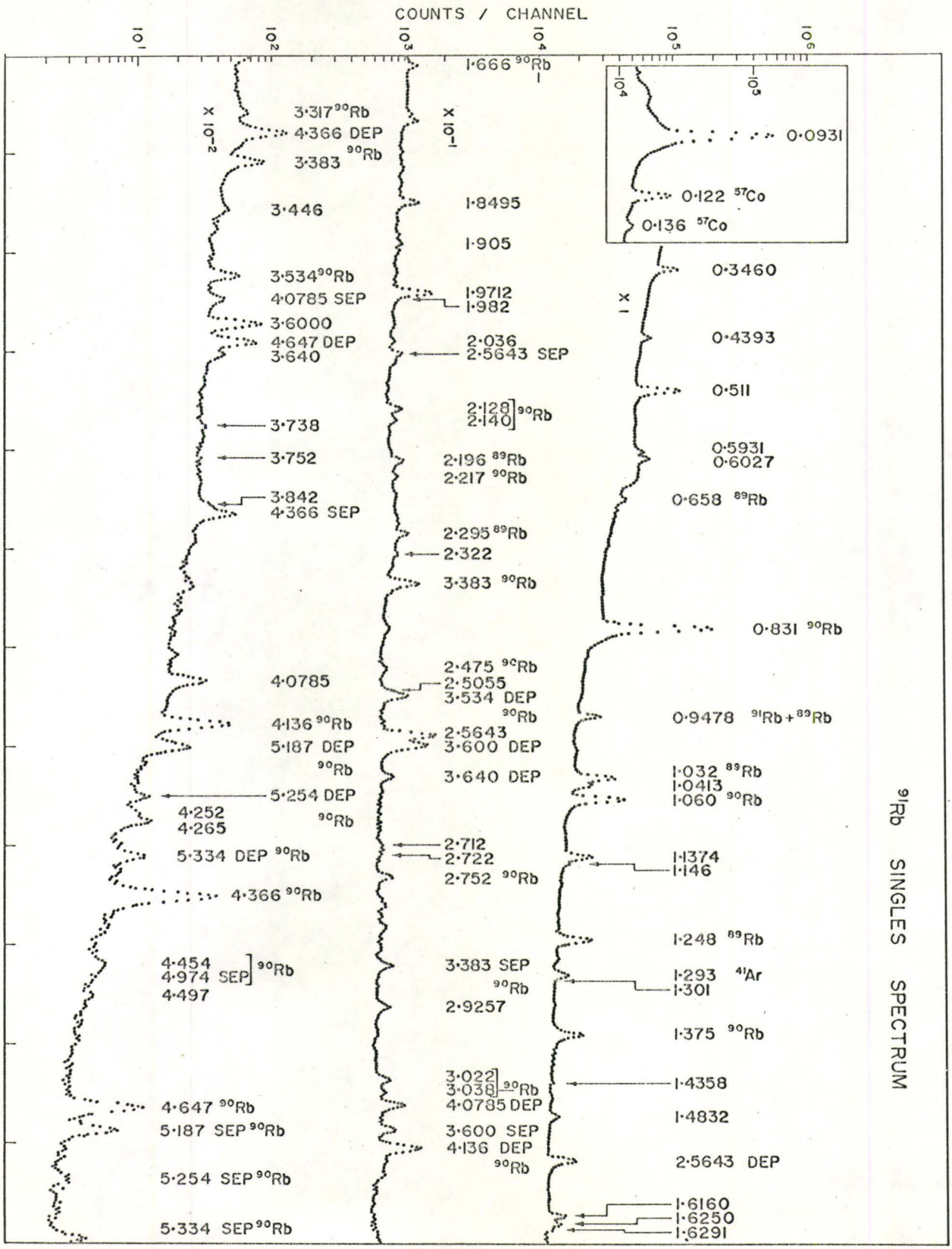

Figure 5.2.2 ^{91}Rb Singles Gamma Spectrum

complicated than previously expected.

The decay of ^{91}Rb has not previously been investigated. However, Carlson et al (1969) have measured the halflife to be 58.2 $\pm$ 0.2 sec and it is assumed that this group will also study the decay scheme as part of a systematic investigation of this region.

5.2 Identification of the Origin of the Gamma Rays

Figures 5.2.1 and 5.2.2 show respectively the singles gamma ray spectra obtained from sources prepared to maximize ^{90}Rb and ^{91}Rb as described in 5.3.1. Both figures have inserts taken from other experiments performed to examine the low energy portion of the spectrum in finer detail. In the case of the ^{91}Rb insert, the full energy peaks associated with two energy standard transitions are also included. Using the procedure outlined in 5.3.2 an attempt was made to identify the decay to which each peak belonged. Table 5.2.1 shows a representative sample of the values involved, to indicate the quality of the distinction. In many cases of weak peaks which appeared in the ^{91}Rb spectrum, there were no corresponding peaks occuring in the ^{90}Rb spectrum. These peaks were tentatively assigned to the ^{91}Rb decay. One line, at 1.4547 MeV, was assigned to the ^{90}Rb decay by comparison with the results of Talbert (1969).

5.3 ^{90}Rb Decay

5.3.1 ^{90}Rb Energy and Intensity Measurements

The results of energy and intensity measurements as outlined in Chapter 3 are summarized in Table 5.3.1. The energies are the averages of at least two and in some cases three separate determinations

TABLE 5.2.1

Ratios of Some Peaks Observed in Rubidium Singles Experiment

(Ratios are Peak Area ^{90}Rb Spectrum/Peak Area ^{91}Rb Spectrum)

E_γ(MeV)	Ratio	Isotope Classification
0.8315	1.19	90
0.9478	1.05	89 + 91
1.0321	2.54	89
1.0606	1.19	90
1.1375	0.19	91
1.1460	0.41	91
1.2482	2.62	89
1.6657	1.50	90
1.8495	0.21	91
1.9712	0.19	91
2.008	2.67	89
2.4745	1.35	90
2.5643	0.18	91
2.7520	1.43	90
3.0385	1.69	90
3.0563	0.24	91
3.5342	1.16	90
3.5675	0.25	91
4.0785	0.18	91

i.e. from the ^{90}Rb spectrum, the ^{91}Rb spectrum and the initial calibration of ^{90}Rb with standards. The error in the energy is given as the error in the last significant figure quoted in the energy. Intensities are normalized to the strong transition of 0.8315 MeV as 100. Errors in intensities are not given individually but are believed to be of the order of 10% on the stronger peaks where the error is largely generated from uncertainties in the detector efficiency curve, and rising to the order of 20% or greater on the weaker peaks where a further error is introduced in determining the area of the full energy peak.

Also included in the table are the energy and intensity measurements of Talbert (1969). The position of the gamma ray in the decay scheme is indicated by the column headed "Classification" and the basis for this assignment is summarized in the form of coincidence probabilities with the0.8315 MeV (γ_1), 1.0606 MeV (γ_2) or other gamma rays as listed. These latter columns were prepared from an analysis of the coincidence data as outlined below.

5.3.2 ^{90}Rb Coincidence Measurements and Decay Scheme Construction

Figure 5.3.1 shows the Ge(Li) projection from the "Hi-Lo" Rubidium experiment along with a singles spectrum containing approximately the same total number of counts as the projection, taken with the same experimental configuration. The absence or severely attenuated intensity of the prominent full energy peaks associated with the 3.0385, 3.3833, 4.1360, 4.3660, 4.6466, 4.974, 5.070, 5.1878, 5.2545 and 5.3336 MeV gamma rays indicates that these are ground state transitions and establishes levels at these energies. These classi-

TABLE 5.3.1

Gamma Rays Observed in the Decay of ^{90}Rb

Energy (MeV)				Intensity		Classification	Basis for Classification			
Present Work		Talbert (1969)		Present Work	Talbert (1969)		E	γ_1	γ_2	Other Gammas
0.1064	5	0.1069	3	0.12		253 sec isomeric transition in ^{90}Rb				
0.315	1	0.3149	3	0.4	0.35	2.2068→1.8921	E	0.5	0.45	
0.551	1	0.5514	3	0.3	0.4	2.2068→1.6555	E	0.33		0.33(0.824)
		0.5863	6		0.2	4.0360→3.4497	E			
		0.7204	4		0.35	2.9275→2.2068	E			
0.8240	2	0.8237	1.5	3.8	4.2	1.6555→0.8315	E	3.8		
0.8315	1	0.83115	1.5	100	100	0.8315→0	E		20.5	
0.838				0.2*		4.974 →4.1360	E			0.2(4.136)
0.871	1			0.3*		2.5271→1.6555	E	0.3		0.3(0.824)
0.9525	2	0.9524	2	0.7	0.85	3.4497→2.4972	E	0.7		0.6(1.666)
				0.3		4.3355→3.3833	E			0.3(3.383)
0.9972	2	0.9975	2	0.9	0.5	4.0360→3.0385				0.9(3.038)
		1.0320	6		0.3					
		1.0388	3		0.6	5.1876→4.1485	E			0.4(3.317)
1.0606	1	1.0604	2	19	19	1.8921→0.8315	E	19		
1.1186	6			0.3		5.2545→4.1360	E			0.2(4.136)

Energy (MeV)				Intensity		Classification	Basis for Classification			
Present Work		Talbert (1969)		Present Work	Talbert (1969)		E	γ_1	γ_2	Other Gammas
1.1426	20	1.1412	4	0.4	0.4			0.7		
1.2426	2	1.2427	2	1.1	1.6	3.4497→2.2068	E	1.3		1.1(1.375)
1.2720	2	1.2716	3	0.8	0.9	2.9275→1.6555	E	0.8		0.8(0.824)
		1.3268			0.6	4.3660→3.0385	E			0.3(3.0385)
1.3752	1	1.3754	2	8.1	9.8	2.2068→0.8315		8.4		1.1(1.240) 2.1(2.128) 1.3(2.834)
1.377				0.4*		3.5835→2.2068				0.4(1.375)
1.4547	30	1.4562	7	0.4**	0.3					
		1.4895	7		0.35	3.3833→1.8921	E			
1.6657	2	1.6653	2	2.8	3.0	2.4972→0.8315	E	2.6		
1.6961	6	1.6960	5	0.7	0.75	2.5271→0.8315	E	1.1		
1.7397	4	1.7386	4	1.3	0.85	2.5712→0.8315	E	1.2		0.3(0.61) 0.3(1.03)
1.7939	8	1.7938	7	0.4	0.4	3.4497→1.6555	E	0.35		0.35(0.824)
1.8039	4	1.8039	4	1.1	1.1	5.1876→3.3833	E			1.2(3.383)
1.8380	10	1.8386	7	0.5	0.4	4.3355→2.4972	E			
1.8922	6	1.8921	4	1.1	1.0	1.8921→0	E			
2.1279	2	2.1282	7	2.0	2.5	4.3355→2.2068	E	2.4		2.1(1.375)
2.1404	6	2.1393	7	1.0	0.5	4.0325→1.8921		0.8		
2.1480	10	2.1484	7	0.3	0.45	5.1876→3.0385	E			0.3(3.0385)
2.169	1			0.8*				0.7		

Energy (MeV)				Intensity		Classification	Basis for Classification			
Present Work		Talbert (1969)		Present Work	Talbert (1969)		E	γ_1	γ_2	Other Gammas
2.1820	10	2.1829	7	0.4	0.4			0.6	0.5	
2.2076	8	2.2072	5	1.3	0.75	3.0385→0.8315	E	1.3		
2.2170	8	2.2162	5	0.9	0.85			1.3		
2.2430	2	2.2430	10	0.6	0.7	3.8985→1.6555	E	0.8		0.8(0.832)
2.254	3	2.2570	8	0.5	0.35	4.1485→1.8921	E	<0.6	<0.5	
2.4745	5	2.4737	4	1.3	1.1	4.3660→1.8921	E	1.3	1.1	
2.525	2			0.6		2.5271→0	E			
2.551	2			0.4*		3.3833→0.8315	E	0.4		
2.566	2			0.4*				0.4		
2.7520	3	2.7527	3	5.2	5.6	3.5835→0.8315	E	4.0		
2.754	2			0.2*		4.6466→1.8921	E		0.2	
2.834	2	2.8345	4	1.0	1.15	5.0397→2.2068	E	1.2		1.0(1.375)
3.0385	5	3.0389	4	2.9	1.9	3.0385→0	E			0.8(0.99) 0.3(2.148)
3.1475	10	3.1487	4	2.3	1.8	5.0397→1.8921	E	1.3	1.3	
3.2953	6	3.2954	6	1.3	1.3	5.1876→1.8921	E	1.5	1.4	
3.3046	6	3.3043	5	1.5	1.5	4.1360→0.8315	E	1.6		
3.3170	2	3.3171	4	5.0	7.3	4.1485→0.8315	E	4.3		~0.15(1.03)
3.3603	10	3.3616	5	2.4	1.6	5.2540→1.8921	E	2.4	1.6	

Energy (MeV)				Intensity		Classification	Basis for Classification			
Present Work		Talbert (1969)		Present Work	Talbert (1969)		E	γ_1	γ_2	Other Gammas
3.3833	3	3.3833	4	13	12.3	3.3833→0	E			0.4(0.95) 1.2(1.80)
3.5053	10	3.5036	6	1.1	1.0	4.3355→0.8315	E	0.8		
3.5342	2	3.5342	4	8.3	7.5	4.3660→0.8315	E	7.0		
3.654	2			0.3*						
3.8150	10	3.8149	5	1.2	0.9	4.6466→0.8315	E	1.2		
3.889	2			0.6						
4.060	2	4.062		0.3*	trace	4.891 →0.8315		0.3		
4.089	2	4.0871	9	0.8	0.75	4.921 →0.8315		0.7		
4.1360	3	4.1353	5	14	12	4.1360→0	E			0.2(0.838)
4.206	3	4.2099	10	0.4*	0.45	5.0397→0.8315	E	0.4		
4.260	2	4.258		0.4*		5.091 →0.8315		0.4		
4.332	2	4.332		0.4		5.163 →0.8315		0.5		
4.356	2			0.6*		5.1876→0.8315	E	0.6		
4.3660	2	4.3659		15	14.6	4.3660→0	E			no γ-γ
4.454	2	4.4537	9	0.6	0.5	5.285 →0.8315		0.7		
4.6466	6	4.6460	7	4.4	4.1	4.6466→0	E			no γ-γ
4.974	2	4.9739	7	0.4	0.4	4.974 →0				no γ-γ
5.070	1	5.0699	8	0.28	0.3	5.070 →0				no γ-γ

Energy (MeV)				Intensity		Classification	Basis for Classification			
Present Work		Talbert (1969)		Present Work	Talbert (1969)		E	γ_1	γ_2	Other Gammas
5.1878	2	5.1878	7	2.1	2.3	5.1876→0	E			no γ-γ
5.2545	6	5.2545	7	0.47	0.5	5.2540→0	E			no γ-γ
5.3336	3	5.3329	7	0.85	0.85	5.3336→0	E			no γ-γ

Notes

* Indicates transition seen only in coincidence.

** Indicates assignment made to the decay of this nuclide by comparison with Talbert's results.

E Indicates energy fit.

fications are supported by the further absence of these full energy peaks from the "Hi-Lo" NaI gate associated with the strong 0.8315 MeV transitions as presented in Figure 5.3.2. This gate has been split at approximately 4.5 MeV with the upper section plotted on a linear scale.

Also shown in Figure 5.3.2 is the "Hi-Lo" NaI gate associated with the 1.0606 MeV transition. The appearance of several gamma rays in both gates indicates that the 1.0606 and 0.8315 MeV pair form a cascade (which is supported by directly observed coincidences in the "Lo-Lo" experiment described below) with the 0.8315 MeV member lower because of its intensity, and that the transitions in common with the two gates populate a level at 1.8921 MeV. The depopulated levels are then at 5.2545 and 5.1878 MeV as previously defined by ground state transitions, de-excited by the 3.3603 and 3.2953 MeV gamma rays respectively and at 5.040 MeV, a new level for which there is other supporting evidence, de-excited by the 3.1475 MeV. Of the transitions which appear only in the 0.8315 MeV gate, the ones at 4.454, 4.332, 4.260, 4.089, 4.060 and 3.3170 MeV have been used to define levels at 5.285, 5.163, 5.091, 4.921, 4.891 and 4.1485 MeV respectively for which they are the only evidence, while the one at 3.5053 MeV is used to define a level at 4.3355 MeV for which there is other support. The remaining gamma rays in this gate de-excite previously defined levels with the 4.356, 4.206, 3.8150, 3.5342 and 3.3046 MeV transitions connecting levels at 5.1878, 5.040, 4.6466, 4.3660, 4.1360 MeV respectively with the first excited state at 0.8315 MeV, while the 2.834 MeV connects levels at 5.040 and 2.2068 MeV respectively. This latter terminal level

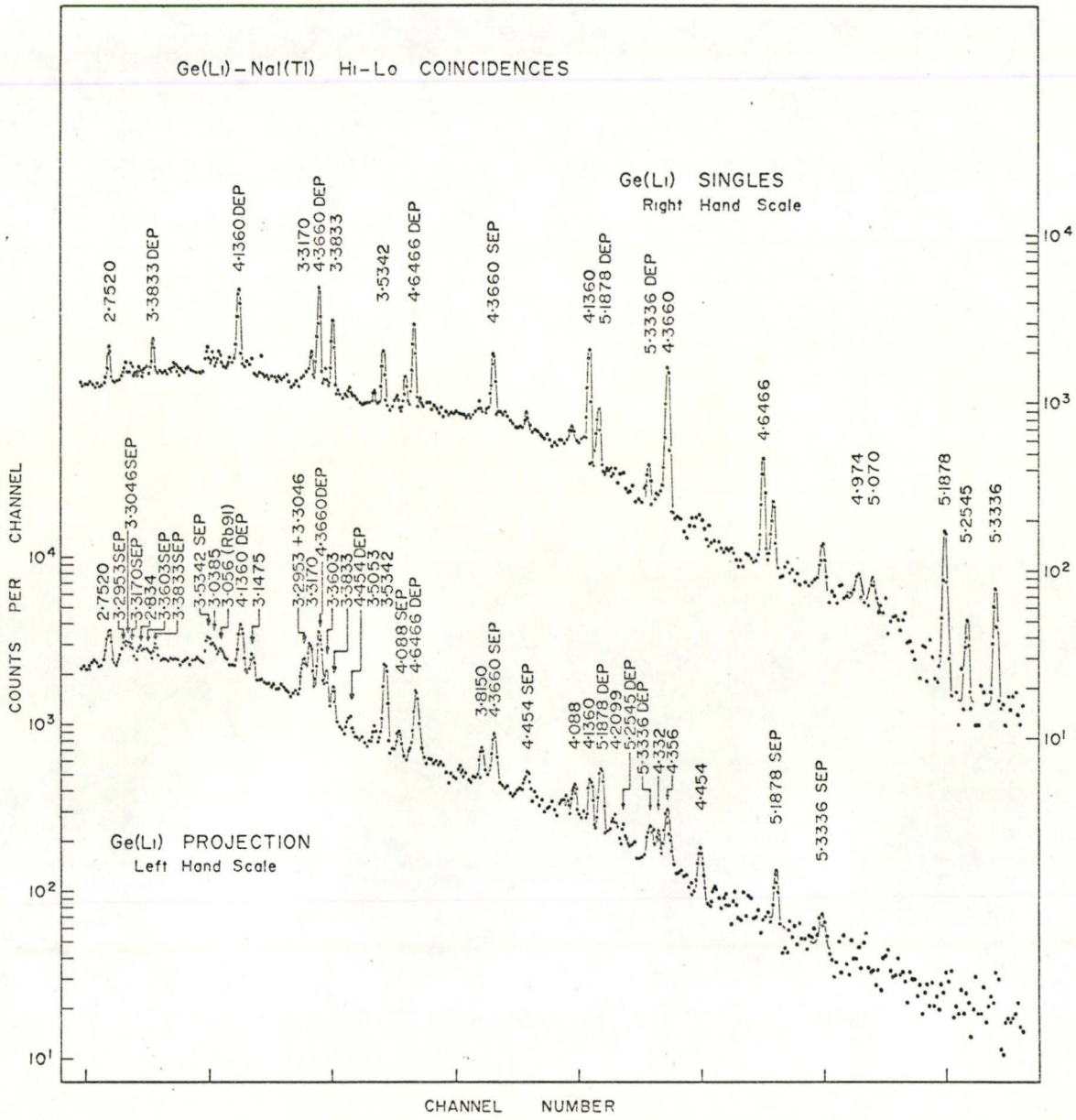

Figure 5.3.1 ^{90}Rb Gamma Coincidence Spectra - Ge(Li) Projection and Singles from "Hi-Lo" Experiment

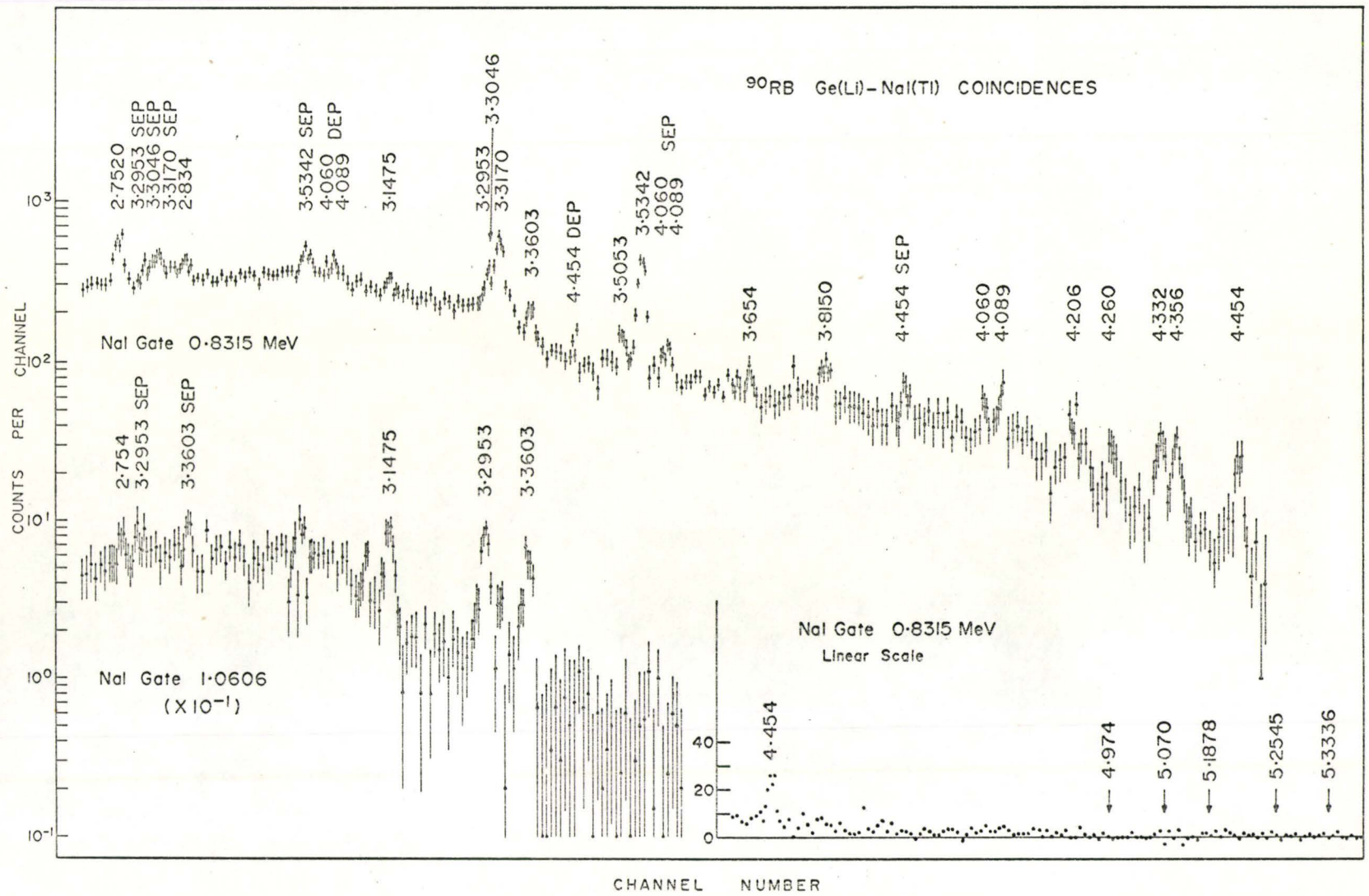

Figure 5.3.2 ^{90}Rb Gamma Coincidence Spectra - 0.8315 and 1.0606 MeV NaI Gates from "Hi-Lo" Experiment

is established from "Lo-Lo" coincidence evidence to be discussed below, and is connected with the 0.8315 MeV state by the appropriate radiation to generate these observed coincidences.

The relatively strong peak occuring at 2.7520 MeV in the 0.8315 MeV gated spectrum has the correct intensity to establish a direct 2.7520-0.8315 cascade. The small peak of approximately the same energy in the 1.0606 MeV gated spectrum has much too small a coincidence probability to indicate a 2.7520-1.0606-0.8315 cascade. This intensity relationship is also evident from the 2.7520 Ge(Li) gated spectrum shown in Figure 5.3.3. To be in triple cascade the 1.0606 MeV NaI full energy peak in this spectrum should be approximately 2/3 the height of the 0.8315 MeV full energy peak as illustrated by the 3.1475 MeV Ge(Li) gated spectrum also in Figure 5.3.3. The presence of the weaker peaks at approximate energies of 1.06 MeV in the Ge(Li) gated spectrum and at 2.752 MeV in the NaI gated spectrum does indicate, however, that there are coincidences between lines of approximately these energies. Two arrangements may be used to account for this data, both of which cause another gamma ray to depopulate the level previously established at 4.3660. One of these involves using a 2.754 MeV gamma ray to connect this state to the one at 1.8921 MeV which is de-excited by the 1.0606 MeV transition. The other would place a 1.063 MeV line between the 4.3660 MeV level and the level at 3.5835 MeV as established by the 2.7520-0.8315 coincidences. The first of these has been indicated on the decay scheme and included in Table 5.3.1.

Figure 5.3.3 also shows the NaI spectra in coincidence with 3.0385, 3.3170, 3.3833 and 4.1360 MeV Ge(Li) full energy peaks. The

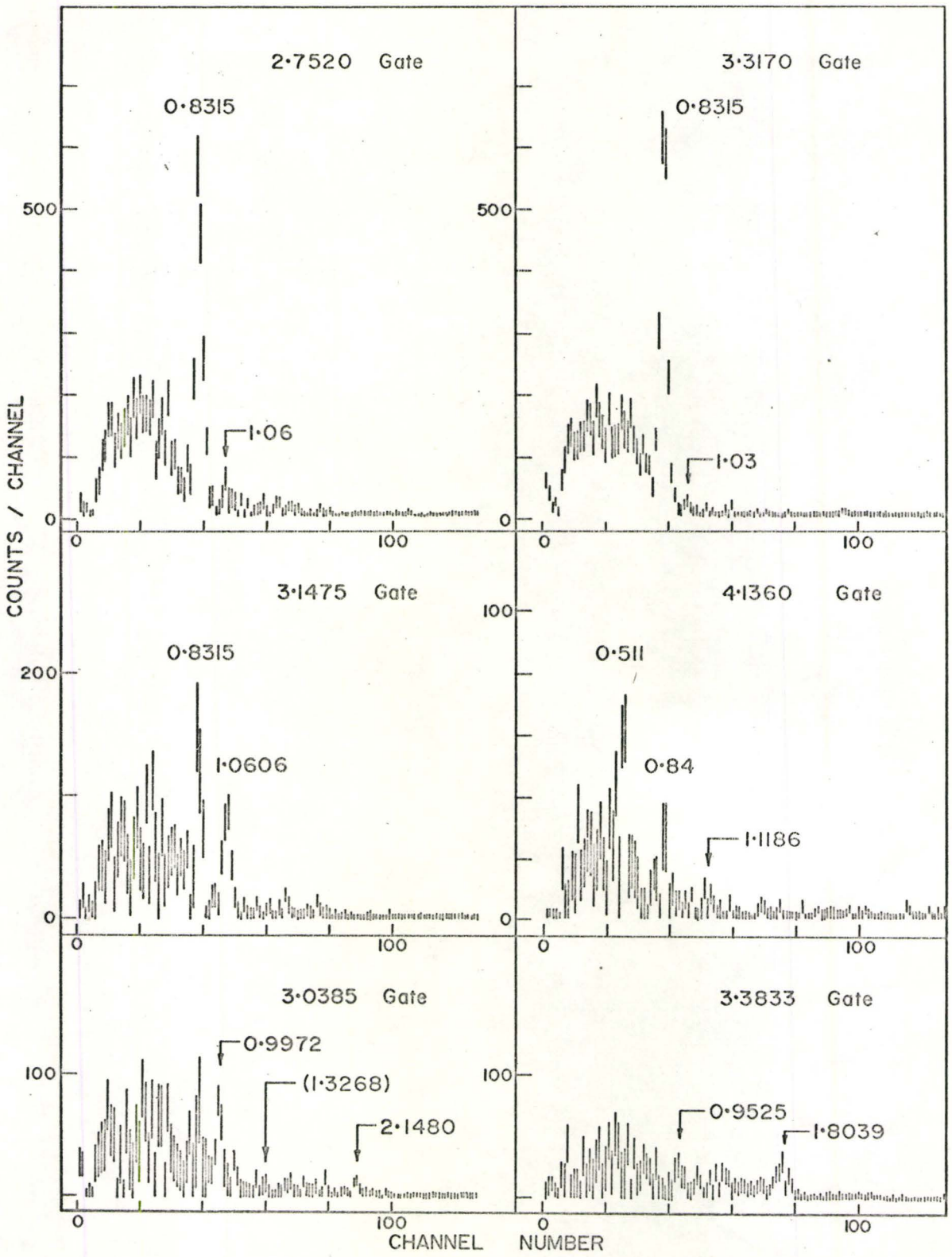

Figure 5.3.3 ^{90}Rb Gamma Coincidence Spectra - Ge(Li) Gates

3.0385 MeV gate is very poor as a result of the quality of the data in the region from which it was generated, as may be seen from the projection. However, there is a hint of a coincidence peak at 2.1480 MeV and also at 1.3268 MeV and a definite one at 0.9972 MeV. Using the 3.0385 as the ground state transition of this group, the 2.1480 and 1.3268 MeV lines fit well in between this and the levels at 5.1878 and 4.3660 MeV which have been previously well defined. The 0.9972 MeV gamma ray, on the other hand defines a new level at 4.0360 MeV for which the only other supporting evidence is the energy fit of the 0.5863 MeV transition observed by Talbert between this level and the well defined state at 3.3833 MeV.

The 3.3170 MeV Ge(Li) gate indicates clearly that this transition feeds the first excited state as concluded from the 0.8315 MeV NaI gate. However, it also shows that a weaker transition of approximately 1.03 MeV feeds the 4.1485 MeV level which the 3.33170 MeV gamma ray de-excites. From energy fit and coincidence probability calculations as listed in Table 5.3.1, this was taken to be the 1.0388 MeV transition observed by Talbert which would then depopulate the level at 5.1878 MeV. The 1.8039 MeV gamma ray observed in the 3.3833 MeV gate also de-excites this level, leading to the state defined by the ground state gating transition. The 0.9525 coincidences observed in this same gate provide supporting evidence for the level previously defined by 3.5053-0.8315 MeV coincidences. However, this transition does not contain the whole strength of the 0.9525 decay as indicated by the coincidence probability in Table 5.3.1. The remaining strength has been placed through its appearance in the 0.8315 MeV "Lo-Lo" gate as will be outlined below.

The remaining 4.1360 MeV Ge(Li) gate, which also contains some 4.6466 MeV single escape peak, shows coincidences with peaks of energy around 0.84 and 1.12 MeV. Since the intensity of the 0.84 MeV peak is much too weak to allow a 4.1360-0.8315 MeV cascade, a gamma ray of energy 0.838 MeV was introduced to connect the well defined levels at 4.974 and 4.1360 MeV. The 1.1186 MeV transition fits well between the previously defined 5.2545 MeV level and that defined by the gating transition.

The 0.8315 and 1.0606 MeV NaI gates for the "Lo-Lo" coincidence experiment are shown in Figures 5.3.4 and 5.3.5 respectively. The former has had the underlying background subtracted while the latter has not. The peaks due to impurities either from other nuclides or underlying Comptons in the 1.0606 MeV gate have been enclosed in brackets. The reciprocal occurence in these gates of the gating transitions themselves, establishes directly the 1.0606-0.8315 MeV cascade inferred previously, with the 0.8315 MeV transition obviously the lower member because of its higher intensity. This level is also de-populated by a 1.8922 MeV transition on the basis of energy fit.

The strong 1.3752 MeV transition which occurs in the 0.8315 MeV gate, establishes a level at 2.2068 MeV which was mentioned above. However, this mode contains only 90% of the transition strength of the 1.3752 MeV decay as evident from the 1.3752 MeV Ge(Li) gated spectrum shown in Figure 5.3.6. This indicates that approximately 10% of this transition strength goes between a previously defined level at 3.5835 MeV and the 2.2068 MeV state. This NaI spectrum also shows coincidences at 1.2426, 2.1279 and 2.834 MeV. The 2.834-1.3752 MeV relationship was noted in the "Hi-Lo" analysis and is confirmed

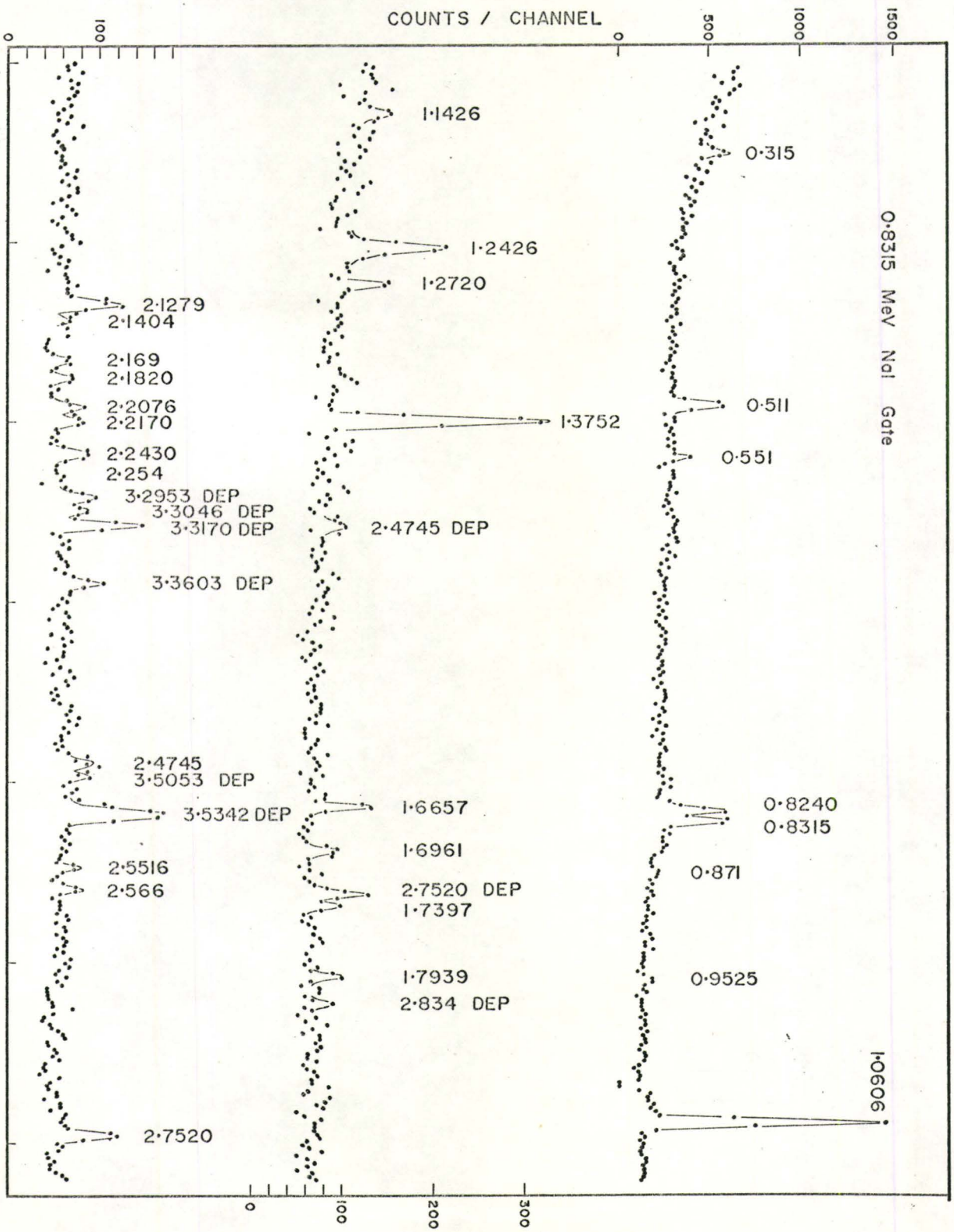

Figure 5.3.4 ^{90}Rb Gamma Coincidence Spectrum - 0.8315 MeV NaI Gate from "Lo-Lo" Experiment

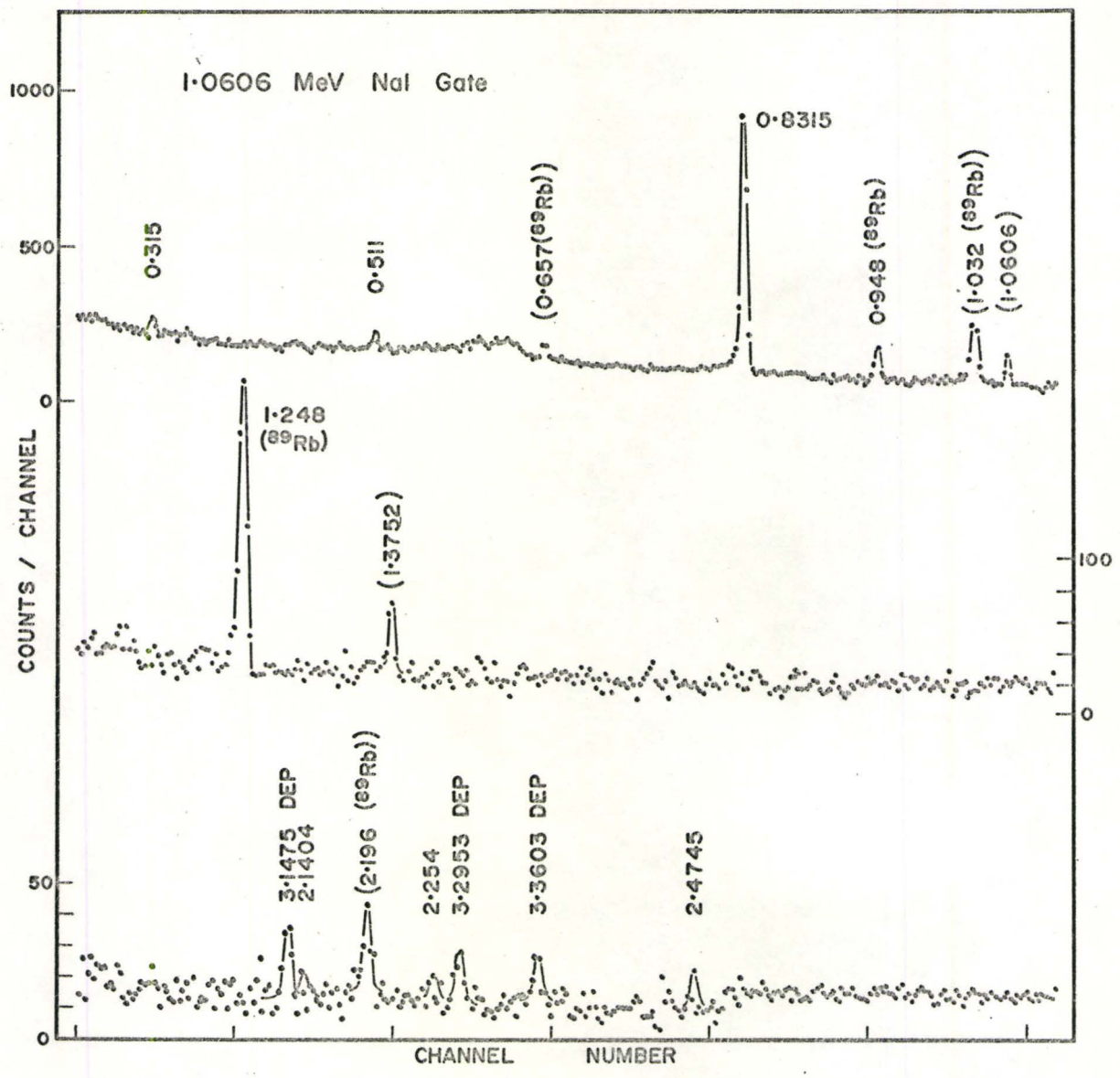

Figure 5.3.5

^{90}Rb Gamma Coincidence Spectrum - 1.0606 MeV NaI Gate from "Lo-Lo" Experiment

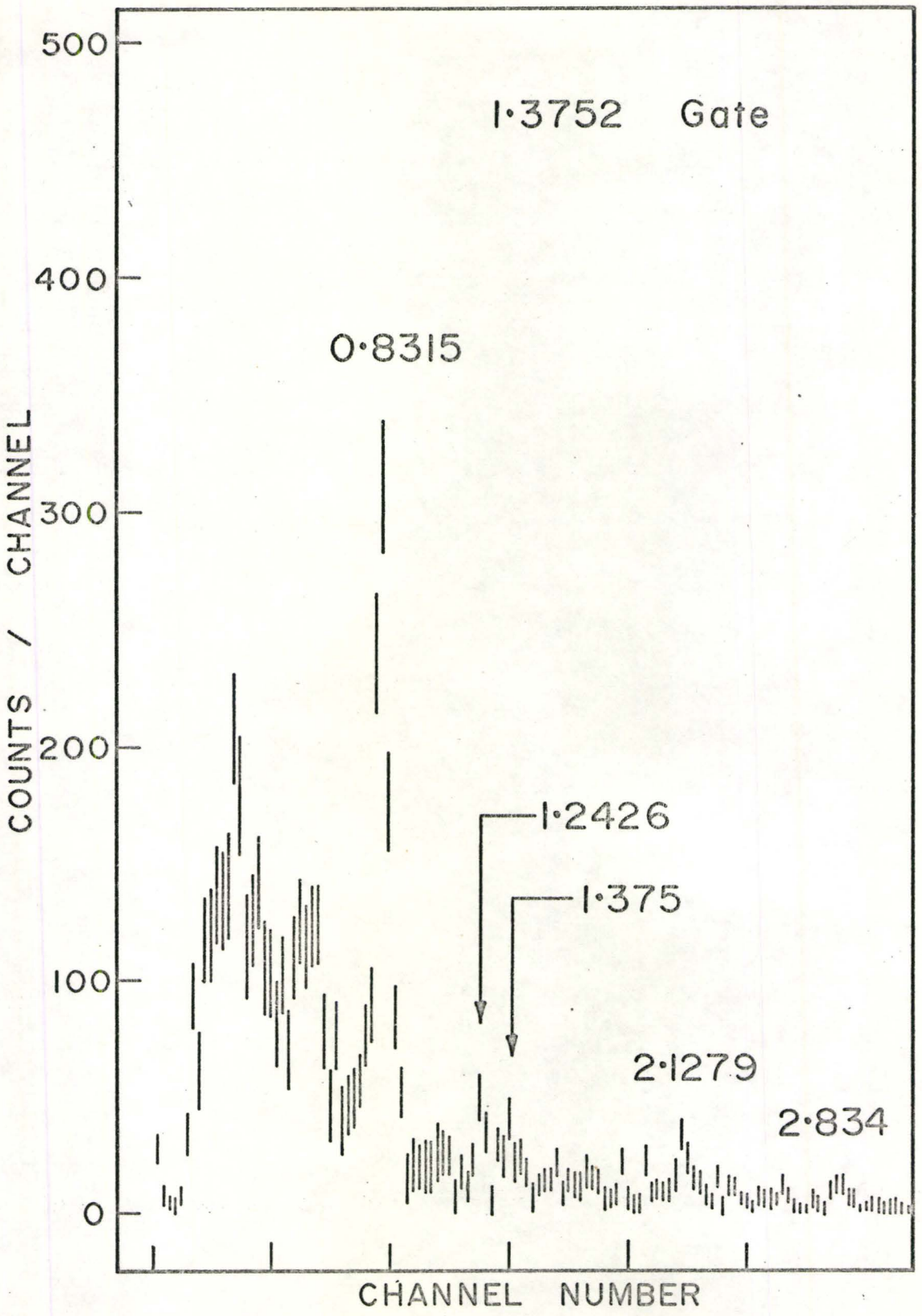

Figure 5.3.6

^{90}Rb Gamma Coincidence Spectrum - 1.3752 MeV Ge(Li) Gate from "Lo-Lo" Experiment

here. The 2.1279 MeV transition is found to depopulate the well established 4.3360 MeV level while the 1.2426-1.3752 MeV cascade establishes a new level at 3.4497 MeV for which there is other support.

The 0.315, 2.254 and 2.4745 MeV gamma rays which occur in both the 1.0606 and 0.8315 MeV gates have been placed between the 1.8921 MeV state and previously well established levels as indicated in Table 5.3.1. The 2.1404 MeV radiation has been used to define a new level at 4.0325 MeV for which it is the only evidence.and the

The occurence in Figure 5.3.4 of the 0.8240 MeV full energy peak indicates 0.8240-0.8315 MeV coincidences. Furthermore, since these radiations will be unresolved in NaI, the gating region for this spectrum will contain both, thus accounting for the 0.8315 MeV peak of the same area in this gate. For this reason also, any gamma rays which populate the level at 1.6555 MeV defined by these two transitions should occur with twice the coincidence probability otherwise expected. Such transitions include the 0.551, 0.871, 1.2720, 1.7939 and 2.2430 MeV gamma rays. All these coincidence relationships with the exception of the 0.871 and 2.2430 MeV provide supporting evidence for the existence of previously established levels. The 0.871 MeV transition establishes a new level at 2.5276 MeV whose existence is confirmed by a possible 2.525 MeV ground state transition and observed 1.6961-0.8315 MeV coincidences. The 2.2430 MeV gamma ray defines a new level at 3.8985 MeV for which it is the only evidence.

Of the remaining transitions observed in the 0.8315 MeV gated spectrum of Figure 5.3.4, the ones at 1.6657 and 1.7397 MeV have been

used to establish levels at 2.4972 and 2.5712 MeV respectively, while the ones at 2.2076 and 2.551 MeV have been placed between the established levels at 3.0385 and 3.3833 MeV respectively and the first excited state.

In addition to the data discussed above, several coincidence probabilities are quoted in Table 5.3.1 for which the corresponding data are not shown. Most of these involve the analysis of NaI spectra in coincidence with weak Ge(Li) full energy peaks and as a result energy and area determinations are very imprecise. Generally the possible coincidences observed do not correspond to transitions observed in singles experiments, or to energy differences between well established levels and consequently have been omitted from the decay scheme.

5.3.3 ^{90}Rb Decay Scheme and Discussion

The results of the preceeding coincidence observations are summarized pictorially in the decay scheme of Figure 5.3.7. Transitions which have been observed in coincidence are indicated with a solid dot at the terminal level. Level energies indicated have been calculated using all possible decay chains and as a result may differ slightly from the corresponding values referred to in the text. Using the level structure deduced from coincidence data, several other gamma rays have been inserted on the basis of energy fit alone. These are at energies of 0.5863, 0.7204, 1.1186, 1.3268, 1.4895 and 1.8380 MeV and the positions are indicated in Table 5.3.1. In addition the transitions at 1.1426, 2.169, 2.1820 and 2.2170 MeV which have been weakly observed in coincidence have been omitted, as have gamma rays

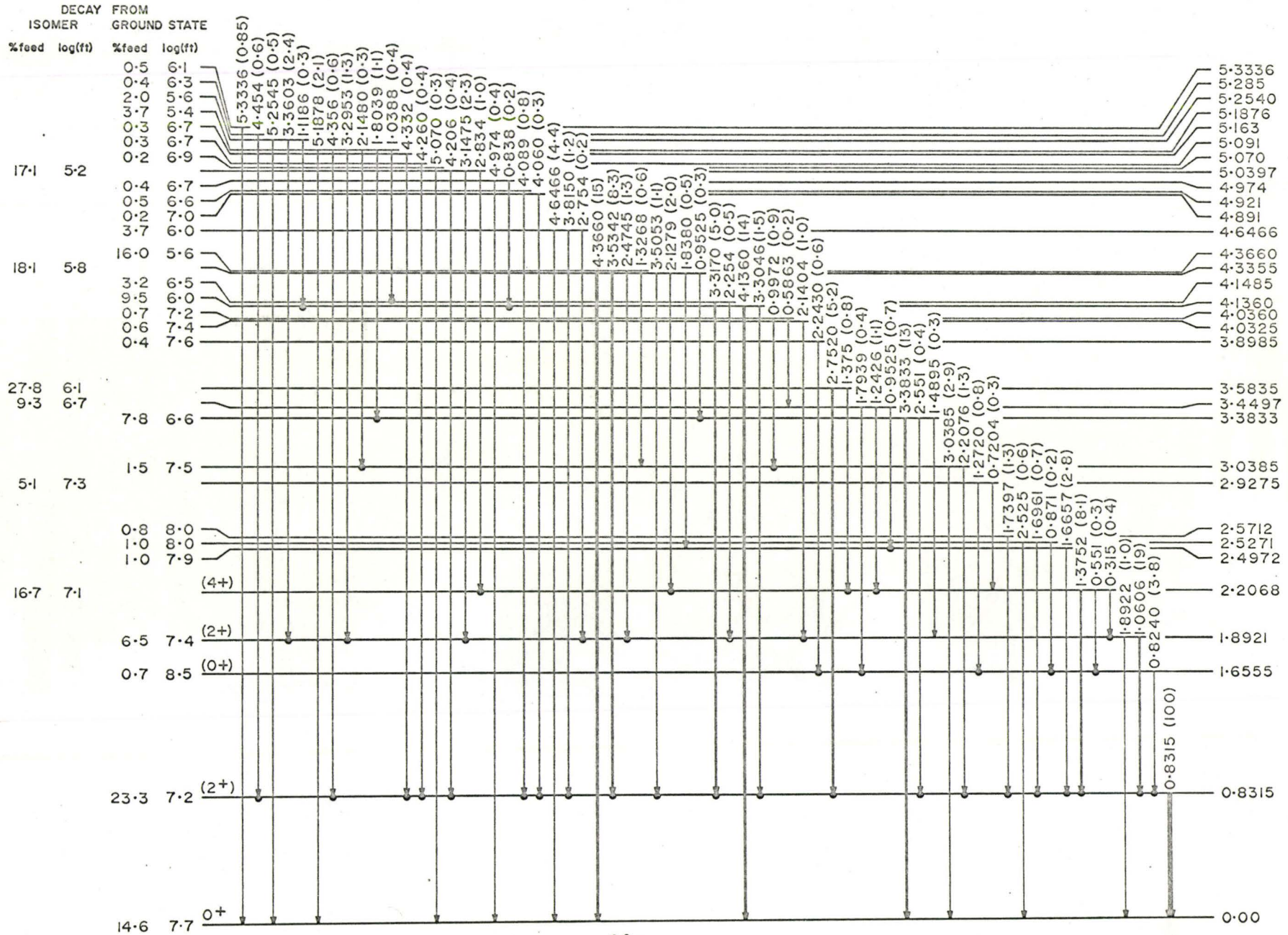

Figure 5.3.7 ^{90}Rb Decay Scheme

at 3.889 and 3.654 MeV, which were observed in singles but not in coincidence.

An estimate of the relative intensities of the beta decays from the 0.1069 MeV isomeric state and the ground state of ^{90}Rb can be made using the observation of Carlson et al (1969) that the 1.3752 MeV gamma ray exhibits only a 253 sec half-life. This indicates that the level at 2.2068 MeV and all other levels which populate this state by gamma emission must be populated by beta decay from the isomeric state. Thus the levels at 2.9275, 3.4497, 3.5835, 4.3355, 5.0397 and 2.2068 MeV would be populated only from the isomer with beta feeds of total intensity 20.3 relative to the 0.8315 MeV gamma ray as 100. This would also mean that the decay of the 0.8315 MeV transition would exhibit a 20% component with the longer half-life. The difference between this and the 33% reported by Carlson et al (1969) can be readily accounted for by assuming that his prescription for source preparation included a longer delay time before counting than the one used in this work.

The measurement by Johnson et al (1964) that the 0.8315 MeV transition occurs in 56% of the decays implies a total beta intensity of 178 and a ground state feed of 23 relative to the 0.8315 MeV gamma ray as 100. The observation by Carlson et al (1969) that all beta rays with energy >4.5 MeV exhibit the 153 sec half life indicates that this ground state group as well as those to the 0.8315, 1.6555 and 1.8921 levels all originate from the ^{90}Rb ground state.

With these considerations it is possible to separate the levels in ^{90}Sr into two groups one of which is fed entirely from the isomer and the other of which is fed mainly from the ground state.

In determining the relative intensities of the partial beta feeds within the group originating from the isomer, the total intensity of the 0.1064 MeV transition from the isomer to the ground state of ^{90}Rb is required. Since this transition has a half life of 253 seconds, it behaves like a transition in ^{90}Sr and appears in Table 5.3.1. From the discussion of ^{90}Rb spins in chapter 4, this transition is most probably M3 and therefore has a total internal conversion coefficient of 11. Thus the total intensity of the transitions de-exciting with the isomers in 20.3 + 1.3 = 21.6. While some of the levels in Figure 5.3.7, assumed to be fed from the 1^- ground state may in fact be fed from the 4^- isomer, the intensity of these partial feeds is almost certainly small and so the above procedure can give reasonably reliable log (ft) values.

The ratio R of the populations of the isomeric and ground states, at the time when the ^{90}Rb collection is completed, can be calculated from the expression

$$R = [1-\exp(-\lambda_{gs}\ t_{cnt})] \cdot [1-\exp(-\lambda_{is}\ t_{cnt})]^{-1} \cdot R_c$$

where R_c is the ratio of the intensities associated with the isomeric and ground state decays as derived above.

The value, R = 0.18, derived from this calculation is in fair agreement with the lower limit of 0.13 derived from the ^{90}Rb intensity balance of Figure 4.3.7.

Since $^{90}_{38}Sr_{52}$ is an even-even nucleus with only two particles outside a closed shell it might be expected to behave like a "soft deformed nucleus", to use the terminology of Baranger and Sorenson (Scientific American (1969)), and exhibit a typical vibrational

spectrum. In this case the first excited state would be 2^+. From the observation mentioned above, concerning the beta feeding to the 2.2068 MeV level, a tentative designation of this state as the 4^+ member of the expected 0^+, 2^+, 4^+ two-phonon triplet, may be made. That is, if the isomer is indeed 4^- level, or at least a high spin configuration, it would be expected to feed a high spin level in the daughter. This assignment is supported by the strong transition to

the first excited state and the absence of a transition to the ground state. A similar gamma decay pattern for the 1.8921 MeV level with a relatively weak ground state transition rather than none at all, suggests that this may be the 2^+ member of the multiplet. The single transition from the 1.6555 MeV level to the first excited state with no ground state transition indicates that this may be the 0^+ member. The log (ft) values for the corresponding beta feeds are also compatable with these assigmments. The 0.5514 MeV gamma ray, however, placed between the 2.2068 and 1.6555 MeV levels would seem to be a contradiction. However, since the single particle level spacing is only $\sim$ 1 MeV as indicated by the level structure of ^{89}Sr (Kitching and Johns (1966)) states in this energy region may not be very pure and such weak transitions could be due to admixtures.

Recently Ball (1969) has demonstrated that nuclei in this region (in particular nuclei with N=50) are particularly amenable to shell model calculations. Thus he has successfully calculated the low lying level structure ($\lesssim$ 4 MeV) of ^{88}Sr and ^{90}Zr among others. It might be expected then, that the structure of ^{90}Sr and possibly ^{91}Sr, which follows, would also be readily calculable. In this case, the spins tentatively assigned above on the basis of the vibrational picture would be expected to be reproduced. In addition a 3^- state which appears consistently at just below 3 MeV in ^{86}Kr, ^{88}Sr, ^{90}Zr and ^{92}Mo might be identified with the level at 3.0385 MeV. In the vibrational interpretation this configuration would be due to the excitation of octupole oscillations and consequently would decay to the ground state with essentially no branching. As with the 0.5514 MeV transition the observed branching could be due to admixed impurities

because of the relatively high excitation compared to the single particle level spacing. In view of this it would appear that the shell model calculation approach would be the most fruitful for level interpretation.

5.4 ^{91}Rb Decay

5.4.1 ^{91}Rb Energy and Intensity Measurements

Table 5.4.1 presents a compilation of the energies and intensities of the gamma rays assigned to the decay of ^{91}Rb. The intensities are normalized to that of the relatively strong 0.6027 MeV transition. This transition was chosen for this purpose since it was the strongest transition to appear well resolved in experiments done both with and without absorber and in each case occured at a point on the detector efficiency curve which was relatively unaffected by the addition of the absorber. The transitions preceeded by an asterisk were assigned to this decay solely on the basis of the appearance of a peak in the spectrum accumulated from sources expected to enhance the activity due to this nuclide. The remaining photons were identified from their ratio in this spectrum to that acquired from sources enhanced in ^{90}Rb activity. The remarks made in Section 5.3.1 concerning the errors in intensities and energies also apply here.

The basis for classification is given as coincidence probabilities determined from gating transitions at 0.0931 (γ_1), 0.3460 (γ_2), 0.6027 (γ_3) and other gamma rays as listed. These columns were prepared from an analysis of the coincidence data as outlined below.

TABLE 5.4.1

Gamma Rays Observed in the Decay of ^{91}Rb

Energy (MeV)		Intensity	Classification	Basis for Classification				
				0.0931 MeV	0.3460 MeV	0.6027 MeV	Other	
0.0931	3	930	0.0931→0					E
0.3460	5	288	0.4392→0.0931	288(n)		81(n)		E
0.4393	5	68	0.4392→0			20		E
0.5931	2	43	2.6574→2.0643	33			1.9712	E
0.6027	2	100	1.0414→0.4392	62	81(n)			E
0.641	2	33			23			
0.707	1	33	1.146 →0.4392		26			E
0.9478	3	70	1.0414→0.0931	67				E
1.0413	3	85	1.0414→0					E
1.1374	2	117	1.2306→0.0931	132				E
1.146	1	20	1.146 →0					E
*1.301	2	20						
*1.4358	10	23						
1.4832	8	38						
*1.6160	5	85	2.6574→1.0414	43	45	53		E
*1.6250	7	39	2.0643→0.4392	48	28			E

Energy (MeV)		Intensity	Classification	Basis for Classification				
				0.0931 MeV	0.3460 MeV	0.6027 MeV	Other	
*1.6291	8	32	3.6932→2.0643					E
1.8495	2	95	1.9426→0.0931	110				E
1.905	2	34	2.340 →0.4392		43			E
1.914	1	35			35			
1.9712	3	244	2.0643→0.0931	250			0.5931	E
*1.982	2	19						
*2.036	2	18						
*2.322	1	28	4.265 →1.9426					E
*2.5055	10	55	3.737 →1.2305	62			1.137	E
2.5643	2	492	2.6574→0.0931	490				E
*2.712	1	27	3.752 →1.0414					E
*2.722	2	21						E
*2.9257	6	90	2.9257→0	no γ-γ				E
3.446	1	60						
3.6000	3	341	3.6932→0.0931	315				E
3.640	1	87	4.0785→0.4395	85				E
*3.738	2	30	3.737 →0	no γ-γ				E
*3.752	2	33	3.752 →0	no γ-γ				E

Energy (MeV)		Intensity	Classification	Basis for Classification			
				0.0931 MeV	0.3460 MeV	0.6027 MeV	Other
*3.842	1	52	3.935 →0.0931	40			E
4.0785	5	143	4.0785→0	no γ-γ			E
*4.252	1	22	4.252 →0	no γ-γ			E
*4.265	1	50	4.265 →0	no γ-γ			E
*4.497	3	88	4.497 →0	no γ-γ			E

Note

* Indicates transition assigned to decay of ^{91}Rb by virtue of peak occuring in this spectrum but not that of ^{90}Rb.

(n) Indicates this coincidence used as normalization.

E Indicates energy fit.

5.4.2 ^{91}Rb Coincidence Measurements and Decay Scheme Construction

Figures 5.4.1, 5.4.2, and 5.4.3 show the three coincidence gates which provided essentially all the coincidence information for the construction of the decay scheme. The first two show the 0.3460 and 0.6027 MeV NaI gated spectra generated from the "Lo-Lo" Rubidium experiment and the final one presents the delayed coincidences with the 0.0931 NaI gate from the separate experiment described in Section 3.5. Analysis of these gates provided the coincidence probabilities listed in Table 5.4.1. Within each gate the calculations were normalized to the cascade indicated in the table as it was believed that the coincidence probabilities for these cascades were well known.

The occurence of the 0.3460 and 0.6027 MeV peaks in the 0.0931 MeV gated spectrum and the reciprocal occurence of these radiations in their own gates indicates the presence of a triple cascade. Their intensity relationship suggests a 0.6027-0.3460-0.0931 MeV ordering which is supported by the appearance of the 0.4393 MeV radiation in the 0.6027 gated spectrum and its absence from the others, as well as the 0.0931 + 0.3460 energy fit. This establishes levels at 0.0931, 0.4392 and 1.0414 MeV, the uppermost of which is verified by the 0.9478-0.0931 coincidences and the energy fit of the possible 1.0413 MeV ground state transition.

The presence of the 1.6160 MeV radiation in all three gated spectra suggests a level at 2.6574 MeV whose existence is confirmed by the energy fit of the observed 2.5643-0.0931, 0.5931-0.0931, 1.9712-0.0931 and 0.5931-1.9712 MeV coincidences. The last of these has not been presented since the NaI gated spectrum in which it was observed contained considerable contamination from ^{89}Rb or

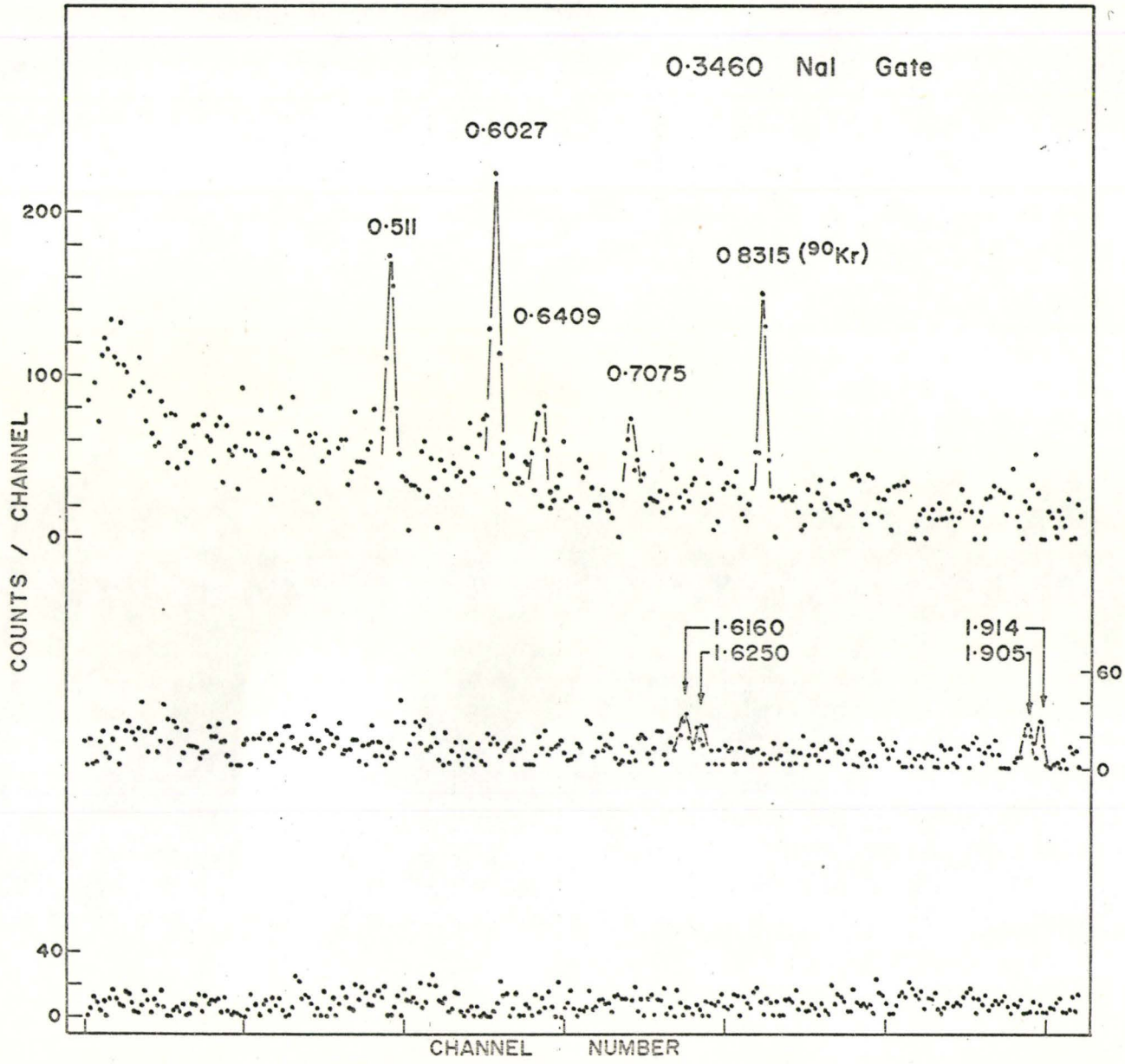

Figure 5.4.1 ^{91}Rb Gamma Coincidence Spectrum - 0.3460 MeV NaI Gate

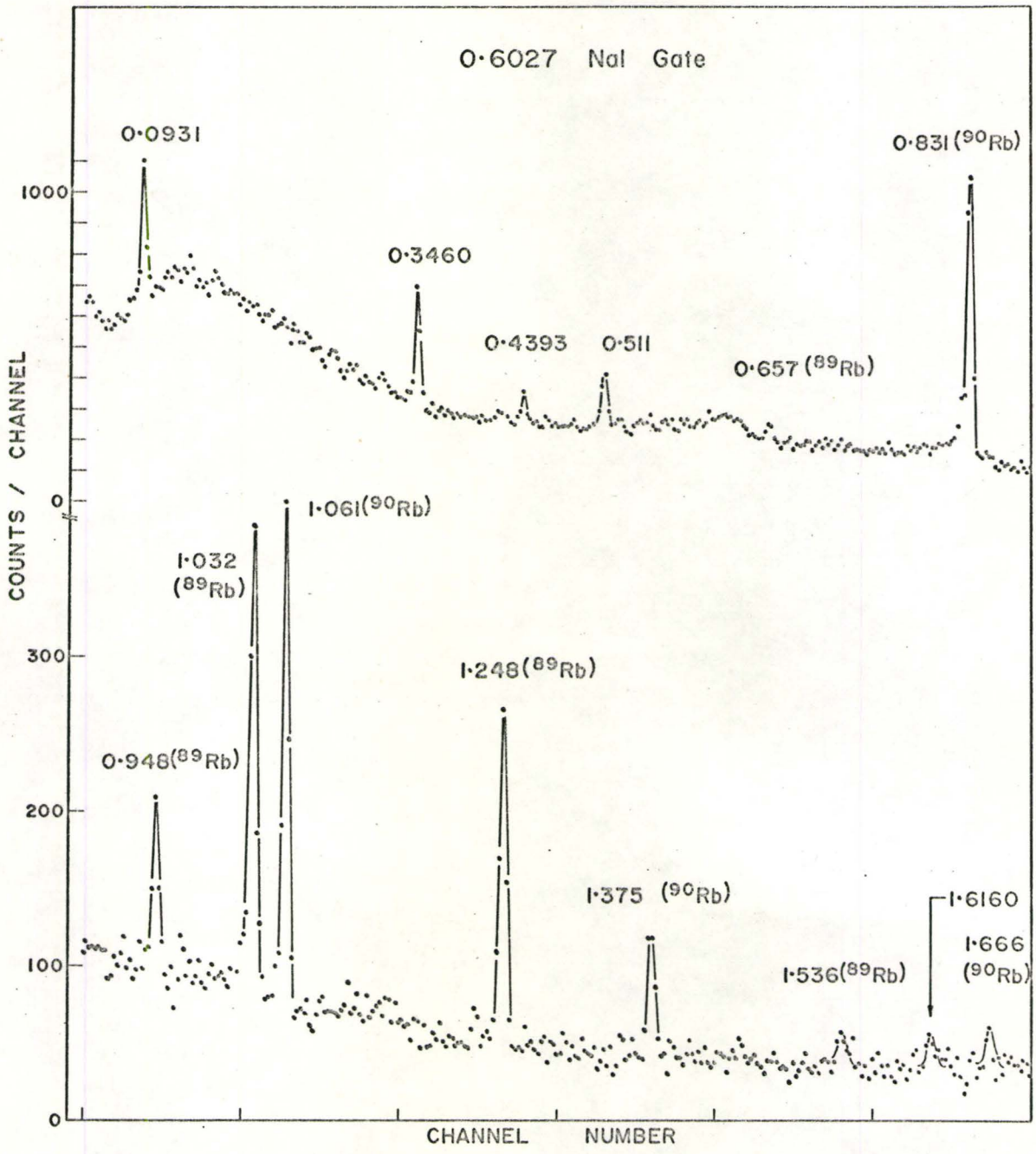

Figure 5.4.2 ^{91}Rb Gamma Coincidence Spectrum - 0.6027 MeV NaI Gate

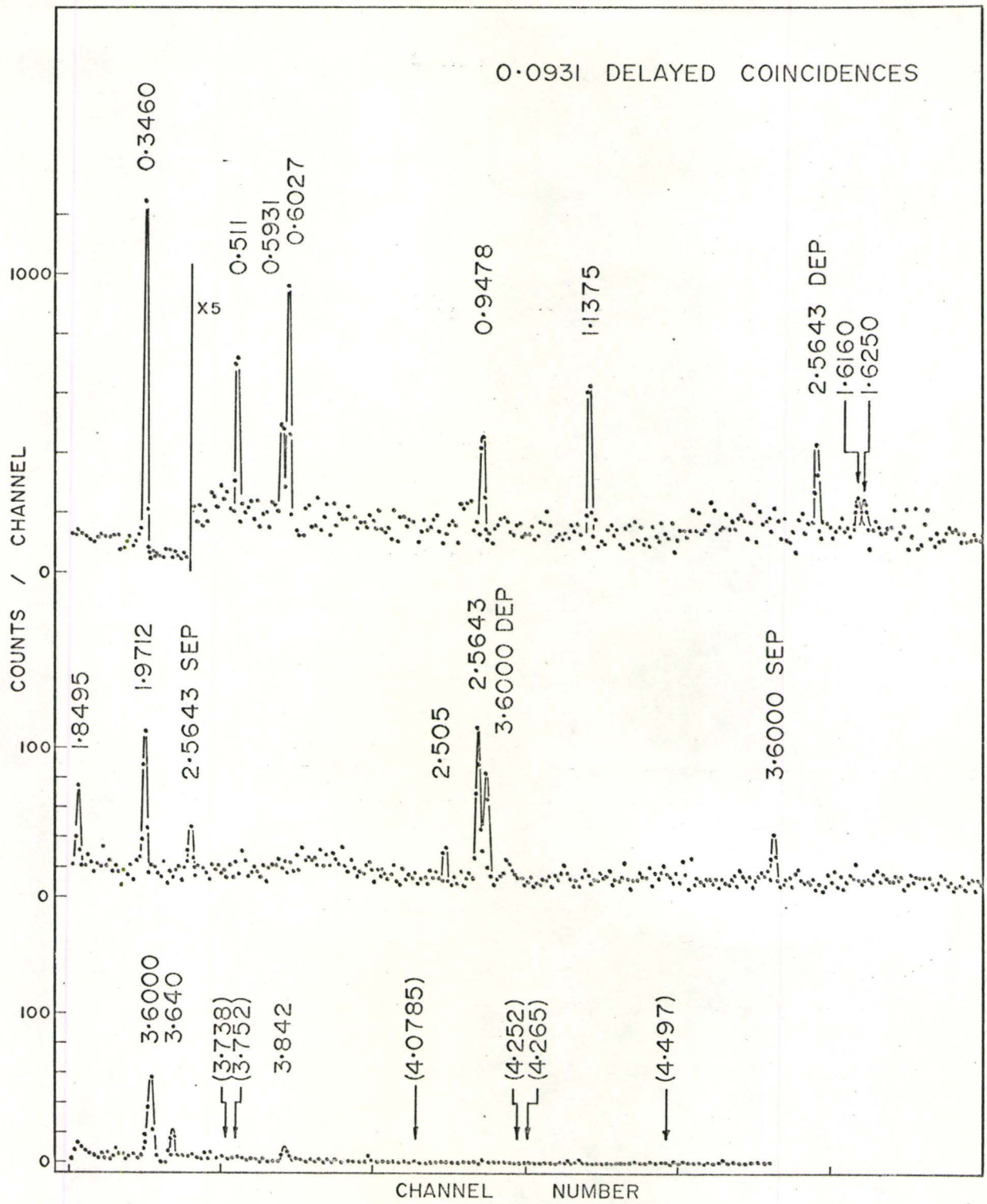

Figure 5.4.3 ^{91}Rb Delayed Coincidence Spectrum

^{90}Rb events but only the single ^{91}Rb coincidence peak. The level defined in this manner at 2.0643 MeV from the 1.9712-0.0931 MeV cascade, is supported by the presence of the 1.6250 MeV gamma ray in both the 0.3460 and 0.0931 MeV gated spectra.

The observed 1.8495-0.091 MeV and 1.1374-0.0931 MeV coincidences establish levels at 1.9426 and 1.2306 MeV respectively which are useful for delineating the higher lying portion of the decay scheme. Levels can then be established at 4.497, 4.265, 4.252, 4.0785, 3.782, 3.737 and 2.9257 MeV because of the absence of these transitions from any of the NaI gated spectra and in particular from the 0.0931 MeV gated spectrum. Since each of the levels so far established is strongly connected either directly or in cascade to the first excited state all these full energy peaks should appear in the delayed coincidence spectrum if the corresponding transition populates any of these levels. In addition, population of any of these levels by these gamma rays would require levels either close to or above the estimated ground state Q-value of 5.5 MeV (Lederer (1967)). Furthermore, some of these levels have supporting evidence. Thus the 4.265 MeV state is supported by the energy fit of the 2.322 MeV transition to the 1.9426 MeV level; the 4.0785 MeV assignment is supported by the observed 3.640-0.0931 MeV coincidences and the energy fit of the 3.640 MeV transition if it is taken to populate the 0.4392 MeV level; the 3.752 MeV placement is supported by the 2.712 MeV energy fit to the 1.0414 MeV level; and the 3.737 MeV state is supported by the observed 2.5055-1.1374 MeV coincidences.

The strong 3.6000-0.0931 MeV coincidences, not yet accounted for, defines a new level at 3.6931 MeV which allows the 1.6291 MeV

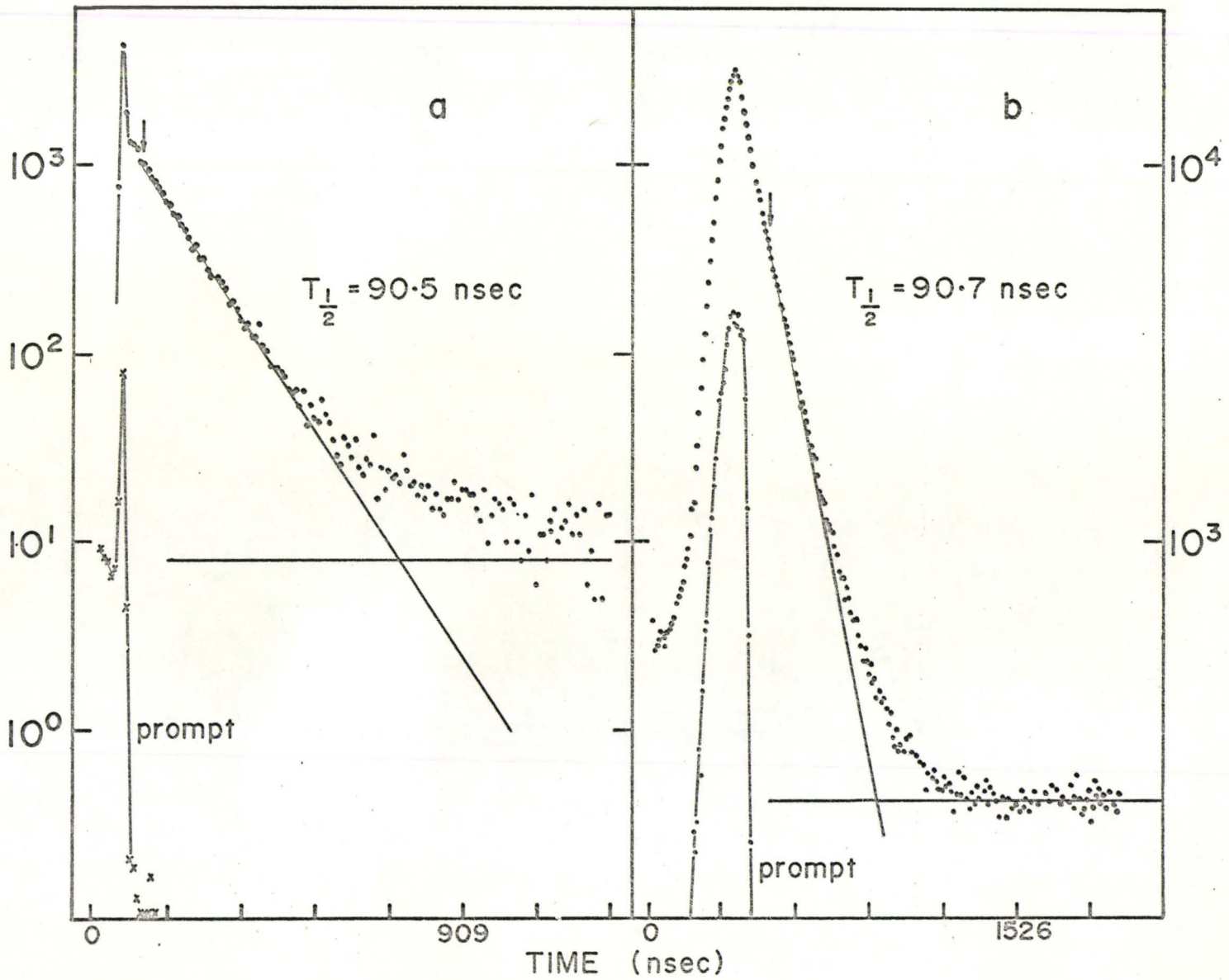

Figure 5.4.4 ^{91}Rb - Lifetime Measurement of 0.0931 MeV Level

gamma ray to be placed between this state and the one at 2.0643 MeV on the basis of energy fit. The weak transition at 0.645 MeV observed in the 0.3460 MeV NaI gate (Figure 5.4.1) has not been placed.

5.4.3 Lifetime of the First Excited State

Using the procedure outlined in Section 3.5 the lifetime of the 0.0931 MeV state was determined. The data from which the lifetime was obtained is presented in Figure 5.4.4, along with the "prompt" response curves. Figure 5.4.4(a) consists of the data acquired with the fast electronics discussed explicitly in Section 3.5 while 5.4.4(b) contains the data acquired during the delayed coincidence experiment. The lifetimes were determined from these data by an iterative least squares technique (Archer et al (1960)) using only those points to the right of the arrows indicated in the figure. A second calculation was also performed, in each case, omitting further data points from the low time end of the spectrum, to ensure that none of the prompt response was included. The results of these calculations yielded a lifetime of 90 ± 5 ns. The error, which is an order of magnitude larger than the statistical error generated from the data by the computer analysis, is made intentionally large to account for any systematic errors in the equipment which may not have been eliminated.

5.4.4 ^{91}Rb Decay Scheme and Discussion

Figure 5.4.5 presents pictorially the information gleaned from the analysis of the coincidence data as well as the lifetime measurement. Unfortunately it is not possible to determine the intensities of the beta feeds to the various levels since nothing is known

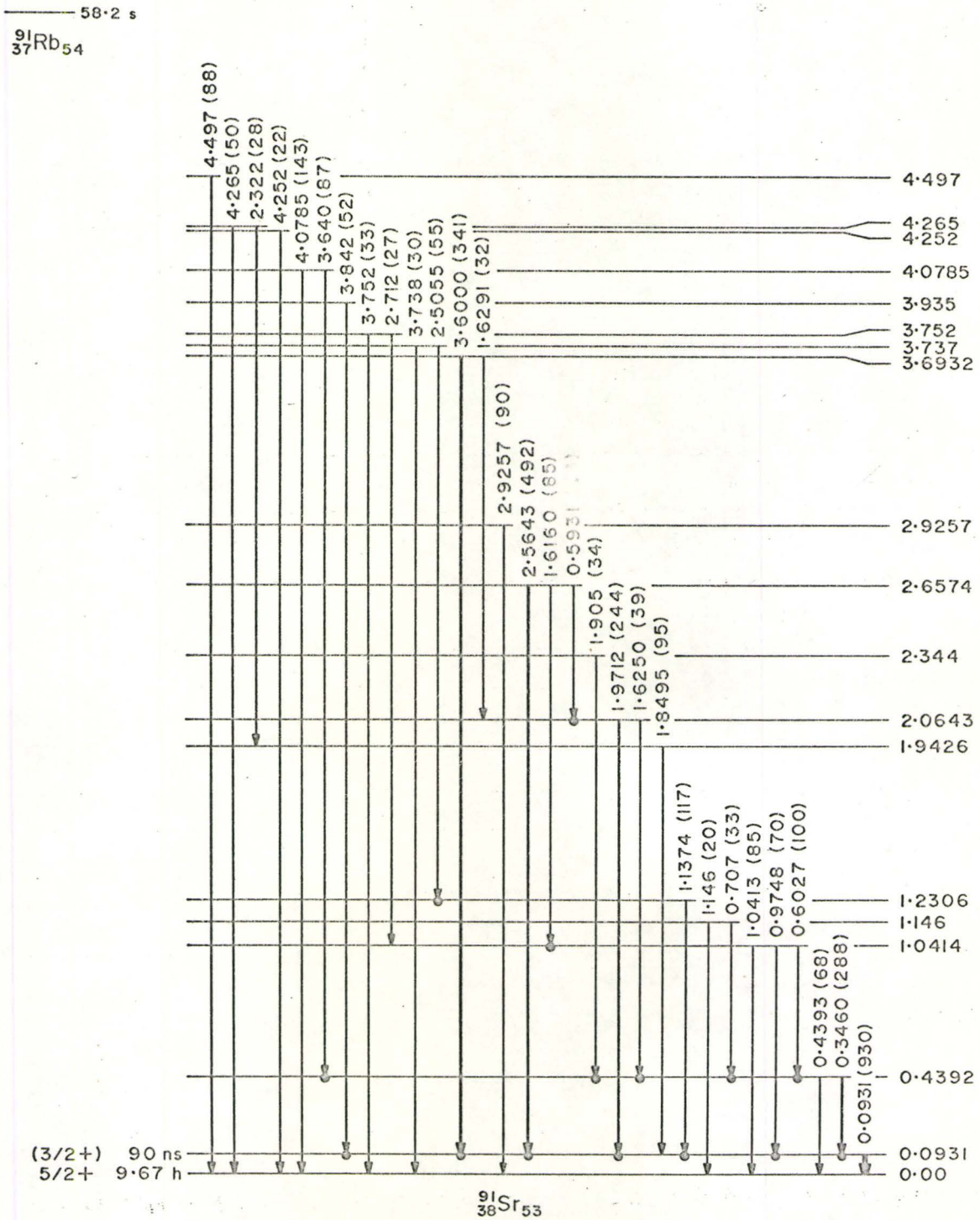

Figure 5.4.5 ^{91}Rb Decay Scheme

about the ground state or first excited state feeds,and therefore, the gamma ray intensities cannot be normalized to photons/100 decays. The ground state of ^{91}Sr is $5/2^+$ as expected from shell model systematics and the ground state of ^{91}Rb is probably $(p_{3/2})^{-1}$ as a result of the promotion of a proton from the $p_{3/2}$ shell model level to fill the $f_{5/2}$ level, thus gaining the advantage of the pairing energy. On this assumption, the ground state beta transition would be expected to be first forbidden. Assuming a representative value of 7 for the log (ft) of such a transition results in an intensity of the order of 2%. However, should the log (ft) be closer to 6 or 8 the intensity might vary from 0.2 to 20%. In view of this any prediction of the ground state beta intensity seems unreasonable.

In addition, the use of the photon intensity of the 0.0931 MeV transition to determine total ground state feeding is unacceptable inasmuch as this transition is expected to be highly converted. Using the gamma rays feeding this level and the ground state, with the exception of the 0.0931 MeV line, encounters the problem of the beta feed to the first excited state similar to that of the ground state. The problem is also compounded in this case due to a lack of knowledge of the spin of the isomer.

A tentative assignment of $3/2^+$ may be made for this state from comparison with ^{93}Zr which has the same neutron configuration. Since both these Sr and Zr isotopes contain an even number of protons, the properties of the low lying states in each might be expected to be largely determined by the neutrons and hence to exhibit some similarity. In fact the first excited state of ^{93}Zr at 0.267 MeV also has a lifetime measured to be 1.45 ± 0.05 ns. (Prestwich

et al (1969)). Using the K shell internal conversion coefficient determined by Knight et al (1959), which indicates at mixing ratio of 28/72 M1/E2, it is possible to calculate the hinderance and enhancement, respectively, of these radiations with respect to the Weisskopf single particle transition probabilities.

In order to make corresponding calculations for the ^{91}Sr case, it is necessary to estimate the internal conversion coefficient of the 0.0931 MeV transition. This can be obtained from the gamma ray intensity measurement and the relationship

$$\alpha_K = \frac{I_\beta + \sum_\kappa I_{\gamma\kappa} - I_{0.0931}}{I_{0.0931}}$$

where $I_\beta + \sum_\kappa I_{\gamma\kappa}$ represent the total intensity of all radiations populating the 0.0931 MeV level. Although I_β is not known, the assumption $I_\beta = 0$ will yield a lower limit for the conversion coefficient. Such a calculation gives $\alpha_K = 0.87 \pm 0.15$ which corresponds to 75 $\pm$ 16% E2 or an M1/E2 mixing ratio of 25/75, which corresponds closely to that in ^{93}Zr. The errors that have been indicated resulted from the assumption that the intensities involved were statistically independent variables each with an error of 10%. The hinderance and enhancement factors corresponding to this mixing ratio are listed in Table 5.4.2 along with the corresponding values for ^{93}Zr and ^{95}Mo (Prestwich et al (1969)), both of which have the same neutron configuration as ^{91}Sr.

One possible explanation for the severe retardation of the M1 transition probability is that the first excited state is the 3/2 member of the multiplet produced from the coupling of the

$|\nu(d_{5/2})^3 ; J^\pi = 5/2^+ >$ ground state to the 2^+ one-phonon vibrational state of the ^{90}Sr core. In this case the transition to the ground state would involve the annihilation of a quadrupole phonon and as a result would be limited to this multipolarity. Any M1 transition strength could only arise from admixtures of other shell model states into the wave functions. In addition, because of the collective nature of the excited state, the strength of the E2 transition would be expected to be enhanced, as is observed.

TABLE 5.4.2

Comparison of Reduced Transition Probabilities

Isotope	E(MeV)	B(E2) W.U.	B(M1) W.U.
^{91}Sr	0.093	27	$7.7 * 10^{-5}$
^{93}Zr	0.267	7.4	$2.3 * 10^{-4}$
^{95}Mo	0.204	17.5	$3.3 * 10^{-3}$

On the other hand, the first excited state might be formed from a re-coupling of the neutrons to a $|\nu(d_{5/2})^3; J^\pi = 3/2^+ >$ configuration. In this event, the expected M1 transition between this and the ground state would be L-forbidden and therefore strongly hindered, again only existing through admixtures of other configurations. In this case, however, no natural explanation for the enhancement of the E2 portion of the radiation exists except for the observation that these transitions are generally enhanced.

REFERENCES

Amarel, I., Bernas, R., Foucher, R., Jastrzebski, J., Johnson, A., Teillac, J., and Gauvin, H. (1967). Phys. Lett. 24B, 402.

Archer, N. P., Prestwich, W. V., and Keech, G. L. (1960). Nucl. Inst. Meth. 44, 114.

Archer, N. P. (1965). Ph.D. Thesis, McMaster University.

Ball, J. B. (1969). Invited Paper, A.P.S. Meeting (Washington); Bull. Am. Phys. Soc. 14, 545; also ORNL-TM-2602.

Baranger, M. and Sorenson, R. A. (1969). Scientific American 221, 58 (Aug. (1969)).

Bardeen, J., Cooper, L. N., and Schreiffer, R. (1957). Phys. Rev. 108, 1175.

Bohr, A., Mottelson, B. R., and Pines, D. (1958). Phys. Rev. 110, 936.

Brennan, M. H. and Bernstein, A. M. (1960). Phys. Rev. 120, 927.

Carlson, G. C., Schick, W. C. Jr., Talbert, W. L. Jr., and Wohn, F. K. (1969). Nucl. Phys. A125, 267.

Goodman, R. H., Kitching, J. E., and Johns, M. W. (1964). Nucl. Phys. 54, 1.

Hager, R. S. and Seltzer, E. C. (1968). "Nuclear Data" Section A Vol. 4, Academic Press.

Haxel, O., Jensen, J. H. D., and Suess, H. E. (1949). Phys. Rev. 75, 1766.

Haxel, O., Jensen, J. H. D., and Suess, H. E. (1950). Z. Physik 128, 295.

Johnson, N. R., O'Kelley, G. D. and Eichler, E. (1964). Phys. Rev. 135B, 36.

Kennett, T. J., Archer, N. P. and Hughes, L. B. (1967). Nucl. Phys. A96, 658.

Kitching, J. E. and Johns, M. W. (1966). Can. J. Phys. 44, 2661.

Knight, J. D., Hoffman, D. C., Dropesky, B. J. and Frasco, D. L. (1959). J. Inorg. Nucl. Chem. 10, 183.

Kofoed-Hansen, O. and Nielsen, K. O. (1951). Phys. Rev. 82, 96.

Lederer, C. M., Hollander, J. M. and Perlman, I. (1967). "Table of Isotopes", John Wiley and Sons Inc.

Lee, T. D. and Yang, C. N. (1956). Phys. Rev. 104, 254.

Lycklama, H., Hughes, L. B. and Kennett, T. J. (1967). Can. J. Phys. 45, 1871.

Mayer, M. G. (1949). Phys. Rev. 75, 1969.

Mayer, M. G. (1950). Phys. Rev. 78, 16.

Norris, A. E., and Wahl, A. C. (1966). Phys. Rev. 146B, 926.

Okendon, D. W. and Tomlinson, R. H. (1962). Can. J. Chem. 40, 1594.

Pauli, W. (1933). Rapports du Septieme Conseil de Physique, Solvay, Brussels.

Preston, M. A. (1962). "Physics of the Nucleus", Addison-Wesley Co. Inc., Reading, Mass.

Prestwich, W. V., Arad, B., Boulter, J., and Fritze, K. (1968). Can. J. Phys. 46, 2321.

Reines, F. and Cowan, C. L. (1959). Phys. Rev. 104, 254.

Segrè, E. (1965). "Nuclei and Particles", W. A. Benjamin Inc., New York.

Slavinskas, D. D., Kennett, T. J., and Prestwich, W. V. (1965). Nucl. Inst. and Meth. 37, 36.

Talbert, W. L. Jr. (1969). Private Communication.

Wolfsburg, K. (1965). Phys. Rev. 137B, 929.

Wu, C. S., Ambler, E., Hayward, R. W., Hoppes, D. D. and Hudson, R. P. (1957). Phys. Rev. 105, 1413.

Zherebin, A. E., Krylov, A. I., Polikarpov, V. I., Yuzvuk (1967). Soviet J. Nucl. Phys. 5, 1.